Radiative Transfer and Aerosol Remote Sensing

Dissertation

zur

Erlangung der naturwissenschaftlichen Doktorwürde
(Dr. sc. nat.)

vorgelegt der

Mathematisch-naturwissenschaftlichen Fakultät

der

Universität Zürich

von

Felix C. Seidel

von

Pfäffikon ZH

Promotionskomitee

Prof. Dr. Michael E. Schaepman (Vorsitz und Leitung der Dissertation)

Dr. Alexander A. Kokhanovsky

Prof. Dr. Klaus I. Itten

Zürich, 2011

Author:
Felix C. Seidel
Remote Sensing Laboratories, Department of Geography, University of Zurich,
Winterthurerstrasse 190, CH-8057 Zurich, Switzerland
http://www.geo.uzh.ch/rsl

Seidel, Felix C.
Radiative Transfer and Aerosol Remote Sensing
Remote Sensing Series, Vol. 61 – Zurich: Remote Sensing Laboratories, 2011.
ISBN: 978-3-03703-027-1

This work was approved as a PhD thesis by the Faculty of Science of the University of Zurich in the spring semester 2011 on the basis of expert reviews by Prof. Dr. Michael E. Schaepman (Remote Sensing Laboratories, University of Zurich, Switzerland), Dr. Alexander A. Kokhanovsky (Institute of Environmental Physics, University of Bremen, Germany) and Dr. Alexei I. Lyapustin (NASA Goddard Space Flight Center, USA).
Die vorliegende Arbeit wurde von der Mathematisch-naturwissenschaftlichen Fakultät der Universität Zürich im Frühjahrssemester 2011 aufgrund der Gutachten von Prof. Dr. Michael E. Schaepman (Remote Sensing Laboratories, Universität Zürich, Schweiz), Dr. Alexander A. Kokhanovsky (Institut für Umweltphysik, Universität Bremen, Deutschland) und Dr. Alexei I. Lyapustin (NASA Goddard Space Flight Center, USA) als Dissertation angenommen.

Doctorate Committee/Promotionskomitee:
Prof. Dr. Michael E. Schaepman (Chair/Vorsitz und Leitung), Dr. Alexander A. Kokhanovsky, Prof. Dr. Klaus I. Itten

Give us the vision which can see our love in the world in spite of human failure.
Give us the faith, the trust, the goodness, in spite of our ignorance and weakness.
Give us the knowledge that we may continue with understanding hearts and show us what each one of us can do to set forward the coming of the day of universal peace.

Adapted from Frank Borman
(Astronaut, Apollo 8 mission, first human spaceflight to leave Earth orbit, 24 Dec 1968)

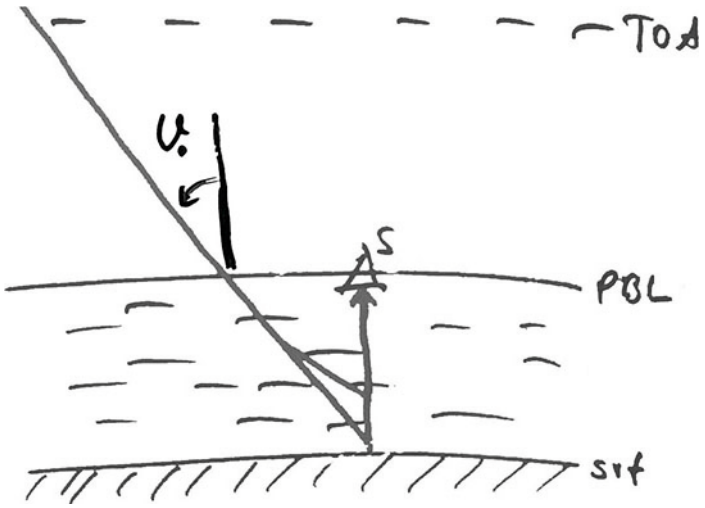

Sketch of the fast and simple model for atmospheric radiative transfer as presented in this thesis.

Acknowledgments

The PhD endeavor has taken away a lot of time from my private life, including long evenings and weekends. I am very grateful for the understanding and continuous support by my personal environment. I would like to emphasize my deepest gratitude to Beatrice Caprez, to my parents, to my brother and sister and to my closest friends Bettina Ryser, Damaris Reist, Daniel Thomas and Jonas Hinn.

This work would not have been possible without the support and friendship of my advisors and many colleagues, for which I am very grateful. To name just a few in alphabetical order: Alexander Kokhanovsky, Andreas Hüni, Daniel Schläpfer, Désirée Treichler, Erich Meier, Jens Nieke, Klaus Itten, Markus Kurmann, Mathias Kneubühler, Michael Schaepman, Philippe Meuret, Robert Höller, Tobias Kellenberger, Urs Baltensperger, Urs Frei, Yves Bühler, as well as Adrian Schubert, Alexander Damm, Bruno Weber, Damien Markulin, Daniel Henke, Daniel Odermatt, David Small, Edoardo Alberti, Felix Morsdorf, Francesco Dell'Endice, Jason Brazile, Jeffrey Bowles, Johannes Keller, Jörg Weyermann, Jürg Schopfer, Lola Suarez, Lucia Yanez, Lucie Homolová, Lukas Zuberbühler, Michael Jehle, Natália Archinard, Othmar Frey, Petra D' Odorico, Rita Ott, Sandra Altorfer, Wolfgang von Hoyningen-Huene, and last but not least Zbyněk Malenovský.

Abstract

Atmospheric particles (aerosols) are the objective of intensive research. In addition to effects on our health, they also have a significant influence on climate. Aerosols can be measured *in-situ* or be retrieved using optical remote sensing instruments. Such instruments measure the upwelling solar radiance, which is scattered in the atmosphere as well as partially reflected from the Earth's surface. The separation of measured radiance into these components is one of the great challenges for quantitative remote sensing.

A radiative transfer algorithm was developed in the course of this thesis to generate an approximate solution to this problem. It combines analytical equations in a novel way with parameterizations and other approximations to achieve fast computations. An extended version of this algorithm was developed specifically to retrieve aerosol optical depth. Interesting findings were derived from this algorithm: e.g. the influence of surface albedo and its uncertainty on aerosol retrieval. The thesis is dived into the following three parts:

In the first part, an analysis of the instrument performance requirements for aerosol retrieval is provided. This entirely theoretical study shows that a high sensor sensitivity is needed with a signal to noise ratio on the order of 10^2 to 10^3. Even higher signal to noise ratio is required for reliable retrievals over bright surfaces with a surface albedo greater than 0.3. In the second part, the proposed fast algorithm is described in detail. The underlying equations are able to approximate most effects of the atmosphere and surface on the solar radiation. Comparisons with a widely used and recognized radiative transfer model show its fast computation and accuracy. In the last part, a promising application of the suggested aerosol retrieval algorithm is presented. Tests with synthetic and real remote sensing data show its efficiency and relatively high accuracy. The algorithm is then used to quantify the influence of the surface reflectance factor on aerosol retrieval. Results concerning the so-called "critical" surface albedo indicate that it may significantly complicate the aerosol retrieval problem.

The presented algorithm for the fast and simple radiative transfer computation provides a promising basis for many applications in the fields of remote sensing and climatology whenever quick calculations and flexibility are preferred. Pointwise aerosol retrievals using remote sensing data, as demonstrated in this thesis, is one example. It is possible to extend the proposed approach in the future to account for the spatial distribution of aerosols. Further, the accuracy of the radiative transfer computation can be enhanced by incorporating higher orders of scattering and a more comprehensive representation of the surface, with its influence on radiation, into account.

Kurzfassung

Partikel in der Atmosphäre (Aerosole) werden intensiv erforscht. Neben gesundheitlichen Auswirkungen und klimawirksamen Eigenschaften beeinflussen sie die Erfassung der Erdoberfläche mittels Fernerkundung durch Streuung und Absorption des Sonnenlichtes. Da viele Anwendungen der Fernerkundung an der Charakterisierung von Oberflächeneigenschaften interessiert sind, muss der atmosphärische Einfluss am gemessenen Signal anhand von Modellrechnungen quantifiziert und separiert werden. Dies ist nach wie vor eine grosse Herausforderung, da unter anderem die optischen Eigenschaften der Aerosole bekannt sein müssen.

In der vorliegenden Dissertation wird eine Methode zur effizienten Lösung dieses Problems entwickelt. Sie ermöglicht die Extraktion des optischen Einflusses der Aerosole direkt aus Fernerkundungsdaten. Der vorgestellte Algorithmus setzt vorhandenes Wissen neu zusammen und bietet hiermit eine neue, vereinfachte und effiziente Methode an. Erste Anwendungen dieses Algorithmus resultierten bereits in interessanten Ergebnissen, welche in dieser Arbeit vorgestellt werden. So wurde beispielsweise der Einfluss des Bodenreflexionsfaktors auf die Detektion von Aerosolen untersucht. Diese Erkenntnis kann möglicherweise zur Reduktion von Unsicherheiten bezüglich der Strahlungswirksamkeit der Aerosole in heutigen Klimamodellen beitragen.

Die Arbeit besteht aus drei zusammenhängenden Teilen. Der erste Teil eruiert die notwendige Messgenauigkeit eines optischen Fernerkundungssensors zur zuverlässigen Detektion von Aerosolen. Diese rein theoretische Sensitivitätsstudie zeigt, dass hierfür ein mindestes 10^2 bis 10^3 fach stärkeres Signal als das Sensorrauschen notwendig ist. Der mittlere Teil der Arbeit beschreibt im Detail den vorgeschlagenen Algorithmus. Die zugrunde liegenden analytischen Formeln erlauben eine gute Schätzung der Beeinflussung des Sonnenlichtes durch die Atmosphäre und den Boden. Der Vergleich mit einem Referenzmodell zeigt die hohe Effizienz und die zugehörige Genauigkeit der vorgestellten Methode. Der letzte Teil zeigt dessen Anwendung zur Detektion von Aerosolen aus simulierten und gemessenen Fernerkundungsdaten. Der Algorithmus wird zudem verwendet, um den Einfluss des Bodenreflexionsfaktors auf die Aerosol-Detektion zu ermitteln. Die Resultate deuten auf eine sogenannten "kritische" Albedo hin, welche die Aerosol-Detektion stark erschweren kann.

Das erarbeitete schnelle Strahlungstransfermodell für die Atmosphäre schafft einen Mehrwert für Anwendungen in der Fernerkundung und Klimatologie. Die punktweise Aerosol-Bestimmung aus Fernerkundungsdaten, wie sie in der vorliegenden Dissertation gezeigt wird, ist ein Beispiel dafür. Dieser Ansatz kann in Zukunft um eine flächendeckende Charakterisierung erweitert werden. Eine Genauigkeitssteigerung des vorgestellten Modells kann unter Einbezug detaillierterer Streumechanismen und umfassenderer Beschreibungen des Bodens mit dessen Einfluss auf die Strahlung erzielt werden.

Contents

List of Figures

List of Tables

Nomenclature

α	Ångström parameter
ΔL	radiometric resolvability
Δ	absolute difference or absolute error
δ	relative difference or percent error
$\Delta\tau^{aer}$	minimal aerosol retrieval interval
$\in$	A $\in$ B: A is an element of the set B; A $\notin$ B: A is not an element of B.
λ	wavelength or spectral dependence if subscript
NE Δ	noise equivalent difference
μ	cosine of the viewing zenith angle
μ_0	cosine of the solar zenith angle
ω	single scattering albedo
ϕ	viewing azimuth
ϕ_0	solar azimuth
ρ^{sfc}	surface reflectance factor equivalent to surface albedo (a)
τ	optical depth
Θ	scattering angle
θ	viewing zenith angle
θ_0	solar zenith angle
ε	application specific error
$\veebar$	exclusive propositional logic (Statement A $\veebar$ B is true when either A or B, but not both, are true.)
a	surface albedo
a^{crit}	critical surface albedo, also CSA
E_0	solar irradiance
f^{corr}	correction factor

F_0	solar flux (irradiance E_0 on a unit area perpendicular to the beam)
g	asymmetry factor
L	radiance [watt / square meter / steradian / nanometer]
p	air pressure
$P_\lambda(\Theta)$	spectral scattering phase function
R	reflectance
R^2	squared correlation coefficient
s	spherical albedo
sh	scaling factor or scaling height
T	transmittance
6S	Second Simulation of a Satellite Signal in the Solar Spectrum, Vector version 1.1, RTM
µm	micron
aer	aerosol
AOD	aerosol optical depth (vertical column)
AOT	aerosol optical thickness (arbitrary column)
APEX	Airborne PRISM Experiment, imaging spectrometer
APS	Aerosol Polarimetry Sensor
atm	atmospheric
CSA	critical surface albedo, also a^{crit}
dfs	diffuse
drc	direct
ESA	European Space Agency
HG	Henyey-Greenstein
I	layer one (upper)
IDL	Interactive Data Language
II	layer two (lower)
IPCC	Intergovernmental Panel on Climate Change

iSMART	inverted simple model for atmospheric radiative transfer
JPL	Jet Propulsion Laboratory
LUT	Look Up Table
m	meter
MISR	Multi-angle Imaging SpectroRadiometer
mlc	molecular
MODTRAN4	MODerate resolution atmospheric TRANsmission, version 4.3r1, RTM
MS	multiple scattering
MSPI	Multiangle SpectroPolarimetric Imager
nadir	vertically below an observer
NASA	(US) National Aeronautics and Space Administration
nm	nanometer
NRMSE	normalized root mean square error
PBL	planetary boundary layer
RAA	relative azimuth angle
RMSE	root mean square error
RT	radiative transfer
RTM	radiative transfer model
SCIATRAN	SCIAMACHY's RTM and retrieval algorithm
SENSOR	at sensor level
SFC	surface
SMART	simple model for atmospheric radiative transfer
SNR	signal-to-noise ratio
SSA	single scattering approximation or single scattering albedo
SWIR	short-wavelength infrared
SZA	solar zenith angle
TOA	top-of-atmosphere
UV	ultraviolet
VIS	visible spectral region (390 nm – 750 nm)
VZA	viewing zenith angle

1. Introduction

This thesis contributes to aerosol remote sensing based on radiative transfer. Research in this field is extremely important because aerosols are relevant to our climate (Charlson et al., 1992; Kaufman et al., 2002; Rind et al., 2009) and health (Wilson and Spengler, 1996). According to the last report of the Intergovernmental Panel on Climate Change (IPCC), the level of scientific understanding regarding the radiative forcing of aerosols is still medium or low (see Fig. 1.1). Some changes in the energy budget are still difficult to understand due to key uncertainties in local radiative forcing by aerosols and related feedback mechanisms. Fig. 1.1 demonstrates clearly very large global aerosol radiative forcing uncertainties, which are much larger than the uncertainties related to greenhouse gases. It is surprising to see that aerosol radiative forcing uncertainties are on the same order or even larger than its estimated global average radiative forcing. It is not yet sure if the direct radiative effect of aerosols is cooling the Earth with 0.1 or 0.9 W/m^2 (Solomon et al., 2007). The uncertainty of the indirect effect is even larger, which includes aerosol–cloud interactions and other feedback mechanisms. Those uncertainties contribute significantly to the uncertainty of total net anthropogenic radiative forcing, which limits the validity of climate models. It is obvious that much more research is needed to advance our understanding on aerosols and their effect on climate. This includes the development of better methods to measure aerosol optical and micro-physical properties on a local to global spatial scale.

Ground based aerosol *in situ* measurement technologies provide most accurate information on aerosols nowadays. Unfortunately, *in situ* measurements cannot provide information on the spatial distribution, which is important to estimate aerosol global radiative forcing. Aerosol remote sensing is therefore crucial to climate sciences and air quality monitoring. Nevertheless, it is prone to large measurement uncertainties. It is much more difficult to determine aerosol concentrations by passive optical remote sensing techniques than e.g. gas concentrations. This is mainly because aerosols are often a mixture of different particle types. Aerosol scattering and absorption, also known as extinction, is a smooth function of wavelength and depends on various optical and micro-physical properties. Band-ratio and differential absorption methods are therefore not useful and it remains inevitable to use intensity measurements (radiances) for aerosol retrieval. However, one has to rely on accurate remote measurements and radiative transfer (RT) models for separating the upwelling radiance into components, which correspond to the surface or the atmosphere (e.g. molecules, aerosols).

Space based aerosol remote sensing retrieval technologies provide information on aerosol global distribution nowadays. Unfortunately, remote sensing retrievals from space cannot provide information of high spatial resolution to detect the local aerosol distribution with sources and sinks, which is important for air quality applications. APEX, a newly built airborne imaging spectroscopy instrument (Itten et al., 1997;

Schaepman et al., 1998), provides novel data of great unexplored potential to air quality studies on the local scale (Itten et al., 2008).

This dissertation provides contributions to fast RT modeling and aerosol remote sensing using APEX data, as well as to the understanding of aerosol retrieval sensitivities and related sensor requirements.

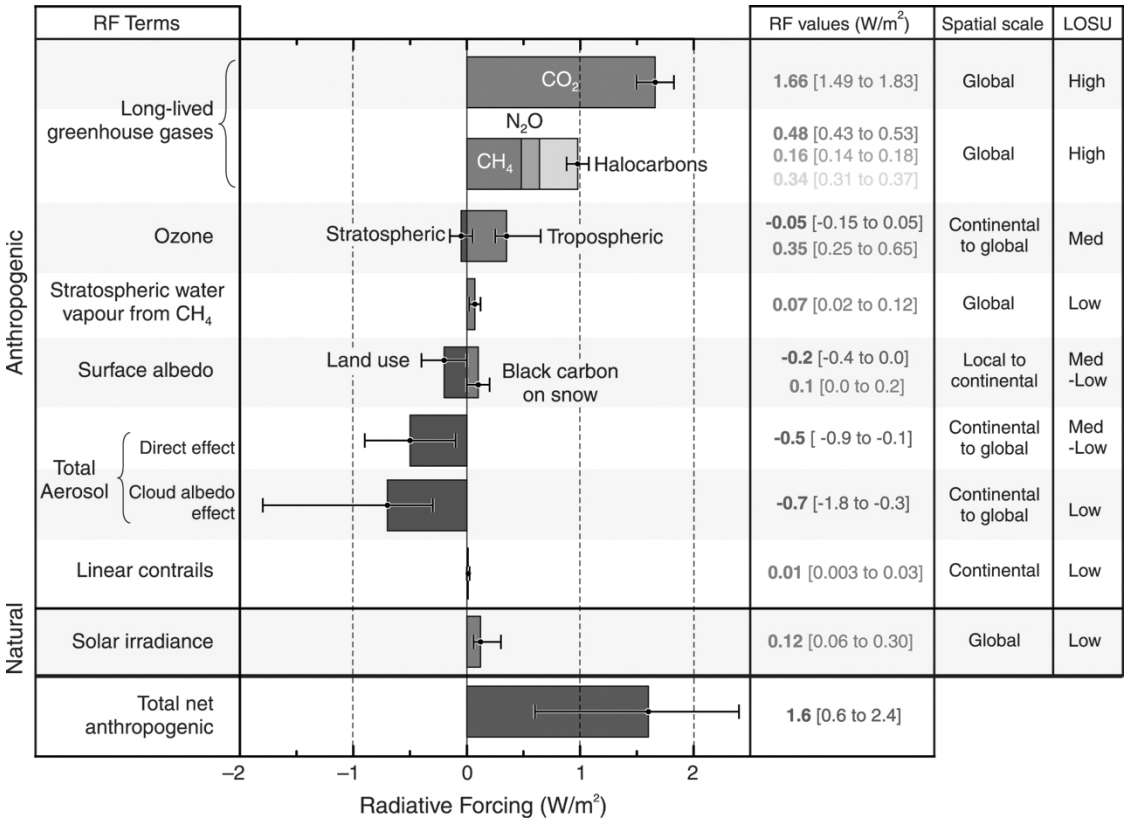

Figure 1.1.: *Global average radiative forcing (RF) in the year 2005 (best estimates and 5 to 95% uncertainty ranges) with respect to the year 1750 for CO_2, CH_4, N_2O and other important agents and mechanisms, together with the typical geographical extent (spatial scale) of the forcing and the assessed level of scientific understanding (LOSU). (IPCC WGI Figure SPM.2, Solomon et al., 2007)*

1.1. Radiative transfer in the atmosphere

RT is the physical phenomenon of energy transfer in the form of electromagnetic radiation. The RT equation describes the interaction of light in a media (atmosphere), namely the effects of extinction, absorption and emission. RT theory was developed mainly in the field astronomy to model gaseous nebulae, stellar and planetary atmospheres (Ångström, 1925, 1930; van de Hulst, 1948; Sobolev, 1956, 1972). Since the 1960s, RT was more and more used and applied in remote sensing problems. Chandrasekhar solved the polarization problem for an atmosphere with Rayleigh scattering and published his pioneering book on RT (Chandrasekhar, 1960). Various methods have been developed since then, such as "successive orders of scattering" (Hansen and Travis, 1974), "discrete ordinates" (Stamnes et al., 1988) (also known as Chandrasekhar method) and "adding-doubling" (van de Hulst, 1948; Hansen and Travis, 1974), to solve the RT problem in scalar and vector formulation (incl. polarization). Iterative Gauss–Seidel and ray-tracing Monte Carlo solvers provide even more methods to solve the RT equation.

A comparison of RT solving techniques is given by Lenoble (1985) and a detailed an historical perspective in a larger context of RT theory is provided by Shore (2002). An incomplete selection of further relevant work in the field of RT modeling contain publications by Tanré et al. (1979), Liou (1980), Zege and Chaikovskaya (1996), Lyapustin (2001), Mishchenko et al. (2002), Thomas and Stamnes (2002), Collins (2003; orig. 1989), Kokhanovsky (2004), Marshak and Davis (2005), Kotchenova et al. (2008), Kokhanovsky (2008), Kokhanovsky et al. (2010a) and others. Some chapters in the book of Kanschat et al. (2009) on numerical modeling of RT in multidimensional geometries provide interesting new methods, which may be applied to atmospheric RT in the near future.

In Earth observation, relatively simple RT models are used for the correction of unwanted atmospheric influences, because the scattering and absorption processes affect the retrieval of quantitative information on surface properties. RT models and their inversions are commonly used to correct for such effects on the propagation of light. Well-known RT models are 6S (Second Simulation of a Satellite Signal in the Solar Spectrum) (Vermote et al., 1997), SCIATRAN (Rozanov et al., 2005), SHARM (Muldashev et al., 1999; Lyapustin, 2005), RT3 (Evans and Stephens, 1991), RTMOM (Govaerts, 2006), RAY (Zege and Chaikovskaya, 1996; Katsev et al., 2009), STAR (Ruggaber et al., 1994) and Pstar2 (Nakajima and Tanaka, 1986; Ota et al., 2010), as well as DISORT (Stamnes et al., 1988), which is used in MODTRAN (Berk et al., 1989), STREAMER (Key and Schweiger, 1998) and SBDART (Ricchiazzi et al., 1998). These accurate but complex RTMs are frequently run in a forward mode, generating look-up tables (LUTs), which are later used during the inversion process for atmospheric compensation (Gao et al., 2009) or aerosol retrieval (Kokhanovsky, 2008; Kokhanovsky and de Leeuw, 2009; Kokhanovsky et al., 2010b), for instance.

1.2. Aerosol retrieval

Comprehensive introductions to the chemistry and physics of atmospheric aerosols and its observations are provided in the books of Seinfeld and Pandis (1998) and Kondratyev et al. (2006). Kokhanovsky and de Leeuw (2009) and Lee et al. (2009) treat specifically remote sensing of aerosols. Some overview and inter-comparison articles on satellite aerosol remote sensing are given by King et al. (1999), Kaufman et al. (2002), Myhre et al. (2004), Kahn et al. (2007) and Kokhanovsky et al. (2010b), as well as Kahn et al. (2010) specifically for the Multi-angle Imaging SpectroRadiometer (MISR) instrument.

Global AOD retrievals from satellite remote sensing data are well established (King et al., 1999; Kaufman et al., 2002; Lee et al., 2009; Kokhanovsky and de Leeuw, 2009), although uncertainties exist mainly due to sub-pixel clouds and approximations regarding effects at the surface (Levy et al., 2010), especially on the scale of single pixels (Kokhanovsky et al., 2007). Mishchenko et al. (2007) finds significant differences among well established satellite instruments in a long-term study over ocean. This critical review article by Mishchenko et al. (2007) provides also an overview of potential future strategies for aerosol climatologies using satellite remote sensing.

There are, however, only few studies available using airborne high spatial resolution imagers for aerosol retrievals on the local scale, except for Bassani et al. (2010). Although, precise measurements of aerosol scattering is of vital importance to the atmospheric correction of such data (Guanter et al., 2005; Gao et al., 2009).

The retrieval of AOD from remote sensing data is performed using RT model inversion. Inverse problems using radiance spectra are usually ill-posed and ill-conditioned, even in case when concurrent spectral measurements with calibrated instruments from multiple directions of the scattered solar radiation would be available. Furthermore, *a priori* knowledge of the spectral bidirectional reflectance function (BRDF) of the underlying surface and its surrounding area is needed to account for three-dimensional effects at the surface (Lyapustin, 2001). Concurrent measurements of all these variables are often not available and assumptions on surface properties and aerosol types are required to constrain the problem. A recent inter-comparison study by Kokhanovsky et al. (2010b) has shown that many existing retrieval algorithms cannot always properly retrieve AOD even using simulated data with a black surface. It is therefore clear that remote sensing of aerosol over land is still a challenging problem, even with comprehensive and computationally extensive retrieval algorithms.

1.3. Objectives and research questions

The original motivation of this thesis was to find an optimal method to retrieve aerosol properties from APEX airborne remote sensing data for environmental observations. An accurate and easy to use RT algorithm is the main prerequisite for such a method. Unfortunately, it was found that existing RT algorithms have often been developed for specific applications or specific satellite instruments and many of them require expert knowledge to use and understand. This has led to the two main objectives: first, the development of a fast and flexible RT algorithm, and then its application for AOD retrieval using APEX data. Based on these objectives, the following research questions are addressed in this thesis:

1. What are the sensor performance requirements for aerosol retrieval with remote sensing instruments? (investigated in Chap. 2)

2. Is it feasible to simulate radiative transfer in the atmosphere faster and with less complexity than in existing algorithms? What is the trade-off between computational speed and accuracy? (investigated in Chap. 3)

3. How well can aerosol optical depth be retrieved with a simplified radiative transfer model? How large is the influence of the surface albedo on such a retrieval? (investigated in Chap. 4)

A summary of the main findings with answers to the research questions is provided in Sect. 5.1.

1.4. Outline

This paper-based dissertation is organized as follows:

Chapter 1 introduces the topics of radiative transfer and aerosol retrieval with their relevance to remote sensing and climate research. It states the objectives and the deduced research questions, which will be addressed in this thesis.

Chapter 2 assesses the basic requirements for retrieval of atmospheric aerosols by means of airborne optical remote sensing. The measurement sensitivity of a sensor is one of the limiting factors in this respect. This chapter analyzes the smallest possible ratio between signal and noise of an instrument that is needed to retrieve aerosol optical depth with a predefined degree of accuracy.

Chapter 3 describes a newly developed fast and simple model for atmospheric radiative transfer, which is based on analytical equations, parameterizations and other approximations. It is compared to a benchmark radiative transfer model with respect to calculation time and accuracy.

Chapter 4 describes the above model in an inverse configuration allowing retrieval of aerosol optical depth from remote sensing data. It is applied to simulated and measured remote sensing data in order to validate the feasibility of retrieval. The presented algorithm is used to analyze the influence of the surface albedo on retrieval of aerosol optical depth. The study provides insights on the sensitivity of aerosol retrieval to surface albedo uncertainties.

Chapter 5 recapitulates the main findings in relation to the original research questions and synthesizes them with respect to ongoing issues in the same field. The outlook summarizes what can be done to extend the presented radiative transfer model and addresses missing links to spatial continuous aerosol retrieval.

Appendix A provides additional results on the influence of different aerosol types on the simulated radiance using radiative transfer calculations and it provides further results to Chap. 4, which may have an impact on the level of scientific understanding with regard to large uncertainties in aerosol radiative forcing.

2. Sensor performance requirements for the retrieval of atmospheric aerosols by airborne optical remote sensing

This chapter is published in the special issue *Remote Sensing of Natural Resources and the Environment* of the *Sensors* journal as:

Seidel, F., Schläpfer, D., Nieke, J., Itten, K.I, 2008. Sensor performance requirements for the retrieval of atmospheric aerosols by airborne optical remote sensing. Sensors 8 (3), 1901–1914.

Sensor performance requirements for the retrieval of atmospheric aerosols by airborne optical remote sensing

Felix Seidel[1], Daniel Schläpfer[1], Jens Nieke[2] and Klaus I. Itten[1]

[1] Remote Sensing Laboratories, University of Zurich, Winterthurerstr. 190, CH-8057 Zurich, Switzerland
[2] ESA / ESTEC, Noordwijk, Netherlands

Abstract

This study explores performance requirements for the retrieval of the atmospheric aerosol optical depth (AOD) by airborne optical remote sensing instruments. Independent of any retrieval techniques, the calculated AOD retrieval requirements are compared with the expected performance parameters of the upcoming hyperspectral sensor APEX at the reference wavelength of 550 nm. The AOD accuracy requirements are defined to be capable of resolving transmittance differences of 0.01 to 0.04 according to the demands of atmospheric corrections for remote sensing applications. For the purposes of this analysis, the signal at the sensor level is simulated by radiation transfer equations. The resulting radiances are translated into the AOD retrieval sensitivity ($\Delta\tau_{\lambda}^{aer}$) and compared to the available measuring sensitivity of the sensor ($NE\,\Delta L_{\lambda}^{sensor}$). This is done for multiple signal-to-noise ratios (SNR) and surface reflectance values. It is shown that an SNR of 100 is adequate for AOD retrieval at 550 nm under typical remote sensing conditions and a surface reflectance of 10% or less. Such dark surfaces require the lowest SNR values and therefore offer the best sensitivity for measuring AOD. Brighter surfaces with up to 30% reflectance require an SNR of around 300. It is shown that AOD retrieval for targets above 50% surface reflectance is more problematic with the current sensor performance as it may require an SNR larger than 1000. In general, feasibility is proven for the analyzed cases under simulated conditions.

2.1. Introduction

It is known that atmospheric aerosols influence the Earth climate system. Various efforts are being made to investigate the global distribution and concentration of these aerosols and to quantify their forcing on the radiation budget. Numerous data from passive optical Earth observation satellites are used to map aerosol properties on a global scale. Not only atmospheric scientists, but also the remote sensing community relies on aerosol information. Earth observation data in particular have to be corrected for the atmospheric influence in order to provide accurate physical measuring quantities.

During the last two decades, several aerosol retrieval techniques have been developed for satellite instruments. An overview is given by King et al. (1999) and recent inter-comparisons are provided for the retrieval over land by Kokhanovsky et al. (2007) and over sea by Myhre et al. (2004), Mishchenko et al. (2007) and Kahn et al. (2007). In general, relatively large discrepancies between different satellite instruments were found, especially on the scale of single pixels Kokhanovsky et al. (2007). Even long-term studies over the ocean reveal differences between well established satellite instruments of up to 0.1 aerosol optical depth (AOD or τ_{λ}^{aer}) and 0.45 Ångström exponent Mishchenko et al. (2007).

State-of-the-art hyperspectral airborne imagers may be able to outperform the limitations of most current satellite instruments. For example, the typical ground sampling distance (GSD) of spaceborne instruments retrieving AOD routinely is in the range of $1km$ to $30km$. The resulting uncertainty of the surface reflectance is an important contribution to the inaccuracy of the retrieved AOD over land. On the other hand, the GSD of airborne instruments is in the range of meters. One can therefore assume better performances in AOD retrieval over land because the unmixing of the surface and the atmospheric signal is expected to be less difficult. The increased likelihood of observing a uniform surface within one pixel leads to smaller uncertainties in the assumptions about the surface reflectance. This is a major source of error in most satellite-based AOD retrievals. In addition, the use of a hyperspectral sensor allows the avoidance of atmosphere gaseous absorption bands and the use of the complete spectrum from near-UV to SWIR if desired. Furthermore, the spectral and the spatial domain can be binned (adding bands or pixels together) to achieve the desired signal-to-noise ratio (SNR). The Airborne Prism EXperiment (APEX) Nieke et al. (2005) is chosen for this paper as an example for such an airborne hyperspectral instrument.

This study assesses the feasibility of aerosol retrieval with APEX in terms of the SNR and independent of any particular AOD retrieval technique, which was previously proposed by Seidel et al. (2005) and Seidel et al. (2006). A model which translates atmospheric conditions and surface reflectance into radiance values at-sensor is essential for the establishment of feasibility. It needs also to address the multiple scattering of light while being as simple as possible to avoid excessive computational time or alternatively the use of precalculated look-up tables. This study analyses the SNR requirements and limitations of aerosol retrieval with a focus on the influence of the surface reflectance.

All calculations are carried out at the commonly used aerosol reference wavelength of $550nm$ to make the results comparable to other studies. Preliminary analysis at other

wavelengths within the visible spectrum did not reveal qualitative differences to the findings at $550nm$ and are therefore not shown in this paper. The figures are plotted for $0 < \tau^{aer}_{550nm} < 1$ on the x-axis because the minimum expected visibility for an airborne remote sensing campaign will be about $5km$ ($\tau^{aer}_{550nm} \approx 1$). Flights usually will be carried out at visibilities of more than $10km$ ($\tau^{aer}_{550nm} \approx 0.6$).

2.1.1. Sensor characteristics of APEX

APEX is a dispersive push-broom imaging spectrometer, which is expected to provide unique hyperspectral data to geophysical and biochemical studies on land, water and atmospheric processes. APEX will contribute to the Earth observation community by simulating, calibrating and validating future space- and airborne optical sensors. The expected performance of APEX along with a novel spectral, radiometric and geometric calibration methodology provide an opportunity to overcome limitations of currently available remote sensing instruments. This potential is especially important in addressing the requirements for the remote sensing of aerosols.

APEX features more than 500 spectral bands from $385nm$ to $2500nm$ with a sampling interval of $0.4nm$ to $10nm$ in the full spectral mode. The standard spectral mode comprises more than 300 bands, where bands are binned together to increase the SNR. The typical gain in SNR is in the order of 40% per domain (spectral or spatial). This corresponds to a factor of $1.4^2 \approx 2$ for the binning in both domains.

The GSD is governed by 0.028° instantaneous field of view and 1000 pixels across track. It varies from $2.5m$ to $8m$ depending on the flight altitude.

Table 2.1 provides the preflight APEX-specific sensor performance for minimum, average and maximum radiance levels at $550nm$ (L^{sensor}_{550nm}). They correspond to surface reflectances (ρ^{sfc}_{550nm}) of 0%, 30% and 100%. $\rho^{sfc}_{550nm} = 0.3$ represents a relatively bright surface reflectance, which can be expected during typical remote sensing campaigns over land. The minimum and maximum surface reflectance was chosen to account for the extreme values following Schaepman et al. (2002). The sensor performance is expressed by the noise equivalent spectral radiance difference ($NE\,\Delta L^{sensor}_{550nm}$) and based on the standard spectral and spatial binning pattern. The relation between L^{sensor}_{550nm} and $NE\,\Delta L^{sensor}_{550nm}$ is given by :

$$NE\,\Delta L^{sensor}_{\lambda} = \frac{L^{sensor}_{\lambda}}{SNR_{\lambda}}, \tag{2.1}$$

where SNR_{λ} is the band-specific signal-to-noise ratio or sensor efficiency. It consists of the instrument and photon noise. The latter is mainly a function of the spectral radiance level L^{sensor}_{λ}.

The actual sensor performance values are going to be measured in mid 2008 during the first full calibration of APEX. This instrument is currently in assembly and its maiden flight is scheduled later in 2008.

Table 2.1.: *Preflight values at* $550nm$ *for the spectral radiance resolvability of APEX* $\left(NE\,\Delta L^{sensor}_{550nm}\right)$ *for the corresponding minimum* $(\rho^{sfc}_{550nm} = 0.0)$*, average* $(\rho^{sfc}_{550nm} = 0.3)$ *and maximum* $(\rho^{sfc}_{550nm} = 1.0)$ *spectral radiance level at the sensor* $\left(L^{sensor}_{550nm}\right)$*. The values are given in units of* $\left[W \cdot m^{-2} \cdot sr^{-1} \cdot nm^{-1}\right]$*.*

Minimum		Average		Maximum	
$NE\,\Delta L^{sensor}_{550nm}$	L^{sensor}_{550nm}	$NE\,\Delta L^{sensor}_{550nm}$	L^{sensor}_{550nm}	$NE\,\Delta L^{sensor}_{550nm}$	L^{sensor}_{550nm}
0.00019	0.01631	0.00030	0.09762	0.00060	0.51699

2.2. Radiance simulation

Some basic radiation transfer equations are needed to simulate the attenuation of the light traveling from the top of the atmosphere down to a surface pixel and upward to the airborne sensor. The upwelling spectral radiance into an instrument (At-Sensor-Radiance L^{sensor}_{λ}) is a function of successive orders of radiation interactions within the coupled surface-atmosphere system. In theory, it can be decoupled into a contribution from the atmosphere (Path-Radiance L^{atm}_{λ}) and from the underlying surface (L^{sfc}_{λ}). L^{atm}_{λ} can be split into the direct ($L^{atm,drc}_{\lambda}$) and the diffuse ($L^{atm,dfs}_{\lambda}$) reflected spectral radiance from the scattering atmospheric layer.

$$L^{sensor}_{\lambda} = L^{atm}_{\lambda} + L^{sfc}_{\lambda} = L^{atm,drc}_{\lambda} + L^{atm,dfs}_{\lambda} + L^{sfc}_{\lambda} \tag{2.2}$$

2.2.1. Path radiance

If we assume a homogeneous scattering layer and the single scattering approximation (SSA), the atmospheric spectral path-radiance can be derived from the well known Radiation Transfer Equation by Chandrasekhar (1960) as follows:

$$L^{atm}_{\lambda,SSA} = \underbrace{\frac{E_{0\lambda}\mu_0}{\pi}}_{I} \underbrace{\left[1 - e^{-\tau_{\lambda}\left(\frac{1}{\mu_0}+\frac{1}{\mu}\right)}\right]}_{II} \underbrace{\frac{\omega_0 P_{\lambda}\left(\Theta\right)}{4\left(\mu+\mu_0\right)}}_{III}, \tag{2.3}$$

where the incoming spectral radiance (I) is reflected by the scattering atmosphere (II) and scattered directly (single scattering) into the sensor's viewing geometry (III). $E_{0\lambda}\mu_0$ is the solar spectral irradiance, scaled by the cosine of the solar zenith angle. μ describes the sensor viewing geometry, where $\mu = cos(0°) = 1$ is valid for a nadir viewing instrument, such as APEX. The atmospheric single scattering albedo ω_0 is the ratio of the scattering to the extinction coefficient. The atmospheric phase function $P_{\lambda}\left(\Theta\right)$ takes care of the amount of light, which is diverted into the sensor viewing direction. For aerosol remote sensing, the atmospheric optical depth can be decomposed into its molecular and particle (aerosol) extinction part, such that $\tau_{\lambda} = \tau^{mlc}_{\lambda} + \tau^{aer}_{\lambda}$.

The multiple scattering of light at molecules and aerosols is an important contribution to L^{sensor}_{λ} for $\lambda < 800nm$. It leads to increasing errors for smaller λ due to the SSA in Equation 2.3. Unfortunately, multiple scattering is difficult to express in form of a simple

equation. But its influence can be taken into account by introducing a correction factor $f(\tau_\lambda)$ Rozanov and Kokhanovsky (2006):

$$f(\tau_\lambda) = \frac{L_\lambda^{atm}}{L_{\lambda,SSA}^{atm}}. \tag{2.4}$$

It represents the ratio of the exact radiance calculation by a multiple scattering radiation transfer code (i.e. Stamnes et al. (1988) or Rozanov and Kokhanovsky (2006)) to the SSA radiance calculation. $f(\tau_\lambda)$ can be interpreted in Figure 2.1a by taking the ratio between the MODTRAN4 Berk et al. (1989) curve and the SSA curve from Equation 2.3. One finds that the multiple scattering intensifies L_λ^{sensor} by a factor of 1.5 at $\tau_{550nm}^{aer} = 0.2$ and by 2.0 at $\tau_{550nm}^{aer} = 0.85$.

The atmospheric spectral radiance corrected for the multiple scattered light is therefore given by:

$$L_\lambda^{atm} = \frac{E_{0\lambda}\mu_0}{\pi}\left[1 - e^{-\tau_\lambda\left(\frac{1}{\mu_0}+\frac{1}{\mu}\right)}\right]\frac{\omega_0 P_\lambda(\Theta)}{4(\mu+\mu_0)}f(\tau_\lambda). \tag{2.5}$$

2.2.2. Surface contribution

Since L_λ^{sfc} is often the dominating contribution to L_λ^{sensor}, one must account for the underlying surface. The ratio of incoming and outgoing spectral irradiance at the surface level yields the homogeneous Lambertian surface reflectance: $E_\lambda^{\downarrow sfc}/E_\lambda^{\uparrow sfc} = \rho_\lambda^{sfc}$. Since $E_\lambda^{\uparrow sfc} \equiv \pi L_\lambda^{sfc}$ and therefore $E_\lambda^{\downarrow sfc}/\pi\rho_\lambda^{sfc} = L_\lambda^{sfc}$ we find:

$$L_\lambda^{sfc} = \frac{E_{0\lambda}\mu_0}{\pi}\frac{\rho_\lambda^{sfc}T_\lambda^{\updownarrow}}{1 - s_\lambda\rho_\lambda^{sfc}}. \tag{2.6}$$

s_λ is the spherical albedo and describes the portion of the light that is scattered back to the surface as a result of isotropic illumination of the atmosphere by the surface. It is therefore also a function of T_λ and τ_λ. $T_\lambda^{\updownarrow}$ denotes the total spectral transmittance, comprising of the down- and upward direct $T_\lambda^{drc,sca}$ and diffuse $T_\lambda^{dfs,sca}$ scattering transmittance and the absorption transmittance T_λ^{abs}:

$$T_\lambda^{\updownarrow} = \left(T_\lambda^{\downarrow drc,sca} + T_\lambda^{\downarrow dfs,sca}\right)T_\lambda^{\downarrow abs}\left(T_\lambda^{\uparrow drc,sca} + T_\lambda^{\uparrow dfs,sca}\right)T_\lambda^{\uparrow abs}. \tag{2.7}$$

Kokhanovsky et al. (2005) offers a parameterization by polynomial series with a satisfying accuracy to describe the diffuse scattering transmittance and the spherical albedo. Additionally, a non-uniform surface could be considered by adjusting ρ_λ^{sfc} in the denominator of Equation 2.6 to incorporate an environment reflectance according to Tanré et al. (1979) and Tanré et al. (1981) or Vermote et al. (1997).

2.2.3. At-sensor radiance

In the case of an airborne remote sensor, the extinction due to atmospheric molecules has to be adjusted to the reduced atmospheric path length between the surface and the

Table 2.2.: *Variables used in Equation 2.8 to plot the figures of this paper. τ_{λ}^{mlc} is tabulated in Bodhaine et al. (1999).*

Variables independent of τ_{550nm}^{aer}:	μ_0	μ	$\Theta_{\mu_0,\mu}$ [°]	$E_{0;550nm}$ $[W \cdot m^{-2} \cdot nm^{-1}]$	τ_{550nm}^{mlc}
	0.733	1.00	137	1.90	0.097

Variables depending on τ_{550nm}^{aer} :	ω_0	$P_{550nm}(\Theta)$	s_{550nm}
$\tau_{550nm}^{aer} = 0.05$	0.99	0.90	0.10
$\tau_{550nm}^{aer} = 0.5$	0.97	0.87	0.20

sensor. An approximating method would be to use the air pressure ratio (p^*) between the sensor and the surface level to scale the upward optical depth due to molecular scattering: $p^* \cdot \tau_{\lambda}^{\uparrow mlc}$, which is equal to $(T_{\lambda}^{\uparrow mlc})^{p^*}$. The extinction by aerosols above the sensor (ie. background volcanic particles in the stratosphere) is neglected here. For this study, p^* is set to 0.5, which corresponds to a height of about 5500 meters above sea level using the international standard atmosphere.

Finally, the complete spectral radiance at the sensor level is given by adding Equations 2.5 and 2.6:

$$L_{\lambda}^{sensor} = \frac{E_{0\lambda}\mu_0}{\pi}\left[\left[1 - e^{-\tau_{\lambda}\left(\frac{1}{\mu_0}+\frac{1}{\mu}\right)}\right]\frac{\omega_0 P_{\lambda}(\Theta)}{4(\mu+\mu_0)}f(\tau_{\lambda}) + \frac{\rho_{\lambda}^{sfc}T_{\lambda}^{\updownarrow}}{1 - s_{\lambda}\rho_{\lambda}^{sfc}}\right]. \tag{2.8}$$

2.2.4. Verification with MODTRAN4

Equation 2.8 was compared against results from the widely accepted radiation transfer model MODTRAN4 Berk et al. (1989) including the multiple stream algorithm DISORT Stamnes et al. (1988) to account for the multiple scattering. The 1976 U.S. Standard Model Atmosphere was used to describe the vertical profile of gas mixing ratios. The vertical variation of the aerosol optical properties were taken into account by a rural type of aerosol (0.7 small water soluble and 0.3 large dust-like particle mixing ratio) within the planetary boundary layer and a tropospheric type (small water soluble particles) in the free troposphere. Equation 2.8 was fed by the Average Continental model from d'Almeida et al. (1991), which adds a few particles of soot (0.06 mixing ratio) to the troposphere type. These differences in the aerosol models do not affect the results or conclusions because they were derived only by Equation 2.8 as a function of τ_{λ}^{aer} and ρ_{λ}^{sfc}. Further parameters, used with Equation 2.8 and with MODTRAN4 for the verification, are given in Table 2.2.

Figure 2.1 presents the simulation of L_{λ}^{sensor} as a function of τ_{λ}^{aer} . The black lines are the results from Equation 2.8 over different ρ_{λ}^{sfc} while the colored lines with circles referring to the MODTRAN4 reference calculations. Figure 2.1a shows the intermediate step with the single scattering approximation (dashed lines) over a black surface

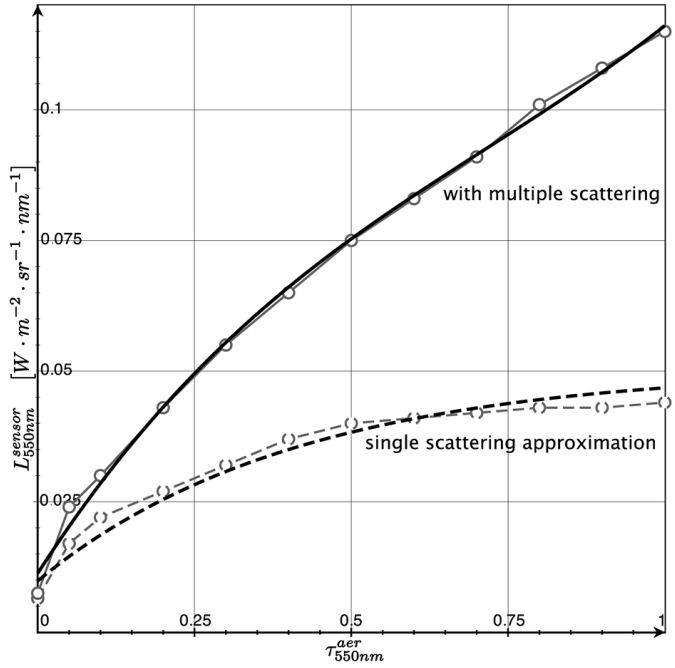

(a) $L^{atm}_{550nm,SSA}$ *and* L^{atm}_{550nm}

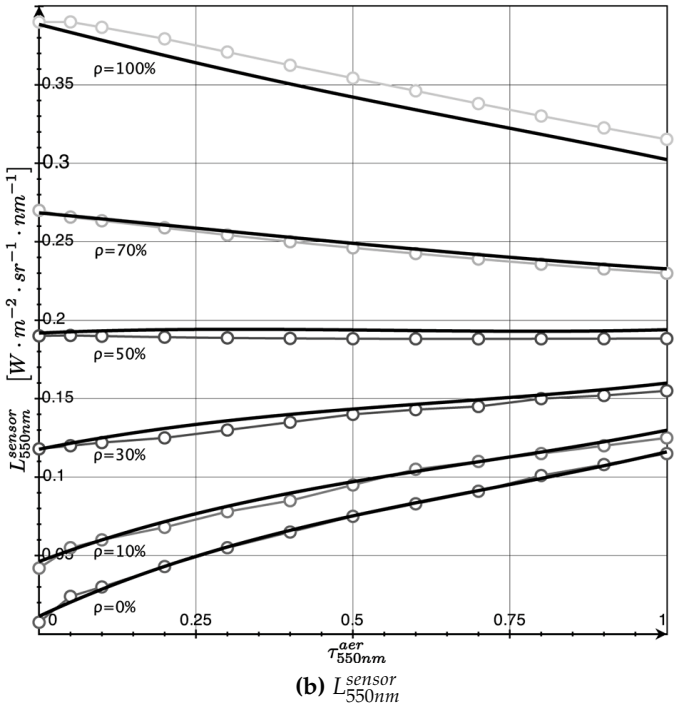

(b) L^{sensor}_{550nm}

Figure 2.1.: *Black lines show the radiance simulations, while the MODTRAN4 reference calculations are given by colored lines with circles. (a) Influence of AOD (τ^{aer}_{550nm}) on the observed path-radiance (ρ^{sfc}_{λ}=0) with the single scattering approximation ($L^{atm}_{550nm,SSA}$) from Equation 2.3 and with multiple scattering (L^{atm}_{550nm}) from Equation 2.5 (black lines). (b) Influence of τ^{aer}_{550nm} on the observed radiance (L^{sensor}_{550nm}) including the surface contribution from Equation* (2.8) *(black lines). ρ = ..% denotes the corresponding surface reflectance ρ^{sfc}_{λ}.*

($\rho^{sfc}_{550nm} = 0$), which is given by Equation 2.3. The influence of the multiple scattering is clearly visible as the offset between the dashed and the solid lines. This offset is represented in the multiple scattering correction factor $f(\tau_\lambda)$ used in Equation 2.5.

The accuracy of the spectral radiance simulation is given by qualitatively comparing the results for $L^{atm}_{550nm,SSA}$ and L^{atm}_{550nm} with the MODTRAN4 reference calculations in Figure 2.1a. The effect of the surface contribution (Equation 2.6) can be seen in Figure 2.1b, where the complete L^{sensor}_λ from Equation 2.8 is given for different surface reflectances along with the MODTRAN4 results.

At $\rho^{sfc}_\lambda \approxeq 0.5$, the model expects to cancel out the change in absorption and the change in scattering due to a changing AOD. L^{sensor}_λ is therefore no longer a function of τ^{aer}_λ, which makes it impossible to retrieve AOD at a surface reflectance of about 50%. Further investigations showed that this critical ρ^{sfc}_λ varies with the aerosol scattering properties ω_0, $P_\lambda(\Theta)$ and with μ_0, μ and s_λ (not shown).

2.3. Sensitivity requirements

2.3.1. AOD retrieval sensitivity requirement

The atmosphere has a distorting effect on L^{sensor}_λ, which has to be compensated for quantitative remote sensing applications. AOD is a crucial parameter for the atmospheric correction process to derive accurate apparent surface reflectances. We define an accuracy requirement of 1% absolute error in surface reflectance according to Richter and Schläpfer (2002). This can be also expressed in terms of transmittance in order to relate it to AOD. A rough estimation of the allowed application specific error (ε) in $T^{\updownarrow drc,sca}_{550nm} = e^{-\tau_{550nm}}$ yields 0.01 transmittance values for dark surfaces, such as water bodies ($\rho^{sfc}_{550nm} \approx 0.05$). The relative influence of L^{atm}_λ on L^{sensor}_λ is decreasing for increasing ρ^{sfc}_λ (Equation 2.8). For example, at $\rho^{sfc}_{550nm} = 0.3$ L^{atm}_{550nm} is only about 25% of L^{sensor}_{550nm} at $\tau^{aer}_{550nm} = 0.1$ (see Figure 2.1b) and therefore ε yields 0.04 transmittance values.

The required retrieval sensitivity of the total optical depth is calculated by:

$$\Delta\tau_\lambda = \frac{\varepsilon}{\left|\frac{d}{d\tau_\lambda} T^{\updownarrow drc,sca}_\lambda\right|} = \left|-\varepsilon e^{\tau_\lambda}\right|. \tag{2.9}$$

The exponential dependence of $\Delta\tau_\lambda$ on the total optical depth and therefore also on AOD is obvious and it is found that $\Delta\tau^{aer}_\lambda \leq 0.01$ is needed for the worst case of a dark surface and low AOD conditions ($\tau^{aer}_\lambda \to 0$). A $\Delta\tau^{aer}_\lambda \leq 0.045$ is satisfactory for $\rho^{sfc}_{550nm} \approx 0.3$. Equation 2.9 is also used later in Figures 2.2 and 2.3 to define AOD retrieval requirements.

2.3.2. Sensor sensitivity requirement

The results from AOD retrieval sensitivity requirements can now be used to define the performance requirements of an optical remote sensing instrument because they are related to the radiometric resolvability (ΔL_λ). This is a prerequisite for the successful

retrieval of aerosols. For obvious reason, the radiance variation induced due to change in AOD must exceed the $NE\,\Delta L_\lambda$ of a sensor Schläpfer and Schaepman (2002):

$$\Delta\tau_\lambda^{aer} \propto \Delta L_\lambda^{aer} \geq NE\,\Delta L_\lambda^{sensor}. \tag{2.10}$$

In order to find the sensor-specific sensitivity on AOD, $NE\,\Delta L_\lambda^{sensor}$ can be translated into $NE\,\Delta\tau_\lambda^{aer}$ with a radiance model, as given for example by Equation 2.8,

$$NE\,\Delta\tau_\lambda^{aer} = \frac{1}{\frac{d}{d\tau_\lambda^{aer}} L_\lambda^{sensor}} NE\,\Delta L_\lambda^{sensor}. \tag{2.11}$$

2.4. Results

2.4.1. SNR Requirements

Figure 2.2 assesses the SNR requirements depending on surface reflectance and AOD. AOD retrieval is feasible as long as $NE\,\Delta\tau_\lambda^{aer} \leq \tau_\lambda^{aer}$. The area where this limit is not fulfilled, because the noise exceeds the signal, is drawn in red in Figures 2.2 and 2.3. The dark orange color denotes the area where the desired minimal aerosol retrieval interval ($\Delta\tau_\lambda^{aer}$) from Equation 2.9 can not be achieved for the $\varepsilon = 0.04$ requirement. The stricter $\varepsilon = 0.01$ is met within the white area.

Over dark surfaces, where L_λ^{atm} dominates L_λ^{sensor}, AOD retrieval sensitivity is best for small AOD. This is because small $NE\,\Delta\tau_\lambda^{aer}$ can be achieved even for relative low SNR values (Figures 2.2a and 2.2b). An SNR of less than 100 is enough to fulfill the strict atmospheric correction accuracy requirement of $\varepsilon = 0.01$, which is needed for dark targets. Assuming a typical case with a surface of $\rho_{550nm}^{sfc} = 0.1$ and $\tau_{550nm}^{aer} = 0.15 \pm 0.1$, a $NE\,\Delta\tau_\lambda^{aer}$ of at least 0.008 for $SNR = 100$ can be expected.

Brighter surfaces ($0.1 < \rho_{550nm}^{sfc} < 0.3$) require greater SNR to keep a certain aerosol retrieval sensitivity compared to dark surfaces. This range of surface reflectances is expected to be the typical case for remote sensing over land. To fulfill $\varepsilon = 0.01$, an SNR between 100 and 300 is now required. In terms of atmospheric correction ε can be relaxed to 0.04, where an SNR between 30 and 100 is sufficient (Figures 2.2c and 2.2d). An SNR of 300 allows an aerosol retrieval sensitivity of less than 0.01 with $\tau_{550nm}^{aer} \leq 0.25$, which is expected to be the typical condition for most flight campaigns.

Very bright surfaces ($0.4 < \rho_{550nm}^{sfc} < 0.6$) are found to be most challenging because L_{550nm}^{sensor} depends weakly on τ_{550nm}^{aer}. Changes in scattering and absorption of light due to a $\Delta\tau_\lambda^{aer}$ may cancel each other out. It can be seen in Figure 2.1b, that Equation 2.8 and MODTRAN4 reveal virtually no influence of the aerosol loading on L_{550nm}^{sensor} in the case of $\rho_{550nm}^{sfc} \approx 0.5$. Due to the derivation of a local minimum in Equation 2.11, $NE\,\Delta\tau_{550nm}^{aer}$ can go to infinity as plotted in Figure 2.2e. This critical surface reflectance of about 50% as well as the position (in terms of τ_{550nm}^{aer}) of $NE\,\Delta\tau_{550nm}^{aer} \to \infty$ depends on many parameters and can vary between different models. This effect is not analyzed in detail here but shows clearly that aerosol retrieval can be difficult for a certain small range of surface reflectances.

Extremely bright targets, such as snow and clouds, provide adequate sensitivity. Figure 2.2f shows an example for $\rho^{sfc}_{550nm} = 0.8$, where an SNR of about 100 is sufficient for $\varepsilon = 0.04$, while 300 is needed for the $\varepsilon = 0.01$ requirement. The sensitivity increases only slightly with τ^{aer}_{550nm} in contrast to the calculations with low surface reflectance.

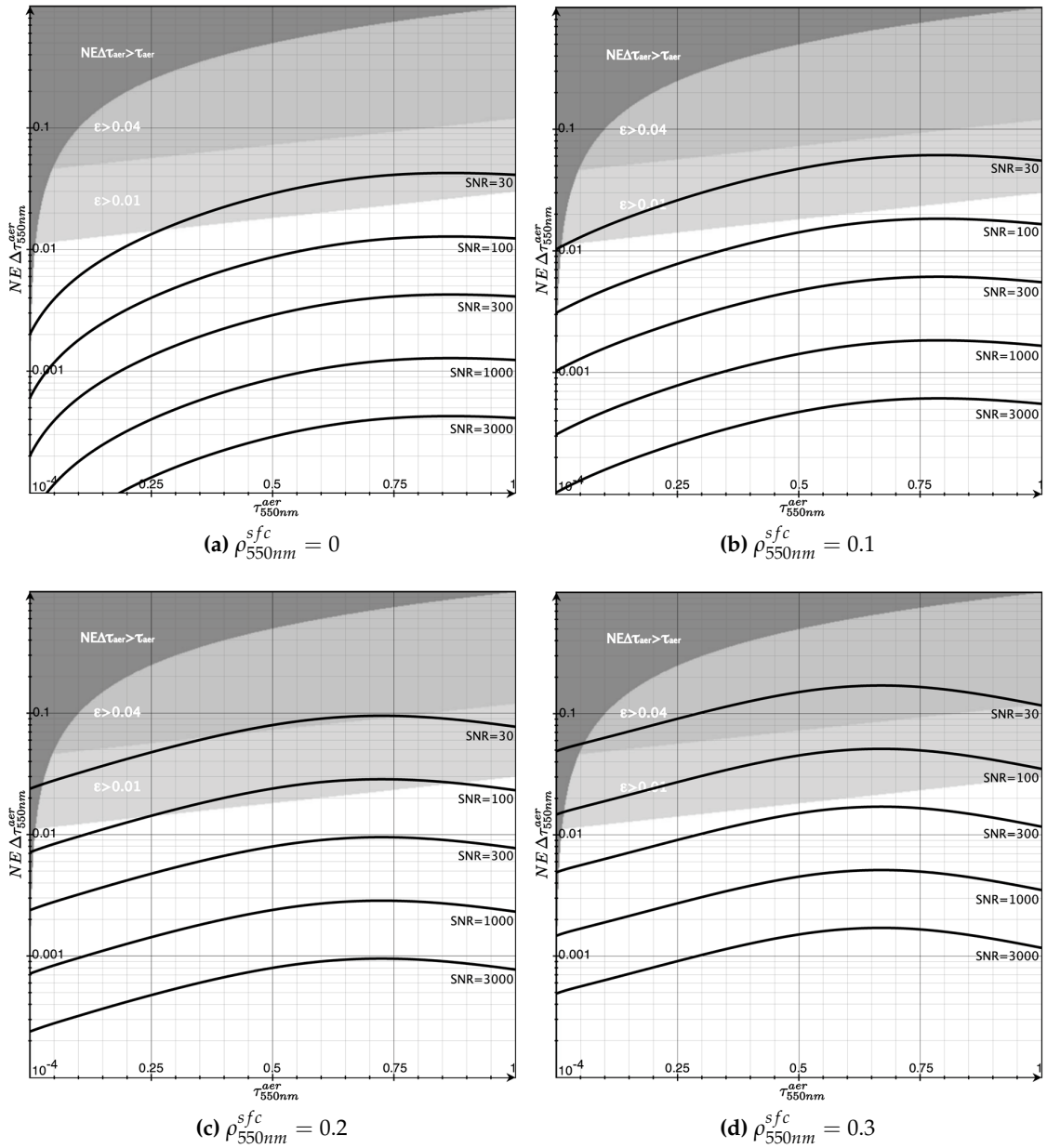

(a) $\rho^{sfc}_{550nm} = 0$ **(b)** $\rho^{sfc}_{550nm} = 0.1$

(c) $\rho^{sfc}_{550nm} = 0.2$ **(d)** $\rho^{sfc}_{550nm} = 0.3$

Figure 2.2.: *AOD (τ^{aer}_{550nm}) influence on the noise equivalent difference aerosol optical thickness ($NE\,\Delta\tau^{aer}_{550nm}$) for different SNR values. AOD retrieval is feasible outside the red area, while the light orange area comply with* $0.01 < \varepsilon < 0.04$ *and the white area* $\varepsilon < 0.01$.

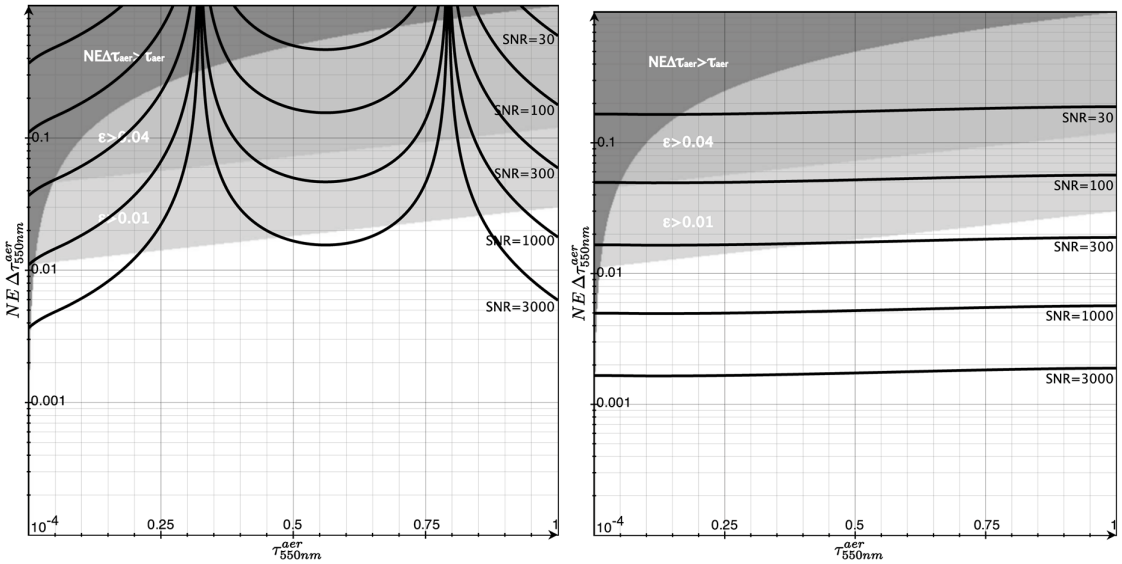

(e) $\rho^{sfc}_{550nm} = 0.5$ **(f)** $\rho^{sfc}_{550nm} = 0.8$

Figure 2.2.: *AOD (τ^{aer}_{550nm}) influence on the noise equivalent difference aerosol optical thickness ($NE\,\Delta\tau^{aer}_{550nm}$) for different SNR values. AOD retrieval is feasible outside the red area, while the light orange area comply with* $0.01 < \varepsilon < 0.04$ *and the white area* $\varepsilon < 0.01$.

2.4.2. Influence of the surface reflectance

The influence of the surface reflectance on aerosol retrieval is highlighted by Figure 2.3. 2.3a reveals clearly, that an $SNR \geq 100$ is needed to detect aerosols over typical surfaces. Such an SNR allows achieving $\varepsilon = 0.01$ with dark surfaces and $\varepsilon = 0.04$ with $\rho^{sfc}_{550nm} = 0.3$. $\rho^{sfc}_{550nm} \leq 0.1$ is mostly unproblematic for instruments with SNR larger than 50. A surface reflectance of $\rho^{sfc}_{550nm} \leq 0.4$ or $\rho^{sfc}_{550nm} \geq 0.8$ requires an instrument with an SNR of about 400 to fulfill the strict requirement (Figure 2.3b). It is possible to achieve $\varepsilon = 0.04$ with the same SNR also for $\rho^{sfc}_{550nm} \leq 0.45$ and $\rho^{sfc}_{550nm} \geq 0.6$. Greater SNR enhances the retrieval sensitivity within the white area, where $\varepsilon < 0.01$ is given.

Much higher SNR are required in order to detect aerosols over a surface reflectance of around 50%. Figures 2.3c and 2.3d show that the requirement of $\varepsilon = 0.04$ can be met within a range of $\tau^{aer}_{550nm} = \{0.01 - 0.25, 0.45 - 0.7, 0.85 - 1.0\}$ with an SNR of 1000. This AOD range becomes smaller for a larger SNR. $\varepsilon = 0.01$ can only be met partially by having an SNR of more than 3000. This can be achieved only by trading off foremost spatial and/or spectral resolution for SNR by binning hyperspectral remote sensing data in the spectral and/or in the spatial domain.

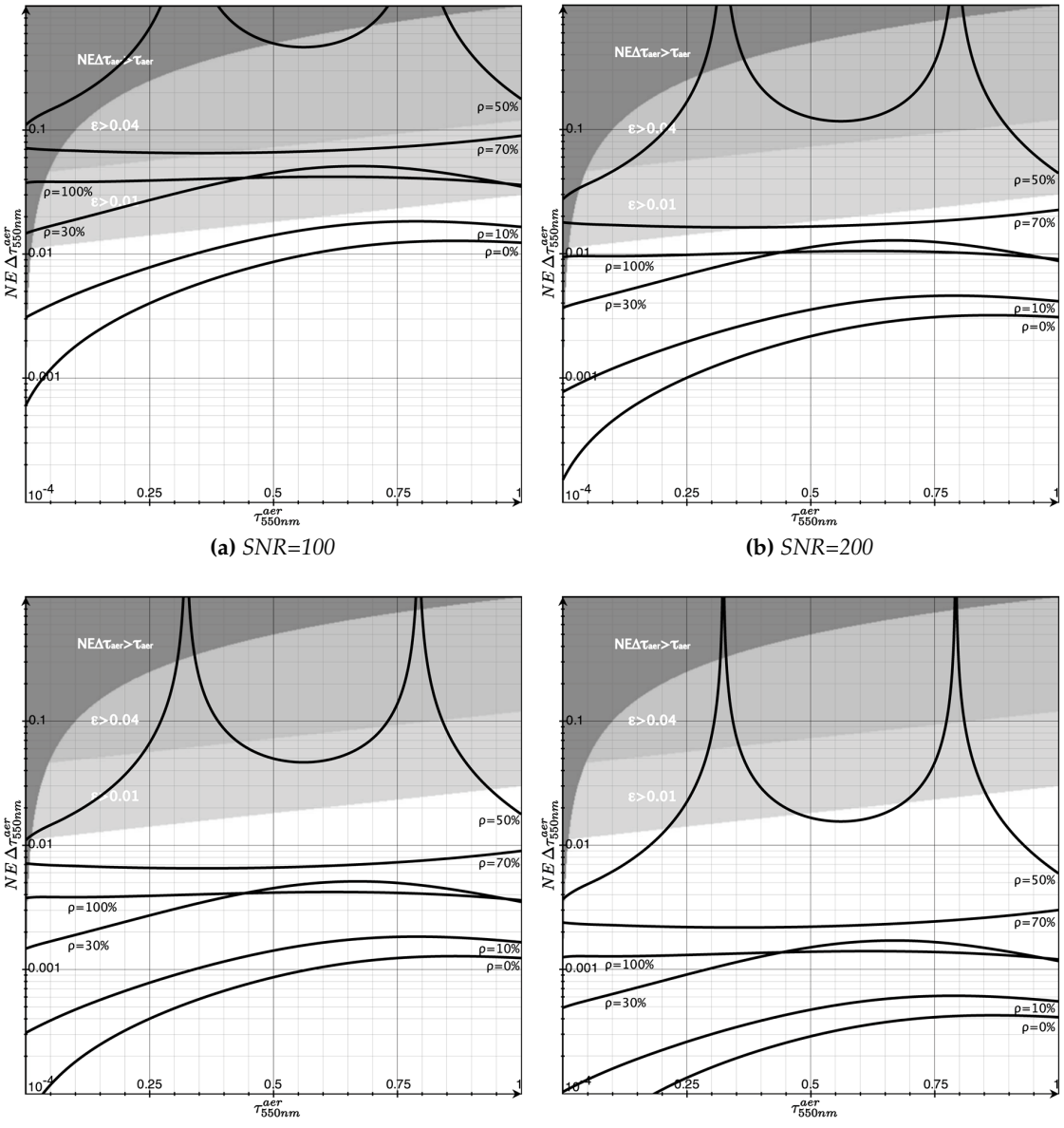

(a) *SNR=100* **(b)** *SNR=200*

(c) *SNR=1000* **(d)** *SNR=3000*

Figure 2.3.: *AOD (τ^{aer}_{550nm}) influence on the noise equivalent difference aerosol optical thickness ($NE\,\Delta\tau^{aer}_{550nm}$) for different surface reflectances ρ^{sfc}_{550nm}. AOD retrieval is feasible outside the red area, while the light orange area complies with $0.01 < \varepsilon < 0.04$ and the white area $\varepsilon < 0.01$.*

Table 2.3.: *Feasibility analysis of the aerosol retrieval with APEX by comparing SNR values at* $550nm$.

Radiance Level	Retrieval Requirement [SNR]	APEX Performance [SNR]	Feasibility
Minimum	55 $\left(\rho^{sfc}_{550nm} = 0.0\right)$	86	OK
Average	250 $\left(\rho^{sfc}_{550nm} = 0.3\right)$	325	OK
Maximum	350 $\left(\rho^{sfc}_{550nm} = 1.0\right)$	862	OK

2.4.3. Feasibility of aerosol retrieval with APEX

The crucial question is whether an aerosol retrieval is possible with an airborne hyperspectral sensor optical system, such as APEX. One must establish if the required signal sensitivity is provided by the instrument. Since APEX has not yet undergone a complete calibration process, one must use preflight SNR requirements for this analysis. These values are given in Table 2.1 with $NE\,\Delta L^{sensor}_{550nm}$ and the corresponding SNR in Table 2.3 along with the retrieval requirement.

The feasibility analysis is based upon three scenarios corresponding to the minimal, average and maximal expected spectral radiance levels according to Table 2.1. Equation 2.8 was solved for ρ^{sfc}_{550nm} =0.0, 0.3 and 1.0. to find the modeled L^{sensor}_{550nm}. The SNR requirements for aerosol retrieval were interpreted from the data, which are shown in Figure 2.2, where the SNR meets the requirement of $\varepsilon = 0.01$ (Equation 2.9).

The comparison between the retrieval requirement and the SNR of APEX reveals clearly the feasibility of aerosol retrieval for the analysed cases. (Table 2.3). However, it might be possible that the SNR does not meet the requirements for aerosol retrieval over the critical surface reflectance around $\rho^{sfc}_{550nm} = 0.5$ without additional binning.

2.5. Summary and conclusions

A spectral radiance simulation at the sensor level has been presented. It is capable of reproducing MODTRAN4 results under the SSA and within typical airborne remote sensing conditions. The multiple scattered path radiance was taken into account by the DISORT code Stamnes et al. (1988). This L^{sensor}_{λ} simulation was used to evaluate the noise equivalent difference aerosol optical thickness $NE\,\Delta\tau^{aer}_{\lambda}$ as a function of τ^{aer}_{λ} for different SNR and surface reflectances at $550nm$. The results reveal the sensor performance requirements for a sufficiently accurate AOD retrieval along with a feasibility analysis regarding APEX.

It has been shown that the detection of aerosols is feasible with APEX for low, average and high spectral radiance levels under the evaluated conditions (ie. viewing and sensor configuration). This finding concerns the sensitivity requirements for an optical remote sensing instrument, such as APEX. The resulting feasibility is based on preflight sensor performance values; the final APEX SNR will be available after full scale calibra-

tion during the 2008 flight season. Further investigations will be performed to assess the sensitivity and the limitations of the radiation transfer calculation and the aerosol retrieval algorithm itself.

We found that the spectral SNR is crucial for aerosol remote sensing and varies strongly with surface reflectance. The latter strongly influences the intensity of L_{λ}^{sensor}, which drives the SNR. It has been shown that dark surfaces ($\rho_{550nm}^{sfc} < 0.1$) have the lowest SNR demands for aerosol retrieval. This is crucial for establishing feasibility because the sensor provides a lower SNR over dark surfaces due to the lower spectral radiance. The analysis showed that APEX is expected to provide sufficiently high SNR values even for black surfaces under the given conditions. More critical are relatively bright surfaces ($0.4 < \rho_{550nm}^{sfc} < 0.6$) because L_{550nm}^{sensor} depends only weakly on τ_{550nm}^{aer}. Extremely bright surfaces require again a lower SNR, but the unmixing of $L_{\lambda}^{atm} + L_{\lambda}^{sfc}$ is expected to be more difficult because of errors in the estimation of ρ_{λ}^{sfc} become dominant. Due to the small GSD of airborne instruments, it is expected that the identification of pure surface materials could be done with an adequate precision compared to satellite platforms. This allows to reduce the uncertainties in allocating a best-guess ρ_{λ}^{sfc} to the observed pixels and therefore alleviate the challenge of the unmixing of L_{λ}^{atm} from L_{λ}^{sensor}.

The finding of indefinitely high SNR requirements might be an artifact of the approximate simulation of L_{550nm}^{sensor} (Equation 2.8) for $\rho_{550nm}^{sfc} = 0.5 \pm 0.05$. It depends strongly upon the aerosol model assumption, in particular the approximation of the phase function and the multiple scattering. Further investigations are needed.

Generally, it was shown that an SNR of 300 or better will provide satisfying aerosol retrieval results for most surface reflectances considered in this analysis. Restricting the ranges to $\tau_{550nm}^{aer} < 0.25$ and $\rho_{550nm}^{sfc} < 0.2$, which are optimal and representative remote sensing conditions, an SNR of 100 is adequate. This is a promising finding in scope of the development of aerosol retrieval methods because most current instruments fulfill such SNR requirements under typical conditions.

Acknowledgments

We would like to acknowledge Dr. Alexander Kokhanovsky for sharing his expertise in the field of radiative transfer and multiple light scattering. We would also like to thank Jason Brazile and all involved individuals for their assistance. As well, we acknowledge the fruitful comments and suggestions of four anonymous reviewers.

3. Fast and simple model for atmospheric radiative transfer

This chapter is published in the *Atmospheric Measurement Techniques* as:

Seidel, F.C., Kokhanovsky, A.A., Schaepman, M.E., 2010. Fast and simple model for atmospheric radiative transfer. Atmos. Meas. Tech. 3 (4), 1129–1141.

Fast and simple model for atmospheric radiative transfer

Felix C. Seidel[1], Alexander A. Kokhanovsky[2] and Michael E. Schaepman[1]

[1] Remote Sensing Laboratories, University of Zurich, Winterthurerstr. 190, CH-8057 Zurich, Switzerland

[2] Institute of Environmental Physics, University of Bremen, O. Hahn Allee 1, D-28334 Bremen, Germany

Abstract

Radiative transfer models (RTMs) are of utmost importance for quantitative remote sensing, especially for compensating atmospheric perturbation. A persistent trade-off exists between approaches that prefer accuracy at the cost of computational complexity, versus those favouring simplicity at the cost of reduced accuracy. We propose an approach in the latter category, using analytical equations, parameterizations and a correction factor to efficiently estimate the effect of molecular multiple scattering. We discuss the approximations together with an analysis of the resulting performance and accuracy. The proposed Simple Model for Atmospheric Radiative Transfer (SMART) decreases the calculation time by a factor of more than 25 in comparison to the benchmark RTM 6S on the same infrastructure. The relative difference between SMART and 6S is about 5% for spaceborne and about 10% for airborne computations of the atmospheric reflectance function. The combination of a large solar zenith angle (SZA) with high aerosol optical depth (AOD) at low wavelengths lead to relative differences of up to 15%. SMART can be used to simulate the hemispherical conical reflectance factor (HCRF) for spaceborne and airborne sensors, as well as for the retrieval of columnar AOD.

3.1. Introduction

The terrestrial atmosphere attenuates the propagation of the solar radiation down to the Earth's surface and back up to a sensor. The scattering and absorption processes involved disturb the retrieval of quantitative information on surface properties. Radiative transfer models (RTMs) and their inversions are commonly used to correct for such effects on the propagation of light. Well-known RTMs are 6S (Second Simulation of a Satellite Signal in the Solar Spectrum) (Vermote et al., 1997), SCIATRAN (Rozanov et al., 2005), SHARM (Muldashev et al., 1999; Lyapustin, 2005), RT3 (Evans and Stephens, 1991), RTMOM (Govaerts, 2006), RAY (Zege and Chaikovskaya, 1996), STAR (Ruggaber et al., 1994) and Pstar2 (Nakajima and Tanaka, 1986; Ota et al., 2010), as well as DISORT (Stamnes et al., 1988), which is used in MODTRAN (Berk et al., 1989), STREAMER (Key and Schweiger, 1998) and SBDART (Ricchiazzi et al., 1998). These accurate but complex RTMs are frequently run in a forward mode, generating look-up tables (LUTs), which are later used during the inversion process for atmospheric compensation (Gao et al., 2009) or aerosol retrieval (Kokhanovsky and de Leeuw, 2009; Kokhanovsky et al., 2010b), for instance. There are also a series of highly accurate, but computationally intensive Monte Carlo photon transport codes available. However, the best accuracy may not be always desirable for a RTM. Approximative equations have been developed before computers were widely available (Hammad and Chapman, 1939; Sobolev, 1972). With regard to the growing size and frequency of remote sensing datasets, approximative and computationally fast RTMs are becoming relevant again (Kokhanovsky, 2006; Katsev et al., 2010; Carrer et al., 2010). In particular, RTMs of the vegetation canopy and further algorithms that exploit data from imaging spectroscopy instruments (Itten et al., 2008) often rely on fast atmospheric RTM calculations.

In this context, we propose the fast Simple Model for Atmospheric Radiative Transfer (SMART). It is based on approximative analytical equations and parameterizations, which represent an favourable balance between speed and accuracy. We consider minimised complexity and computational speed as important assets for downstream applications and define an acceptable uncertainty range of up to 5–10% for the modelled reflectance factor at the sensor level, under typical mid-latitude remote sensing conditions. SMART can therefore be used as a physical model, maintaining a cause-and-effect relationship in atmospheric radiative transfer. Instead of depending on the classic LUT approach, it permits parameter retrieval in near-real-time. This enables the rapid assessment of regional data requiring exhaustive correction, such as imaging spectrometer data. Furthermore, it supports the straightforward inversion of aerosol optical depth (AOD; $\tau_\lambda^{\mathrm{aer}}$) by implementing radiative transfer equations as a function of $\tau_\lambda^{\mathrm{aer}}$. The theoretical feasibility for the retrieval of aerosols in terms of the sensor performance was shown in Seidel et al. (2008) for the APEX instrument (Itten et al., 2008).

In this paper, we describe the two-layer atmospheric model with the implementation of approximative radiative transfer equations in both layers and at the Earth's surface. We then assess the accuracy and performance of SMART in comparison with 6S.

3.2. SMART - a simple model for atmospheric radiative transfer

A remote sensing instrument measures the spectral radiance as a function of the spectral atmospheric properties and the illumination/observation geometry $L_\lambda\left(\tau_\lambda, P_\lambda\left(\Theta\right), \omega_\lambda; \mu_0, \mu, \phi - \phi_0\right)$, where τ_λ is the optical depth, $P_\lambda\left(\Theta\right)$ is the phase function at the scattering angle Θ, ω_λ is the single scattering albedo, $\mu_0 = \cos\theta_0$, $\mu = \cos\theta$, θ_0 and θ represent the solar and viewing zenith angles (SZA, VZA), $\phi - \phi_0$ is the relative azimuth between viewing ϕ and solar direction ϕ_0. However, from a modelling perspective, it is more convenient to use a dimensionless reflectance function. The relationship between radiance and reflectance is given by:

$$R_\lambda = \frac{\pi L_\lambda}{\mu_0 F_{0,\lambda}}, \tag{3.1}$$

where $F_{0,\lambda}$ is the spectral solar flux or irradiance on a unit area perpendicular to the beam. For readability, we omit the arguments. The subscripted wavelength denotes spectral dependence.

SMART assumes a plane-parallel, two-layer atmosphere. We will use the superscript I to denote the upper layer, superscript II for the lower layer. While the lower layer contains aerosol particles and molecules, the upper layer contains only molecules. The surface elevation, the transition altitude of the two layers, as well as the top-of-atmosphere (TOA) altitude can be chosen freely. The planetary boundary layer (PBL) height is a good estimate for the vertical extent of the lower layer. The sensor altitude can be set to any altitude within the atmosphere or to the TOA. Altitudes are related to air pressure p according to the hydrostatic equation. This 1-D coordinate system is used in Eqs. (3.3) and (3.26) to determine τ_λ and to scale the atmospheric reflectance and transmittance function corresponding to a specific altitude within atmosphere.

SMART accepts any combination of τ_λ, θ_0, θ and λ. The current implementation executes on the 2-D array $[\lambda, \tau^{\text{aer}}_{550\,\text{nm}}]$, where $\lambda \in [400\,\text{nm}, 800\,\text{nm}]$ and $\tau^{\text{aer}}_{550\,\text{nm}} \in [0.0, 0.5]$. The spectral dependence of the AOD is approximated by:

$$\tau^{\text{aer}}_\lambda = \tau^{\text{aer}}_{550\,\text{nm}} \left(\frac{\lambda}{550\,\text{nm}}\right)^{-\alpha}, \tag{3.2}$$

according to Ångström's law (Ångström, 1929). Aerosol optical properties, such as the g^{aer}_λ, $\omega^{\text{aer}}_\lambda$ and the Ångström parameter α are taken from d'Almeida et al. (1991) for the following aerosol models: clean-continental, average-continental, urban, clean-maritime, maritime-polluted and maritime-mineral.

3.2.1. Radiative transfer in layer I

By definition, the layer I contains no aerosols and the total optical depth is therefore given by the molecular optical depth $\tau_\lambda^{\mathrm{I}} = \tau_\lambda^{\mathrm{mlc}} \left(1 - h^{\mathrm{PBL}}\right)$, where

$$h^{\mathrm{PBL}} = \frac{p^{\mathrm{SFC}} - p^{\mathrm{PBL}}}{p^{\mathrm{SFC}} - p^{\mathrm{TOA}}} \tag{3.3}$$

is the relative height of the PBL within the atmosphere. It ranges from 0 at the surface (SFC) to 1 at TOA. Values for $\tau_\lambda^{\mathrm{mlc}}$ are computed using semi-empirical equations fromBodhaine et al. (1999).

The downward total transmittance $T_\lambda^{\mathrm{I}\downarrow}$ is the sum of the downward direct transmittance $T_\lambda^{\mathrm{I}\downarrow\mathrm{dir}}$ and the downward diffuse transmittance $T_\lambda^{\mathrm{I}\downarrow\mathrm{dfs}}$:

$$T_\lambda^{\mathrm{I}\downarrow} = T_\lambda^{\mathrm{I}\downarrow\mathrm{dir}} + T_\lambda^{\mathrm{I}\downarrow\mathrm{dfs}} = e^{-\frac{\tau_\lambda^{\mathrm{I}}}{\mu_0}} + \tau_\lambda^{\mathrm{I}} e^{\left(-u_0 - v_0 \tau_\lambda^{\mathrm{I}} - w_0 \left(\tau_\lambda^{\mathrm{I}}\right)^2\right)}. \tag{3.4}$$

$T_\lambda^{\mathrm{I}\downarrow\mathrm{dfs}}$ is approximated by using a fast and accurate parameterization suggested by Kokhanovsky et al. (2005) for $\omega_\lambda = 1$, where

$$u_0 = \sum_{m=0}^{3} h_m \mu_0^m, \tag{3.5}$$

$$v_0 = p_0 + p_1 e^{-p_2 \mu_0}, \tag{3.6}$$

$$w_0 = q_0 + q_1 e^{-q_2 \mu_0}. \tag{3.7}$$

The constants p_0, q_0, p_1, q_1, p_2, q_2 and h_m are parameterized using polynomial expansions with respect to g_λ, e.g.

$$p_0 = \sum_{s=0}^{3} p_{0,s} g_\lambda \tag{3.8}$$

$p_{0,s}$ and all other expansion coefficients are given in Kokhanovsky et al. (2005). The upward transmittance $T_\lambda^{\mathrm{I}\uparrow}$ is defined according to Eqs. (3.4) to (3.8) by substituting μ_0, u_0, v_0, w_0 for μ, u, v, w, respectively.

The transmitted light is scattered in all directions. The ratio of scattering to total light extinction ω_λ and the angular distribution of the scattered light $P_\lambda(\Theta)$ are used to describe the scattering process. To simplify the approach, the total intrinsic atmospheric scattering function can be decomposed into the single scattering approximation (SSA) and multiple scattering (MS). The first order atmospheric reflectance function $R_\lambda^{\mathrm{I,SSA}}$ can be expressed using the analytical equation as given invan de Hulst (1948); Sobolev (1972); Hansen and Travis (1974); Kokhanovsky (2006):

$$R_\lambda^{\mathrm{I,SSA}} = \frac{\omega_\lambda^{\mathrm{mlc}} P_\lambda^{\mathrm{mlc}}(\Theta)}{4(\mu_0 + \mu)} \left(1 - e^{-m\tau_\lambda^{\mathrm{I}}}\right), \tag{3.9}$$

where the molecular single scattering albedo $\omega_\lambda^{\mathrm{mlc}} := 1$ and the molecular (Rayleigh)

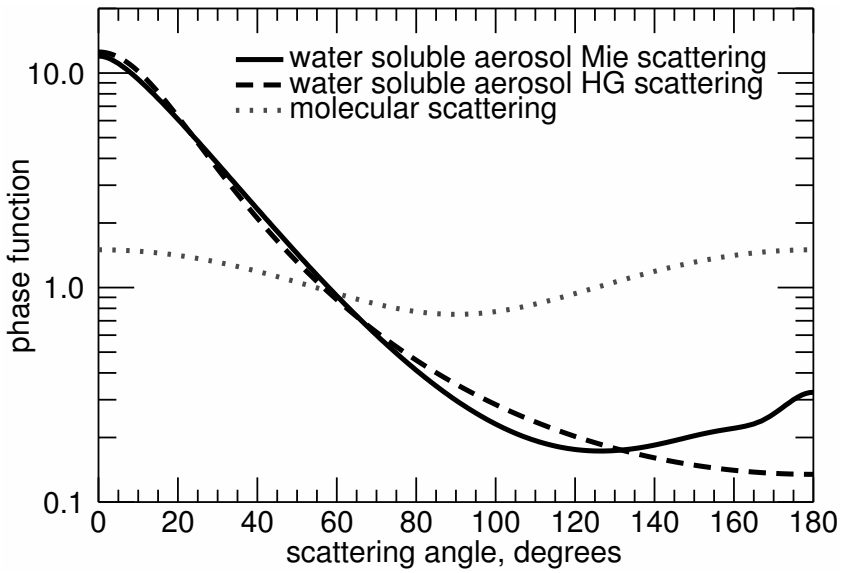

Figure 3.1.: *Phase functions at 550 nm for molecules and dry water soluble aerosols derived from the Henyey-Greenstein (HG) approximation with* $g^{\text{aer}}_{550\,\text{nm}} = 0.63$ *and the exact Lorenz-Mie theory.*

scattering phase function for reflected, unpolarised solar radiation is given by:

$$P^{\text{mlc}}_{\lambda}(\Theta) = \frac{3}{4}\left(1 + \cos^2\Theta\right), \tag{3.10}$$

with the scattering angle

$$\Theta = \arccos\left[-\mu_0\mu + \cos\left(\phi - \phi_0\right)\sqrt{\left(1-\mu_0^2\right)\left(1-\mu^2\right)}\right] \tag{3.11}$$

and the geometrical air mass factor $m = \left(\mu_0^{-1} + \mu^{-1}\right)$. $P^{\text{mlc}}_{\lambda}(\Theta)$ is plotted in Fig. 3.1.

Standard RTMs spend most of their computational time calculating multiple scattering with iterative integration procedures. In the case of layer I, we therefore suggest a generic correction factor f^{corr} to approximate Rayleigh multiple scattering. We derive one f^{corr} per SZA as a function of λ and τ from accurate MODTRAN/DISORT calculations, however without polarisation. The correction factor is defined as the ratio between the total reflectance and the SSA at sensor level:

$$f^{\text{corr}}_{\mu_0}(\lambda,\tau) = \frac{R^{\text{sensor,MODTRAN}}_{\lambda}}{R^{\text{sensor,SSA,MODTRAN}}_{\lambda}}. \tag{3.12}$$

The total reflectance function of layer I is then given by Eqs. (3.9) and (3.12):

$$R^{\text{I}}_{\lambda} = R^{\text{I,mlc}}_{\lambda} = \frac{\omega^{\text{mlc}}_{\lambda} P^{\text{mlc}}_{\lambda}(\Theta)}{4\left(\mu_0+\mu\right)}\left(1 - e^{-m\tau^{\text{I}}_{\lambda}}\right) f^{\text{corr}}_{\mu_0}. \tag{3.13}$$

3.2.2. Radiative transfer in layer II

The down- and upward total transmittances $T_\lambda^{\mathrm{II}\downarrow}$, $T_\lambda^{\mathrm{II}\uparrow}$ in layer II are calculated according to Eq. (3.4) by using g_λ^{aer} and substituting $\tau_\lambda^{\mathrm{I}}$ to the total spectral optical depth of layer II $\tau_\lambda^{\mathrm{II}} = \tau_\lambda^{\mathrm{aer}} + \tau_\lambda^{\mathrm{mlc}} h^{\mathrm{PBL}}$.

The atmospheric reflectance function of layer II is simplified by the decomposition into molecular and aerosol parts. As a consequence, the aerosol-molecule scattering interactions are neglected. The related error is examined in Sect. 3.3.3. The molecular reflectance function $R_\lambda^{\mathrm{II,mlc}}$ is derived directly from Eq. (3.13), where $\tau_\lambda^{\mathrm{I}}$ is changed to $\tau_\lambda^{\mathrm{mlc}} h^{\mathrm{PBL}}$. Thus, the total reflectance function of layer II is given by:

$$R_\lambda^{\mathrm{II}} = R_\lambda^{\mathrm{II,mlc}} + \underbrace{\overbrace{\frac{\omega_\lambda^{\mathrm{aer}} P_\lambda^{\mathrm{aer}}\left(\Theta_{\mathrm{r}}\right)}{4\left(\mu_0+\mu\right)}\left(1-e^{-m\tau_\lambda^{\mathrm{aer}}}\right)}^{\text{first order scattering (SSA)}} + \overbrace{R_\lambda^{\mathrm{aer,MS}}}^{\text{second order}}}_{R_\lambda^{\mathrm{aer}}} . \tag{3.14}$$

The aerosol scattering phase function $P_\lambda^{\mathrm{aer}}(\Theta)$ is defined by the approximate Henyey-Greenstein (HG) phase function (Henyey and Greenstein, 1941), which depends on the aerosol asymmetry factor g_λ^{aer} and the scattering angle Θ:

$$P_\lambda^{\mathrm{aer}}(\Theta) = \frac{1-\left(g_\lambda^{\mathrm{aer}}\right)^2}{\left[1+\left(g_\lambda^{\mathrm{aer}}\right)^2 - 2g_\lambda^{\mathrm{aer}}\cos\Theta\right]^{2/3}} . \tag{3.15}$$

This HG phase function is plotted in Fig. 3.1 with $g_{550\,\mathrm{nm}}^{\mathrm{aer}} = 0.63$ for a dry water soluble aerosol according to d'Almeida et al. (1991). The exact phase function derived from the Lorenz-Mie theory is superimposed to illustrate the imperfection of the HG approximation in the forward scattering domain for $\Theta > 150°$. This influence on the accuracy of SMART is discussed in the second half of Sect. 3.3.2.

The second order (or secondary) scattering is calculated according to the Successive Orders of Scattering (SOS) method described by Hansen and Travis (1974):

$$R^{\mathrm{aer,MS}}\left(\mu,\mu_0,\phi-\phi_0\right) = \frac{\tau^{\mathrm{aer}}\omega^{aer}}{4\pi} \tag{3.16}$$

$$\cdot \int_0^{2\pi}\int_0^1 \left[\frac{1}{\mu} P_{\mathrm{t}}^{\mathrm{aer}}\left(\mu,\mu',\phi-\phi'\right) R^{\mathrm{SSA}}\left(\mu',\mu_0,\phi'-\phi_0\right)\right. \tag{3.17}$$

$$+\frac{1}{\mu_0} R^{\mathrm{SSA}}\left(\mu,\mu',\phi-\phi'\right) P_{\mathrm{t}}^{\mathrm{aer}}\left(\mu',\mu_0,\phi'-\phi_0\right)$$

$$-\frac{e^{-\frac{\tau^{\mathrm{aer}}}{\mu_0}}}{\mu_0} T^{\mathrm{SSA}}\left(\mu,\mu',\phi-\phi'\right) P_{\mathrm{r}}^{\mathrm{aer}}\left(\mu',\mu_0,\phi'-\phi_0\right)$$

$$\left.-\frac{e^{-\frac{\tau^{\mathrm{aer}}}{\mu}}}{\mu} P_{\mathrm{r}}^{\mathrm{aer}}\left(\mu,\mu',\phi-\phi'\right) T^{\mathrm{SSA}}\left(\mu',\mu_0,\phi'-\phi_0\right)\right] d\mu' d\phi'.$$

λ and other non-angular arguments are omitted for the sake of readability. $P_{\mathrm{r}}^{\mathrm{aer}}$ and $P_{\mathrm{t}}^{\mathrm{aer}}$ denote the aerosol HG phase function (Eq. 3.15) using the reflectance scattering angle Θ_r in case of reflectance (Eq. 3.11) and the scattering angle

$$\Theta_{\mathrm{t}} = \arccos\left[\mu_0\mu + \cos\left(\phi - \phi_0\right)\sqrt{\left(1-\mu_0^2\right)\left(1-\mu^2\right)}\right] \tag{3.18}$$

in case of transmittance. The single scattering transmittance T^{SSA} is given in van de Hulst (1948); Sobolev (1972); Hansen and Travis (1974); Kokhanovsky (2006):

$$T_\lambda^{\mathrm{SSA}} = \frac{\omega_\lambda^{\mathrm{aer}} P_\lambda^{\mathrm{aer}}\left(\Theta_{\mathrm{t}}\right)}{4\left(\mu_0 - \mu\right)}\left(e^{-\frac{\tau_\lambda^{\mathrm{aer}}}{\mu_0}} - e^{-\frac{\tau_\lambda^{\mathrm{aer}}}{\mu}}\right). \tag{3.19}$$

In case of $\mu_0{=}\mu$, we modify Eq. (3.19) to avoid indeterminacy with l'Hôpital's (Bernoulli's) rule:

$$T_\lambda^{\mathrm{SSA}} = \frac{\omega_\lambda^{\mathrm{aer}} P_\lambda^{\mathrm{aer}}\left(\Theta_{\mathrm{t}}\right)}{4\mu^2}\tau_\lambda^{\mathrm{aer}} e^{\left(-\frac{\tau_\lambda^{\mathrm{aer}}}{\mu}\right)}. \tag{3.20}$$

We use a numerical approximation to calculate the integrals of Eq. (3.17). This is by far the most computationally intensive step in SMART. Therefore, we currently neglect scattering orders higher than two. A third order term could be added to Eq. (3.17) as given by Hansen and Travis (1974). However, for our accuracy requirements and under favourable remote sensing conditions, second order scattering is sufficient. More details are given in the first half of Sect. 3.3.2.

If fast computation is more important than accuracy, $R_\lambda^{\mathrm{aer,MS}}$ can be substituted by $\cdot f_{\mu_0}^{\mathrm{corr}}\left(\lambda, \tau_{550\,\mathrm{nm}}^{\mathrm{aer}}\right)$ in analogy to Eq. (3.12). The expense is roughly 20% in decreased accuracy.

3.2.3. Radiative transfer at the surface

The modelling of optical processes at the surface can be elaborate due to adjacency and directional effects. Here we assume the simple case with isotropically reflected light on a homogeneous surface according to Lambert's law (Ångström, 1925; Chandrasekhar, 1960; Sobolev, 1972):

$$R_\lambda^{\mathrm{SFC}} = \frac{a_\lambda}{1 - s_\lambda a_\lambda}, \tag{3.21}$$

where a_λ is the surface albedo and s_λ is the spherical albedo to account for multiple interaction between surface and atmosphere. We use the parameterization suggested by Kokhanovsky et al. (2005) for s_λ, where:

$$s_\lambda = \tau_\lambda^{\mathrm{II}}\left(ae^{-\frac{\tau_\lambda^{\mathrm{II}}}{\alpha}} + be^{-\frac{\tau_\lambda^{\mathrm{II}}}{\beta}} + c\right). \tag{3.22}$$

The constants a, α, b, β and c are parameterized according to Eq. (3.8). The corresponding expansion coefficients are given in Kokhanovsky et al. (2005). The resulting R_λ^{SFC} is also known as the hemispherical conical reflectance factor (HCRF) according to Schaepman-Strub et al. (2006).

Table 3.1.: *Definition of the conditions and the related accuracy requirements for SMART. The limited conditions refer to typical airborne remote sensing needs in the mid-latitudes, which SMART was developed for. The analysed conditions refer to the accuracy assessment.*

remote sensing conditions	limited	analysed
$\tau^{\text{aer}}_{550\text{ nm}}$	0–0.5	0–0.5
solar zenith angle, degrees	20–60	nadir–70
viewing zenith angle	nadir	nadir
wavelength, nm	500–700	400–800
surface albedo	0	0
accuracy requirement, %	5	15

3.2.4. At-sensor reflectance function

Finally, we put the above equations together along the optical path to resolve the reflectance function R^{S}_λ. Multiple retro-reflections between layers I and II are neglected. A sensor at TOA or within levels I or II is simulated as follows:

$$R^{\text{S,TOA}}_\lambda = R^{\text{I}}_\lambda + T^{\text{I}\downarrow}_\lambda \left[R^{\text{II}}_\lambda + R^{\text{SFC}}_\lambda T^{\text{II}\updownarrow}_\lambda \right] T^{\text{I}\uparrow}_\lambda \,, \tag{3.23}$$

$$R^{\text{S,I}}_\lambda = R^{\text{I}}_\lambda sh^{\text{I}} + T^{\text{I}\downarrow}_\lambda \left[R^{\text{II}}_\lambda + R^{\text{SFC}}_\lambda T^{\text{II}\updownarrow}_\lambda \right] \left(1 - sh^{\text{I}} + sh^{\text{I}} T^{\text{I}\uparrow}_\lambda \right) \,, \tag{3.24}$$

$$R^{\text{S,II}}_\lambda = T^{\text{I}\downarrow}_\lambda \left[R^{\text{II}}_\lambda sh^{\text{II}} + T^{\text{II}\downarrow}_\lambda R^{\text{SFC}}_\lambda \left(1 - sh^{\text{II}} + sh^{\text{II}} T^{\text{II}\uparrow}_\lambda \right) \right] \,. \tag{3.25}$$

where $T^{\text{II}\updownarrow}_\lambda := T^{\text{II}\downarrow}_\lambda T^{\text{II}\uparrow}_\lambda$,

$$sh^{\text{I}} = \frac{p^{\text{PBL}} - p^{\text{Sensor}}}{p^{\text{PBL}} - p^{\text{TOA}}} \;\text{ and }\; sh^{\text{II}} = \frac{p^{\text{SFC}} - p^{\text{Sensor}}}{p^{\text{SFC}} - p^{\text{PBL}}} \,. \tag{3.26}$$

These scaling factors are used to account for the relative height of the sensor within the corresponding layer. sh^{I} ranges from 1 at TOA to 0 at the PBL, while sh^{II} varies from 1 at the PBL to 0 at the Earth's surface (SFC).

3.3. Accuracy assessment

For typical airborne remote sensing conditions in the mid-latitudes we choose the representative uncertainty of imaging spectroscopy data of approximately 5% (Itten et al., 2008) as the accuracy requirement for SMART. Less typical conditions are analysed as well; in these cases we will accept larger errors. The definition of the conditions is given in Table 3.1. The AOD range was chosen according to the findings of Ruckstuhl et al. (2008), the wavelength range selected with regard to the optimal sensor performance

Table 3.2.: *Summary of the input parameters used in SMART and 6S for the accuracy assessment, with the aerosol and molecular optical depth $\tau^{\text{aer}}_{550\text{ nm}}$ and $\tau^{\text{mlc}}_{550\text{ nm}}$, the solar and viewing zenith angle SZA and VZA, the aerosol asymmetry factor and single scattering albedo $g^{\text{aer}}_{550\text{ nm}}$ and $\omega^{\text{aer}}_{550\text{ nm}}$, the Ångström parameter $\alpha_{550\text{ nm}}$, the surface albedo a_λ, as well as the air pressure at the surface and the planetary boundary layer p^{SFC} and p^{PBL} and the corresponding scaling factor h^{PBL}.*

parameter	$\tau^{\text{aer}}_{550\text{ nm}}$	$\tau^{\text{mlc}}_{550\text{nm}}$	SZA	VZA	$g^{\text{aer}}_{550\text{ nm}}$	$\omega^{\text{aer}}_{550\text{ nm}}$
value	0–0.5	0.097	nadir–70°	nadir	0.638	0.963

parameter	$\alpha_{550\text{ nm}}$	a_λ	p^{SFC}	p^{PBL}	sh^{PBL}
value	1.23	0	1013 mb	800 mb	0.211

(Seidel et al., 2008), while also avoiding strong water vapour absorption. We assume a black surface at the sea level (a_λ=0) to focus on the atmospheric part of SMART. Furthermore, we solely use the nadir viewing direction (μ=1), which is approximated by small field-of-view sensors (FOV<30°).

This section evaluates if the prior accuracy requirements can be met by SMART. We compare SMART with an assumed virtual truth computed by the well known RTM 6SV1.1. It accounts for polarisation and uses the SOS method as well as aerosol phase matrices based on Lorenz-Mie scattering theory (Vermote et al., 1997). It was validated and found to be consistent to within 1% when compared to other RTMs by (Kotchenova et al., 2006). We use the default accuracy mode of 6S with 48 Gaussian scattering angles and 26 atmospheric layers. The use of more calculation angles and layers would be possible, but the accuracy increase would be 0.4% at best (Kotchenova et al., 2006) and therefore is negligible for our study. The two layers of SMART were chosen to interface at 2 km above the surface. The lower layer includes dry water soluble aerosols and molecules distributed along the exponential vertical air pressure gradient. The corresponding aerosol optical parameters g^{aer}_λ, $\omega^{\text{aer}}_\lambda$ and α_λ are taken from d'Almeida et al. (1991) for SMART and 6S. All results in this study are calculated with identical input parameters in SMART and in 6S, which are provided in Table 3.2.

In the following, the accuracy of SMART is investigated for specific approximation uncertainties, as well as for the overall accuracy. As an indicator of the accuracy, we calculate the relative difference or percent error of the reflectance function to the benchmark 6S:

$$\delta R \cdot 100 = \frac{R^{\text{S}}_{\text{SMART}} - R^{\text{S}}_{\text{6S}}}{R^{\text{S}}_{\text{6S}}} \cdot 100\,. \tag{3.27}$$

3.3.1. Rayleigh scattering approximation and polarisation

The total Rayleigh scattering is $R_\lambda^{\mathrm{mlc}} = R_\lambda^{\mathrm{mlc\,I}} + R_\lambda^{\mathrm{mlc\,II}}$ as given by Eqs. (3.13) and (3.14). The associated approximations include the Rayleigh scattering phase function (Eq. 3.10)), the multiple scattering correction factor from MODTRAN (Eq. (3.12)) and) and the neglected polarisation due to the scalar equations. The percent error is a distinct function of the wavelength and SZA, induced mainly by polarisation. Figure 3.2a shows that it grows towards shorter wavelengths and larger SZA. It is known that the scalar approximation can introduce uncertainties of up to 10% in the blue spectral region (van de Hulst, 1980; Mishchenko et al., 1994). The SZA dependency of this uncertainty is shown in Fig. 3.2b. At 550 nm, the Rayleigh scattering uncertainty in the typical SZA range from 20–50° is below 3%.

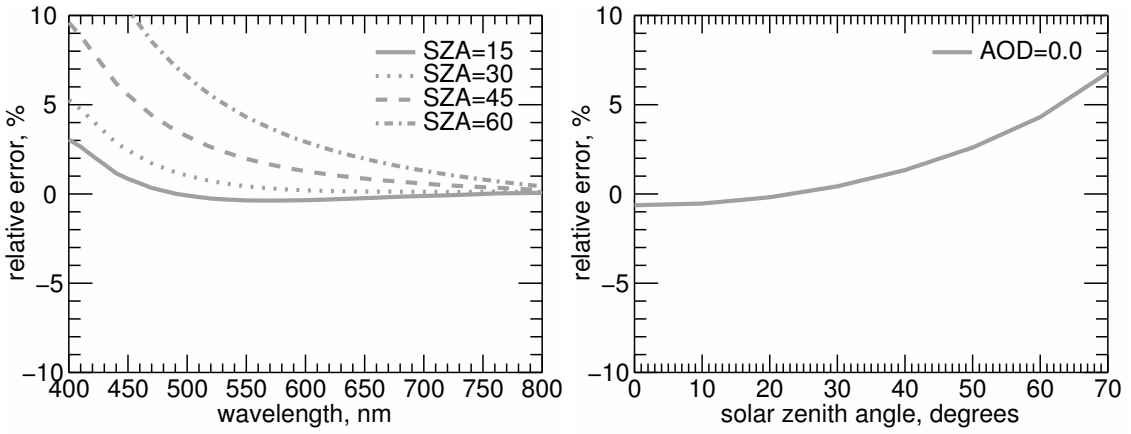

(a) $\delta R_\lambda^{\mathrm{mlc}}(\lambda) \cdot 100$ **(b)** $\delta R_{550\,\mathrm{nm}}^{\mathrm{mlc}}(\mathrm{SZA}) \cdot 100$

Figure 3.2.: *Percent error due to Rayleigh scattering and polarisation with respect to wavelength and solar zenith angle (SZA) at top-of-atmosphere.*

3.3.2. Aerosol scattering approximation

The main approximations for the aerosol scattering are the double scattering (Eq. (3.17)) and the HG phase function (Eq. (3.15)). Initially, we use the exactly same phase function as in 6S in order to study the error induced only by the neglected higher orders of scattering. This phase function for dry water soluble aerosols was derived from the Lorenz-Mie scattering theory. Subsequently, we compare the combined effect of the double scattering and the HG phase function approximation with 6S.

The percent error introduced by the double scattering approximation is plotted in Fig. 3.3. It is almost constant over the spectra due to the higher reflectance at shorter wavelengths (see Fig. 3.3a),. It is obvious that the reflectance function R_λ^{S} is increasingly underestimated by SMART for larger AOD due to the neglected third and higher orders of aerosol scattering (see Fig. 3.3b). Figure 3.3c shows that larger SZA leads to an underestimation of the atmospheric reflectance for the same reason.

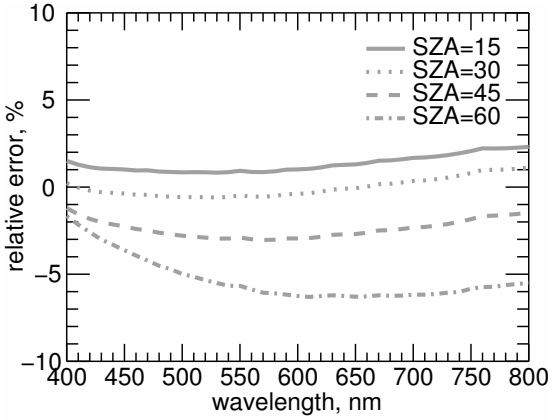

(a) $\delta R^{\text{aer}_{\text{Mie}}}(\lambda) \cdot 100$ *at* $\tau^{\text{aer}}_{550\text{ nm}} = 0.2$

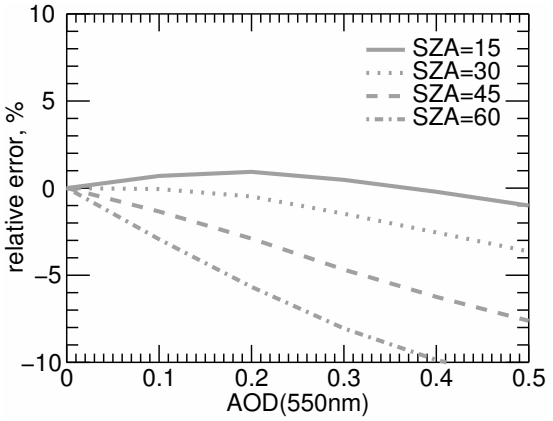

(b) $\delta R^{\text{aer}_{\text{Mie}}}_{550\text{ nm}}(\tau^{\text{aer}}_{550\text{ nm}}) \cdot 100$ *at* $\lambda = 550$ nm

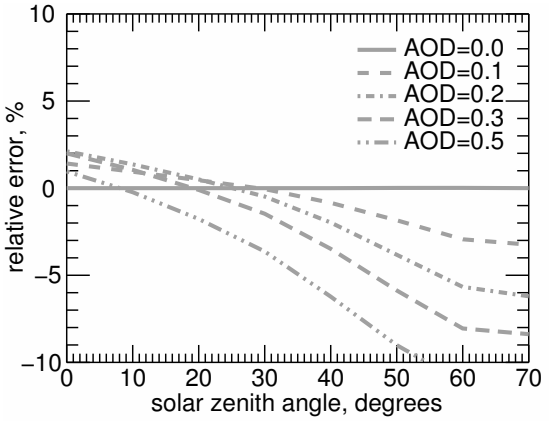

(c) $\delta R^{\text{aer}_{\text{Mie}}}_{550\text{ nm}}(\text{SZA}) \cdot 100$ *at* $\lambda = 550$ nm*]*

Figure 3.3.: *Percent error of the SMART reflectance function due to aerosol scattering with respect to wavelength, aerosol optical depth (AOD) and solar zenith angle (SZA) at top-of-atmosphere. SMART and 6S use the same phase function from Lorenz-Mie theory.*

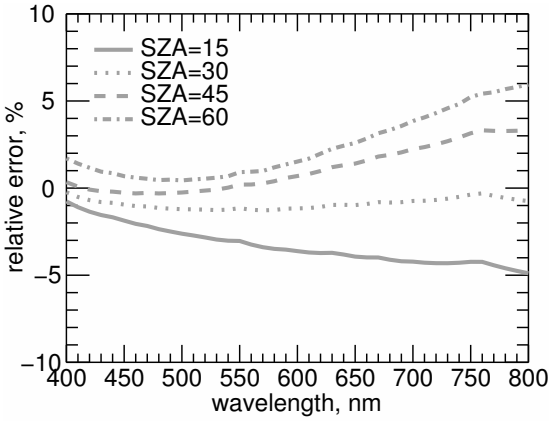

(a) $\delta R^{\text{aer}_{\text{HG}}}(\lambda) \cdot 100$ *at* $\tau^{\text{aer}}_{550\text{ nm}} = 0.2$

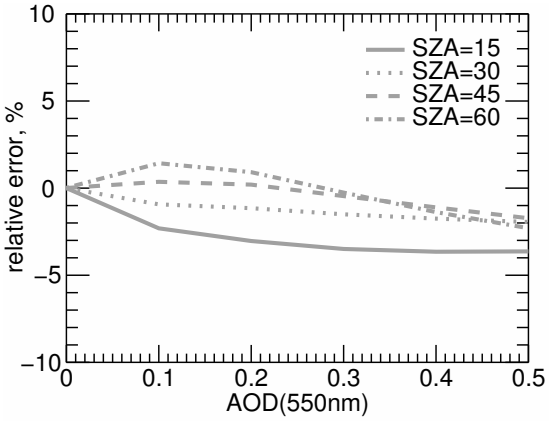

(b) $\delta R^{\text{aer}_{\text{HG}}}_{550\text{ nm}}(\tau^{\text{aer}}_{550\text{ nm}}) \cdot 100$ *at* $\lambda = 550$ nm

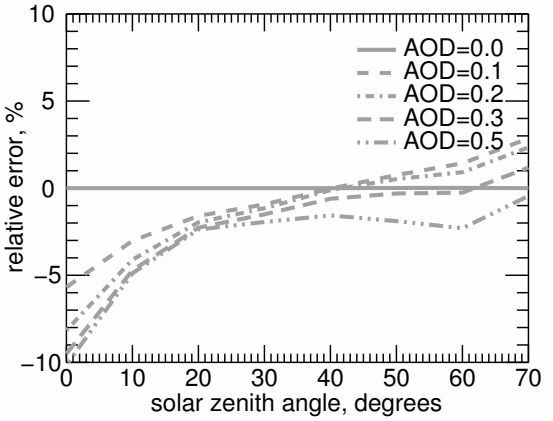

(c) $\delta R^{\text{aer}_{\text{HG}}}_{550\text{ nm}}(\text{SZA}) \cdot 100$ *at* $\lambda = 550$ nm

Figure 3.4.: *Percent error of the SMART reflectance function due to aerosol scattering with respect to wavelength, aerosol optical depth (AOD) and solar zenith angle (SZA) at top-of-atmosphere. SMART uses the HG phase function, 6S the phase function from Lorenz-Mie theory.*

In order to study the accuracy of the total aerosol scattering R_λ^{aer} as part of Eq. (3.14), we include the approximative HG phase function in SMART. 6S still uses the same Mie phase function as before. The input parameter for the HG phase function g_λ^{aer} corresponds to the same dry water soluble aerosol, which is used in 6S. The exact Mie and the approximative HG phase function are shown in Fig. 3.1 for the same aerosol. The latter provides a reasonable approximation for scattering angles around 130°, which corresponds to a 50° SZA for nadir observations. The resulting combination of the aerosol double scattering error with the HG approximation error is examined in Fig. 3.3. It suggests that the use of the HG approximation does not introduce large percent errors within the range of typical SZA, as defined in Table 3.1. Given a range of 20–45° SZA, SMART is quite accurate at all investigated wavelengths and AOD values.

By comparing Fig. 3.3a with 3.4a and Fig. 3.3b with 3.4b, it can be seen that the HG approximation reverses some of the errors due to the aerosol double scattering approximation. The HG phase function for dry water soluble aerosols tends to overestimate of the aerosol scattering, which finally leads to a less distinct underestimation due to the neglected third and higher orders of aerosol scattering.

3.3.3. Coupling of Rayleigh and aerosol scattering

The current version of SMART does not yet account for the scattering interaction between molecules and aerosols. We analyse this effect by comparing 6S computations with the coupling switched on and off. The relative error related to this specific approximation is shown in Fig. 3.5. It remains within about 3%, reaching a maximum at large SZA (see Fig. 3.5c) and short wavelengths (see Fig. 3.5a). With errors of less than 2%, small SZAs are almost not influenced by the coupling and there is no distinct dependency on AOD noticeable (see Fig. 3.5b).

3.3.4. Overall accuracy

Previous Sects. 3.3.1–3.3.3 demonstrated that the approximations in SMART are adequate. Most of them are within the desired accuracy range of ±5% for the limited remote sensing conditions as defined in Table 3.1.. Errors of up to ±15% are found for large SZA, however, they are mainly related to SMART's simple two-layer atmospheric structure.

In the following, we examine the overall accuracy of SMART by comparing it according to Eq. (3.27) with independent computations of 6S. The computations of SMART are performed by Eq. (3.23) for a TOA sensor altitude at 80 km and by Eq. (3.24) for an airborne sensor altitude at 5500 m a.s.l. The percent error due to the excluded coupling between molecules and aerosols is inherent in the results of this subsection.

Figure 3.6 shows the result of two independent calculations using SMART (solid line) and 6S (dashed line) with respect to λ and $\tau_{550\text{ nm}}^{\text{aer}}$. The qualitative agreement between the two models is evident. A quantitative perspective by statistical means of the overall

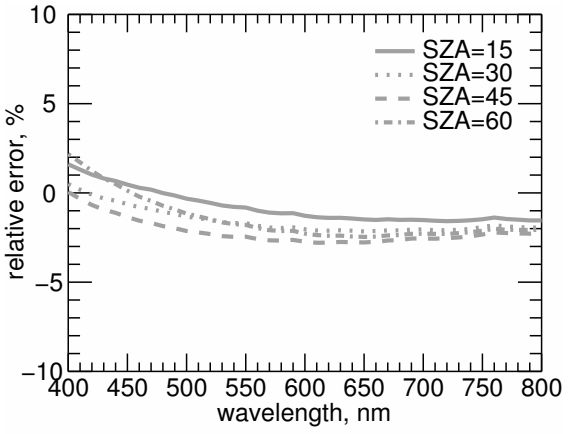

(a) $\delta R^{\text{mlc+aer}}(\lambda) \cdot 100$ *at* $\tau^{\text{aer}}_{550\text{ nm}} = 0.3$

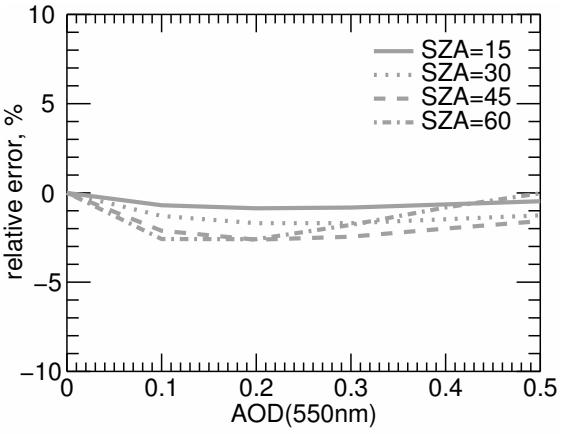

(b) $\delta R^{\text{mlc+aer}}_{550\text{ nm}}(\tau^{\text{aer}}_{550\text{ nm}}) \cdot 100$ *at* $\lambda = 550$ nm

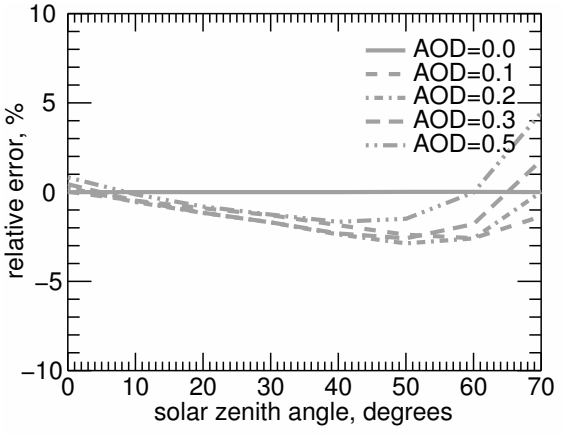

(c) $\delta R^{\text{mlc+aer}}_{550\text{ nm}}(\text{SZA}) \cdot 100$ *at* $\lambda = 550$ nm

Figure 3.5.: *Percent error due to the non-coupling approximation with respect to wavelength, aerosol optical depth (AOD) and solar zenith angle (SZA) at top-of-atmosphere.*

accuracy is provided in Table 3.3, where

$$R^2 = 1 - \frac{\sum \left(R^{\text{S}}_{\text{SMART}} - R^{\text{S}}_{\text{6S}}\right)^2}{\sum \left(R^{\text{S}}_{\text{6S}} - \bar{R}^{\text{S}}_{\text{6S}}\right)^2}, \tag{3.28}$$

is the squared correlation coefficient between the two models,

$$\text{RMSE} = \sqrt{\frac{1}{N}\sum \left(R^{\text{S}}_{\text{SMART}} - R^{\text{S}}_{\text{6S}}\right)^2}, \tag{3.29}$$

is the root mean square error and

$$\text{NRMSE} = \frac{\text{RMSE} \cdot 100}{\max\left(R^{\text{S}}_{\text{SMART}}\right) - \min\left(R^{\text{S}}_{\text{SMART}}\right)}, \tag{3.30}$$

Table 3.3.: *Quantitative comparison between SMART and 6S by statistical means for the limited conditions as defined in Table 3.1. SMART uses the HG phase function; 6S used the phase function from Mie calculations. R^2denotes the squared correlation coefficient, RMSE the root mean square error and NRMSE the normalised RMSE.*

Sensor altitude	R^2	RMSE	NRMSE
TOA	0.998	0.157	1.77%
5500 m	0.998	0.167	3.52%

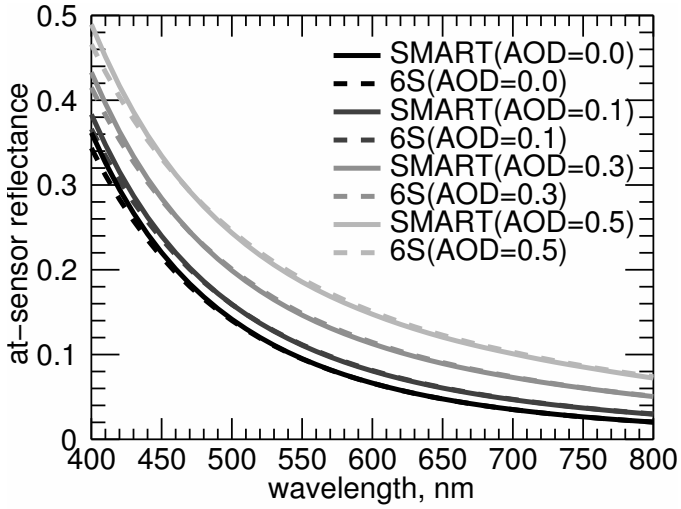

Figure 3.6.: *Results of the at-sensor reflectance function $R_\lambda^{\mathrm{S,TOA}}$ (Eq. 3.23) computed by SMART (solid line) and 6S (dashed line) at TOA, SZA=30° and varying $\tau_{550\,\mathrm{nm}}^{\mathrm{aer}}$. SMART uses the HG phase function, while 6S uses the phase function from Mie theory. Remaining input parameters are given in Table 3.2.*

is the normalised RMSE. The statistics are derived from all combinations of input parameters defined in Tables 3.1 and 3.2 within the limited conditions. The resulting correlation between SMART and 6S is almost perfect. The RMSE is approximately 0.16 reflectance values and the NRMSE is between 1.8% and 3.5%. The differences are smaller at TOA in comparison to those at 5500 m.

In the following, we analyse the overall accuracy of Eq. (3.23) by Eq. (3.27) in more details with respect to wavelength, SZA and AOD. SMART computes very similar results compared to 6S at TOA with an SZA between 30° and 40°. This conclusion can be drawn from the combination of Figs. 3.2b, 3.4c and 3.5c, as well as from the total percent error in Fig. 3.7a. The overall percent error does not exceed$\pm$5% at any investigated wavelength or AOD. At the large SZA of 60°, SMART overestimates $R_\lambda^{\mathrm{S,TOA}}$ by more than 10% at short wavelengths. Nevertheless, the overall accuracy is still well within the acceptable range of 10% at any wavelength larger than 450 nm (see Fig. 3.7b). At 550 nm, only the combination of very small SZA with a strong AOD or a high SZA with low AOD leads to a percent error just outside of the desired 5% margin (see Fig. 3.7c).

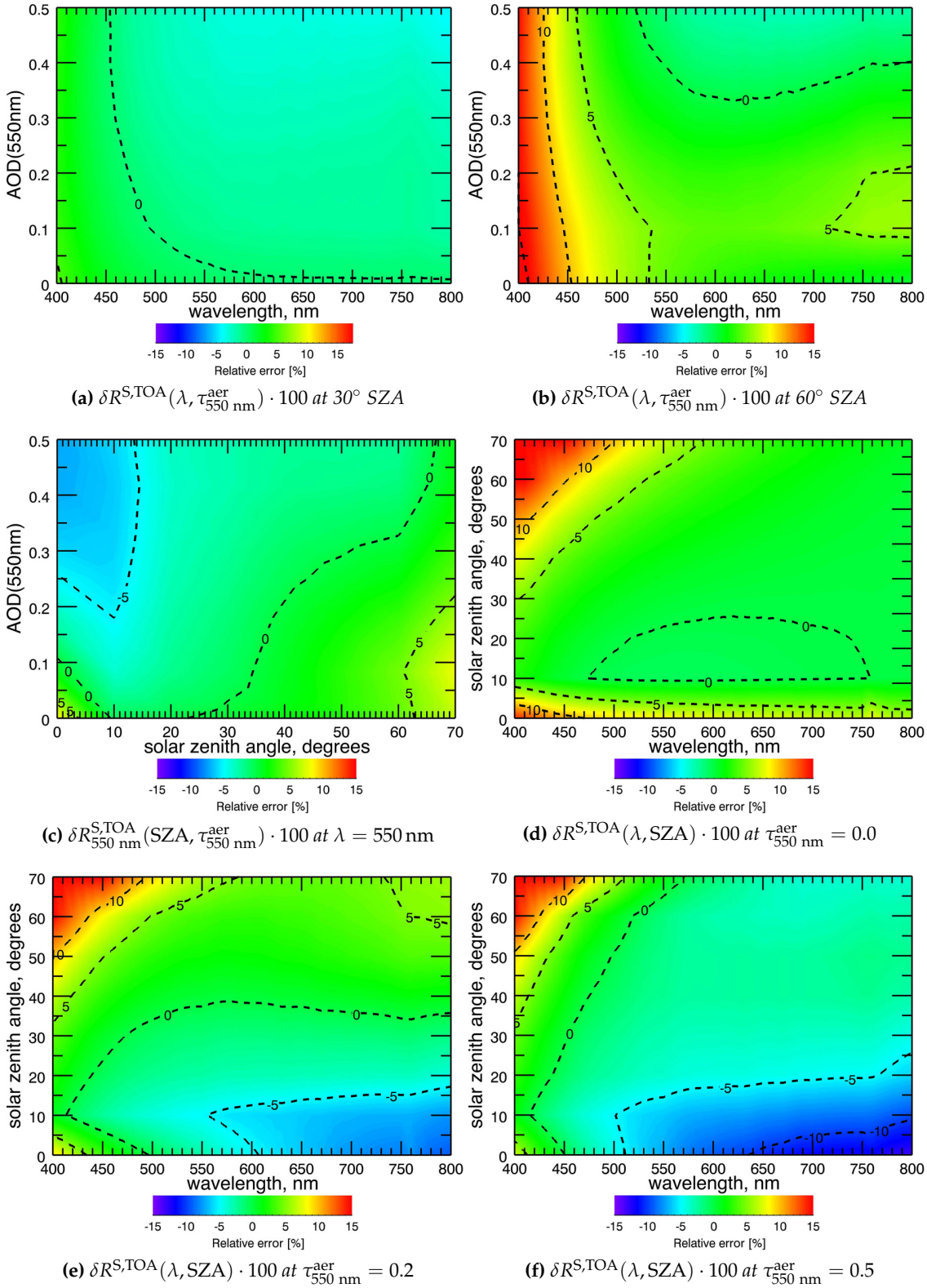

(a) $\delta R^{\mathrm{S,TOA}}(\lambda, \tau^{\mathrm{aer}}_{550\,\mathrm{nm}}) \cdot 100$ *at* $30°$ *SZA*

(b) $\delta R^{\mathrm{S,TOA}}(\lambda, \tau^{\mathrm{aer}}_{550\,\mathrm{nm}}) \cdot 100$ *at* $60°$ *SZA*

(c) $\delta R^{\mathrm{S,TOA}}_{550\,\mathrm{nm}}(\mathrm{SZA}, \tau^{\mathrm{aer}}_{550\,\mathrm{nm}}) \cdot 100$ *at* $\lambda = 550\,\mathrm{nm}$

(d) $\delta R^{\mathrm{S,TOA}}(\lambda, \mathrm{SZA}) \cdot 100$ *at* $\tau^{\mathrm{aer}}_{550\,\mathrm{nm}} = 0.0$

(e) $\delta R^{\mathrm{S,TOA}}(\lambda, \mathrm{SZA}) \cdot 100$ *at* $\tau^{\mathrm{aer}}_{550\,\mathrm{nm}} = 0.2$

(f) $\delta R^{\mathrm{S,TOA}}(\lambda, \mathrm{SZA}) \cdot 100$ *at* $\tau^{\mathrm{aer}}_{550\,\mathrm{nm}} = 0.5$

Figure 3.7.: *Overall accuracy with a sensor at top-of-atmosphere.*

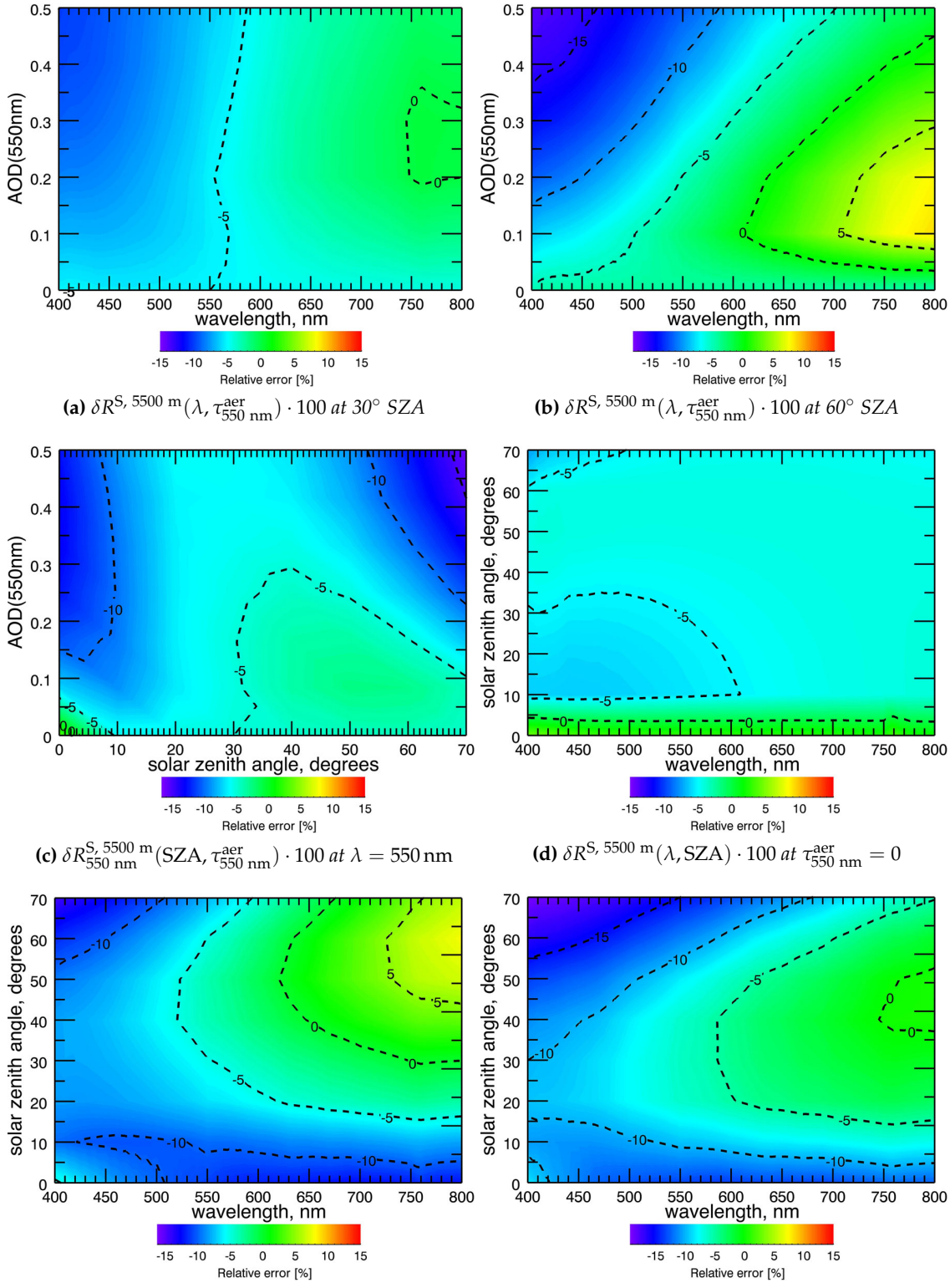

(a) $\delta R^{\mathrm{S,\ 5500\ m}}(\lambda, \tau^{\mathrm{aer}}_{550\ \mathrm{nm}}) \cdot 100$ *at* $30°$ *SZA*

(b) $\delta R^{\mathrm{S,\ 5500\ m}}(\lambda, \tau^{\mathrm{aer}}_{550\ \mathrm{nm}}) \cdot 100$ *at* $60°$ *SZA*

(c) $\delta R^{\mathrm{S,\ 5500\ m}}_{550\ \mathrm{nm}}(\mathrm{SZA}, \tau^{\mathrm{aer}}_{550\ \mathrm{nm}}) \cdot 100$ *at* $\lambda = 550\,\mathrm{nm}$

(d) $\delta R^{\mathrm{S,\ 5500\ m}}(\lambda, \mathrm{SZA}) \cdot 100$ *at* $\tau^{\mathrm{aer}}_{550\ \mathrm{nm}} = 0$

(e) $\delta R^{S,5500\,\mathrm{m}}(\lambda, SZA) \times 100$ *with* $\tau^{aer}_{550\mathrm{nm}} = 0.2$

(f) $\delta R^{\mathrm{S,\ 5500\ m}}(\lambda, \mathrm{SZA}) \cdot 100$ *at* $\tau^{\mathrm{aer}}_{550\ \mathrm{nm}} = 0.5$

Figure 3.8.: *Overall accuracy with a sensor at 5500 m.*

In the blue part of the spectrum, high or low SZA lead to significant percent errors in a pure Rayleigh scattering atmosphere (see Fig. 3.7e). The same is true in an atmosphere containing aerosols, where the aerosols introduce additional percent errors in the red part of the spectrum for small SZAs (see Figs. 3.7d and 3.7f).

SMART is also intended for the use with airborne remote sensing data, we additionally analyse the overall accuracy of Eq. (3.24) by (3.27).

We place the sensor at 5500 m above the assumed black surface at sea level. The airborne scenario is more sensitive to the approximative two-layer setup in SMART. The 26 atmospheric layers in 6S can better account for the vertically inhomogeneous atmosphere. In fact, the percent error is slightly larger in the airborne case in comparison with the TOA case. The error distribution in the contour plots of Figs. 3.8a–3.8d show that SMART underestimates the reflectance factors at 5500 m. Nevertheless, the hypothetical pure Rayleigh atmosphere still performs well, with a maximum percent error of 6% (see Figs. 3.8a, 3.8b and 3.8f). The aerosols worsen the underestimation in the lower half of the visible spectrum, especially at very small and very large SZAs. At 550 nm and a 30° SZA, the percent error is 6% or less for an AOD up to 0.5. With the same constellation but an extreme SZA, the percent errors reach about 10% (see Figs. 3.8c, 3.8e and 3.8f). The largest offset between SMART and 6S is found at 60° SZA, 400 nm and an AOD of 0.5 with 18% relative difference.

However, it should be noted that absolute difference $R^{\mathrm{S}}_{\mathrm{SMART}} - R^{\mathrm{S}}_{\mathrm{6S}}$ is in fact smaller in the airborne case compared to the TOA case (not shown). Nonetheless, the relative error given by Eq. (3.27) is larger due to the smaller $R^{\mathrm{S}}_{\mathrm{6S}}$ in the denominator.

3.4. Performance assessment

SMART is designed to optimally balance the opposing needs for accuracy and computational speed; the speed decreases with increasing model complexity and accuracy. We use the 6S vector version 1.1 (Vermote et al., 1997) as a benchmark RTM (same as in Sect. (3.3)) to assesses the performance of SMART. 6S is compiled with GNU Fortran and SMART is implemented in IDL. Both run on the same CPU infrastructure.

SMART needs only approximately 0.05 s for the calculation of one reflectance factor value. The more complex 6S needs about 1.4 s under identical conditions. Consequently, SMART computes more than 25 times faster. If $R^{\mathrm{aer,MS}}_{\lambda}$ (Eq. 3.17) is substituted by a simple correction factor $f^{\mathrm{corr}}_{\mu_0}(\lambda, \tau)$ for aerosol multiple scattering (similar to Eq. (3.12)), SMART runs 220 times faster than by numerically solving Eq. (3.17) in the presented configuration.

3.5. Summary and conclusions

We introduced SMART, as well as its approximative radiative transfer equations and parameterizations. Results of the atmospheric at-sensor reflectance function computed by SMART were compared with benchmark results from 6S for accuracy and performance. The overall percent error was examined and discussed, as were the individual errors resulting from Rayleigh scattering, aerosol scattering and molecule-aerosol interactions. The aerosol scattering was compared to 6S with and without the effect of the HG phase function approximation.

We found that SMART fulfils its design principle: it is fast and simple, yet accurate enough for a range of applications. One example may include the assessment of atmospheric effects when inspecting the quality of airborne or spaceborne data against ground truth measurements in near-real-time. The generation of atmospheric input parameters for vegetation canopy RTM inversion schemes, could be another application. SMART computes more than 20 reflectance results per second on a current customary desktop computer. This is more than 25 times faster than the benchmark RTM. The overall percent error under typical mid-latitude remote sensing conditions was found to be about 5% for the spaceborne and 5% to 10% for the airborne case. Large AOD or SZA values lead to larger percent errors of up to 15%. In general, the included approximations are sensitive to the strong scattering in the blue spectral region, which leads to larger percent errors. Together with the effect of polarisation, the total percent error of SMART exceeds the desired accuracy goal of 5% only in the blue region. It is therefore suggested that SMART be used preferably in the spectral range between roughly 500 nm and 680 nm, avoiding the blue and strong absorption bands. However, the neglected ozone absorption in this spectral interval leads to a small overestimation of up to 0.007 reflectance units at large SZA and 600 nm. It is also recommended to use SMART for computations with a sensor above the PBL to avoid uncertainties in the vertical distribution of the aerosols.

SMART can be improved by implementing other phase functions instead of the HG approximation, including those derived from Lorenz-Mie theory, geometrical optics (ray-tracing), and T-matrix approaches (Liou and Hansen, 1971; Mishchenko et al., 2002). Further refinements may include the coupling between molecules and aerosols, as well as the implementation of freely mixable aerosol components and hygroscopic growth (Hess et al., 1998). To account for polarisation, the scalar equations can be extended to the vector notation. Furthermore, a similar approach as used for the Rayleigh multiple scattering in this study (Eq. (3.12)) may perhaps be used to perform a rough polarisation correction. Other issues for further developments may include additional atmospheric layers, gaseous absorption (foremost ozone), adjacency effects and the treatment of a directional, non-Lambertian surface.

A recent inter-comparison study for classic RTMs such as 6S, RT3, MODTRAN and SHARM, found discrepancies of $\delta R \leq 5\%$ at TOA (Kotchenova et al., 2008). Even larger errors were found when polarisation was neglected or the HG phase function was used. SMART does not yet account for polarisation and uses the HG approximation by default, however with the option to include pre-calculated Mie phase functions. Therefore, the overall accuracy achieved by SMART under given conditions can be regarded as satisfactory, especially when a computationally fast RTM is required.

Acknowledgements

The work of A. A. Kokhanovsky was performed in the framework of DFG Project Terra. Suggestions from D. Schlaepfer and A. Schubert were very much appreciated. We thank three anonymous referees for their valuable comments on the AMTD version of this publication.

4. Fast retrieval of aerosol optical depth and its sensitivity to surface albedo using remote sensing data

This chapter is in print for the special issue on Remote Sensing of Clouds and Aerosols in *Atmospheric Research*:

Seidel, F.C., Kokhanovsky, A.A., Schaepman, M.E., 2011. Fast retrieval of aerosol optical depth and its sensitivity to surface albedo using remote sensing data. Atmos. Res. In Press, Corrected Proof. doi:10.1016/j.atmosres.2011.03.006

Fast retrieval of aerosol optical depth and its sensitivity to surface albedo using remote sensing data

Felix C. Seidel[1], Alexander A. Kokhanovsky[2] and Michael E. Schaepman[1]

[1] Remote Sensing Laboratories, University of Zurich, Winterthurerstr. 190, CH-8057 Zurich, Switzerland

[2] Institute of Environmental Physics, University of Bremen, O. Hahn Allee 1, D-28334 Bremen, Germany

Abstract

Aerosol remote sensing over land is still a great challenge. The retrieval of optical and micro-physical aerosol properties usually requires comprehensive and computationally extensive retrieval algorithms. An efficient approach for the retrieval of the aerosol optical depth (AOD) is proposed in this paper. It is based on a fast and simple atmospheric radiative transfer model using approximations and analytical equations. The proposed algorithm is validated on both synthetic data from the benchmark radiative transfer model SCIATRAN and on real data from the airborne imaging spectrometer APEX. The promising results confirm the feasibility of retrievals using single wavelength nadir observations under constrained conditions. The AOD retrieval is found to be very sensitive to uncertainties in the surface albedo. In the current experimental setup, 0.01 surface albedo uncertainty leads to approximately 0.2 AOD retrieval uncertainty. Generally, larger AOD leads to the increase of reflectance R at sensor level for underlying "dark" surfaces and to a decrease of R for "bright" surfaces. R does not depend strongly on AOD for a surface albedo in the range of approximately 0.2–0.4. Third and higher orders of aerosol scattering, polarization and three-dimensional effects at the surface–atmosphere interface are not taken into account by this study. Nevertheless, a brief validation shows the feasibility with promising results of the proposed simple and fast AOD retrieval algorithm from remote sensing data.

4.1. Introduction

Aerosols are important to our climate (Charlson et al., 1992; Rind et al., 2009) and health (Wilson and Spengler, 1996). According to the intergovernmental panel on climate change (IPCC), some changes in the energy budget are still difficult to understand due to key uncertainties in local radiative forcing by aerosols and related feedback mechanisms (Solomon et al., 2007). Remote sensing and radiative transfer (RT) models are important instruments for determining micro-physical and optical aerosol properties and better understanding the impact of aerosols on climate (Rind et al., 2009). The aerosol optical depth (AOD) is one of the most often retrieved optical properties. It describes the proportion of the extinction (scattering and absorption) of solar light due to aerosols (Ångström, 1930; van de Hulst, 1948). Operational AOD retrieval algorithms are well established using data from MODIS with the "dark target" approach (e.g. Levy et al., 2007) or the Deep Blue algorithm (e.g. Hsu et al., 2004), from MISR (e.g. Diner et al., 2005; Martonchik et al., 2009), OMI (e.g. Torres et al., 2007) and other sensors (e.g. Tanré, 2010). Still, uncertainties exist mainly due to sub-pixel clouds and approximations regarding effects of the surface (Levy et al., 2010). There are few studies available using airborne high spatial resolution imagers for aerosol retrievals on the local scales (Bassani et al., 2010). Nonetheless, precise measurements of aerosol scattering are of vital importance to the atmospheric correction of such data (Guanter et al., 2005; Gao et al., 2009).

The retrieval of AOD from remote sensing data is performed by RT model inversion. The number of concurrent independent measurements is usually lower than the number of unknowns, which requires ancillary information or assumptions to constrain such a problem. For example, *a priori* knowledge of the spectral bidirectional reflectance function (BRDF) of the underlying surface and its surrounding area is needed to account for three-dimensional effects at the surface (Lyapustin, 2001). Concurrent measurements of all these variables are currently not available and assumptions on the surface properties and the aerosol model have to be made to constrain the problem. A recent intercomparison study by (Kokhanovsky et al., 2010b) has shown that existing retrieval algorithms may retrieve slightly different values of AOD, even when applied to simulated data on black surfaces. Remote sensing of aerosol over land will remain a challenging retrieval problem.

In this paper, we propose a fast and simple AOD retrieval algorithm. The inverse Simple Model for Atmospheric Radiative Transfer (iSMART) is based on approximate analytical solutions of the RT problem. Its minimal complexity and fast computation are important assets for the processing of large datasets, such as imaging spectrometer data. Fast and approximate estimates of AOD permit the prior calculation of probability density functions (PDF), which are used to reduce the ill-conditioned nature of the inverse approach in biophysical parameter modeling, for example. Naturally, computational speed comes at the expense of accuracy, but might still be within the expected uncertainty envelope of comparable algorithms (e.g. MODIS AOD retrieval over land (Remer et al., 2005; Levy et al., 2009)). Another fast, albeit more extensive approach to AOD retrieval was published by Katsev et al. (2010), which is again based on a fast RT model (see Kokhanovsky and de Leeuw, 2009, p. 101–134).

This paper describes an AOD retrieval algorithm. It is validated in Sect. 4.4.1 and 4.4.2 using synthetic and real airborne remote sensing data respectively, which are introduced in Sect. 4.3. iSMART is used in Sect. 4.4.3 to investigate the effect of the critical surface albedo and uncertainties of surface albedo on AOD retrievals.

4.2. iSMART – inverse Simple Model for Atmospheric Radiative Transfer

Spectral radiances L_λ are measured by optical remote sensing instruments and can be simulated by RT models. We approximate L_λ as a function of the optical depth of molecules and aerosols $\tau_\lambda = \tau_\lambda^{mlc} + \tau_\lambda^{aer}$, the scattering phase function $P_\lambda(\Theta)$ at scattering angle Θ, single-scattering albedo ω_λ, surface albedo a_λ, cosine of solar and viewing zenith angles (SZA and VZA) μ_0 and μ, and finally the relative azimuth between viewing and solar direction $\phi - \phi_0$. The subscript λ denotes wavelength dependence. τ_λ^{aer} can be derived from one L_λ value under the condition that all other parameters are known or estimated.

The reflectance values:

$$R_\lambda = \frac{\pi L_\lambda}{\mu_0 F_{0,\lambda}}, \tag{4.1}$$

will be used below, where $F_{0,\lambda}$ is the spectral solar irradiance.

4.2.1. Radiative transfer model

A Simple Model for Atmospheric Radiative Transfer (SMART) is proposed and validated by Seidel et al. (2010). It is based upon analytical equations, parameterizations and a correction factor for molecular multiple scattering to provide fast computations. The accuracy is in the order of 5–10% for typical observational conditions and up to 15% for combinations of large SZA and high AOD in the blue spectral range.

Assuming a sensor at top-of-atmosphere (TOA) and a surface albedo a_λ, R_λ is given by:

$$\begin{aligned} R_\lambda^{TOA} = & \underbrace{\underbrace{\frac{P^{mlc}(\Theta)}{4(\mu_0+\mu)}\left(1-e^{-\tau_\lambda^{mlc}\left(\frac{1}{\mu_0}+\frac{1}{\mu}\right)}\right)}_{R_\lambda^{SSA;mlc}} f_{\mu_0}^{corr}}_{R_\lambda^{mlc}} \\ & + \underbrace{\underbrace{\frac{\omega_\lambda^{aer} P_\lambda^{aer}(\Theta)}{4(\mu_0+\mu)}\left(1-e^{-\tau_\lambda^{aer}\left(\frac{1}{\mu_0}+\frac{1}{\mu}\right)}\right)}_{R_\lambda^{SSA;aer}} + R_\lambda^{aer\,2.SA}}_{R_\lambda^{aer}} \\ & + \underbrace{T_\lambda^{\downarrow}\frac{a_\lambda}{1-s_\lambda a_\lambda}T_\lambda^{\uparrow}}_{R_\lambda^{SFC}}. \end{aligned} \tag{4.2}$$

The molecular reflectance R_λ^{mlc} is the product of the single-scattering approximation (SSA) $R_\lambda^{SSA;mlc}$ and a generic correction factor $f_{\mu_0}^{corr}$ per SZA to approximate molecular multiple scattering. The latter is derived from prior MODTRAN/DISORT (Stamnes et al., 1988; Berk et al., 1989) calculations (Seidel et al., 2010). The Rayleigh scattering phase function for unpolarized solar radiation is given by:

$$P^{mlc}(\Theta) = \frac{3}{4}\left(1 + \cos^2\Theta\right) \tag{4.3}$$

(see Fig. 4.1), where

$$\Theta = \arccos\left[\pm\mu_0\mu + \cos(\phi - \phi_0)\sqrt{\left(1-\mu_0^2\right)\left(1-\mu^2\right)}\right]. \tag{4.4}$$

is the forward (+) or backward (−) scattering angle. The aerosol reflectance approximation R_λ^{aer} is the sum of the first order scattering $R_\lambda^{SSA;aer}$ and the second order scattering $R_\lambda^{2^{nd}S;aer}$ according to the successive orders of scattering method as formulated by Hansen and Travis (1974):

$$\begin{aligned}
R_\lambda^{2^{nd}S;aer}(\mu,\mu_0,\phi-\phi_0) = {} & \frac{\omega_\lambda^{aer}\tau_\lambda^{aer}}{4\pi} \\
& \cdot \int_0^{2\pi}\int_0^{1}\left[\frac{1}{\mu}P_\lambda^{T;aer}\left(\mu,\mu',\phi-\phi'\right)R_\lambda^{SSA;aer}\left(\mu',\mu_0,\phi'-\phi_0\right)\right. \\
& + \frac{1}{\mu_0}R_\lambda^{SSA;aer}\left(\mu,\mu',\phi-\phi'\right)P_\lambda^{T;aer}\left(\mu',\mu_0,\phi'-\phi_0\right) \\
& - \frac{e^{-\frac{\tau_\lambda^{aer}}{\mu_0}}}{\mu_0}T_\lambda^{SSA;aer}\left(\mu,\mu',\phi-\phi'\right)P_\lambda^{aer}\left(\mu',\mu_0,\phi'-\phi_0\right) \\
& \left. - \frac{e^{-\frac{\tau_\lambda^{aer}}{\mu}}}{\mu}P_\lambda^{aer}\left(\mu,\mu',\phi-\phi'\right)T_\lambda^{SSA;aer}\left(\mu',\mu_0,\phi'-\phi_0\right)\right] d\mu' d\phi'.
\end{aligned} \tag{4.5}$$

$P_\lambda^{aer}(\Theta)$ is calculated according to the Lorenz–Mie scattering theory. $P_\lambda^{T;aer}$ denotes the transmittance phase function using the forward scattering angle of Eq. (4.4). van de Hulst (1948); Sobolev (1972); Hansen and Travis (1974); Kokhanovsky (2006) and others derived an analytical equation for the aerosol single-scattering transmittance:

$$T_\lambda^{SSA;aer} = \frac{\omega_\lambda^{aer}P_\lambda^{aer}(\Theta)}{4(\mu_0-\mu)}\left(e^{-\frac{\tau_\lambda^{aer}}{\mu_0}} - e^{-\frac{\tau_\lambda^{aer}}{\mu}}\right) \tag{4.6}$$

or in case of $\mu_0 = \mu$:

$$T_\lambda^{SSA;aer} = \frac{\omega_\lambda^{aer}P_\lambda^{aer}(\Theta)}{4\mu^2}\tau_\lambda^{aer}e^{-\frac{\tau_\lambda^{aer}}{\mu}}. \tag{4.7}$$

Eq. (4.5) allows approximating the total aerosol scattering exclusively by using SSA equations (see Eqs. 4.2 and 4.6) integrated over the scattering directions μ and ϕ. R_λ^{SFC} in

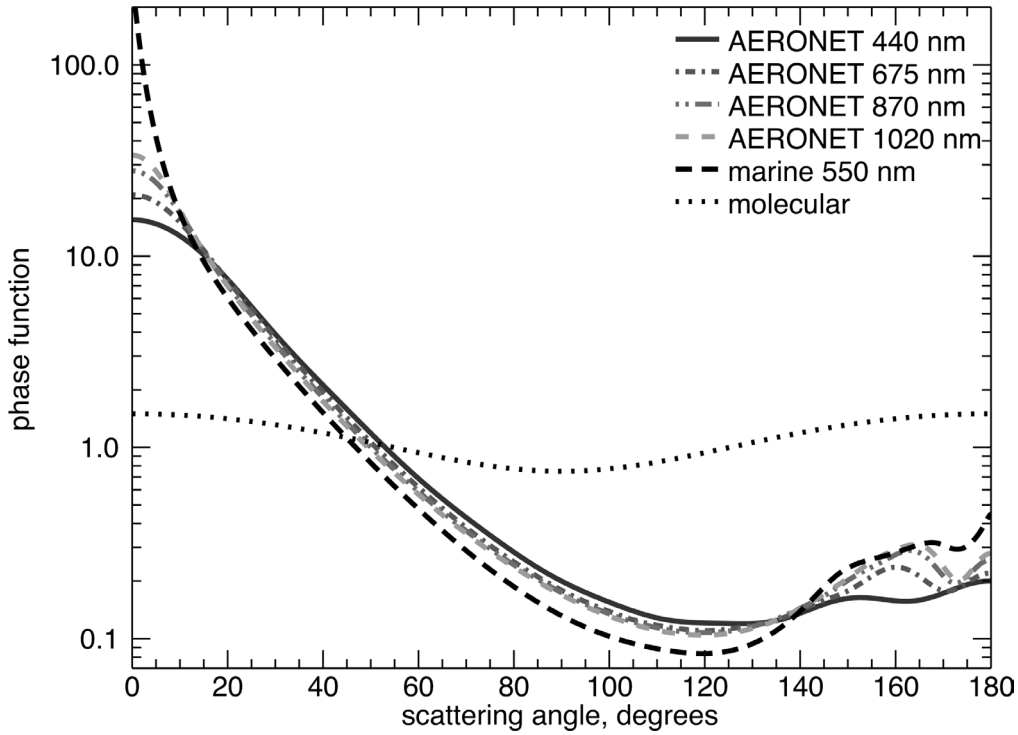

Figure 4.1.: *Phase functions $P_\lambda(\Theta)$ as function of the scattering angle Θ for molecular (Eq. 4.3) and aerosol scattering. The latter is calculated for marine particles using Lorenz–Mie scattering theory (see Sect. 4.3.1) and derived from AERONET measurements (see Sect. 4.3.2).*

Eq. (4.2) describes the reflectance function of an underlying homogeneous Lambertian surface according to Ångström (1925); Chandrasekhar (1960); Sobolev (1972) and others with the surface albedo a_λ, the spherical albedo s_λ of the atmosphere for illumination from below as well as the down and upward transmittance $T_\lambda^\downarrow$ and $T_\lambda^\uparrow$, respectively. A parameterization with respect to τ_λ^{aer} and the asymmetry parameter g for s_λ, $T_\lambda^\downarrow$ and $T_\lambda^\uparrow$ was used as suggested in Kokhanovsky et al. (2005).

Seidel et al. (2010) provides a complete description of SMART including an extended formulation of Eq. (4.2) for airborne remote sensing and a validation with 6S (Vermote et al., 1997).

Fig. 4.2 shows calculations of $R_{550\,nm}^{TOA}$ using SMART (lines) at $a_{550\,nm} \in [0.0\,(0.2)\,1.0]$[1]. Corresponding benchmark results using SCIATRAN (Rozanov et al., 2005) are plotted as reference (circles). Both models were run independently using the same phase function for marine aerosols as described in Sect. 4.3.1 and shown in Fig. 4.1. A good agreement between both models was found for $a_{550\,nm} \leq 0.8$ and $\tau_{500\,nm}^{aer} \leq 0.5$. SMART is generally less accurate in the blue spectral region due to neglected coupling of molecular and higher orders of aerosol scattering, as well as polarization effects.

[1] See Appendix A.2 for additional results.

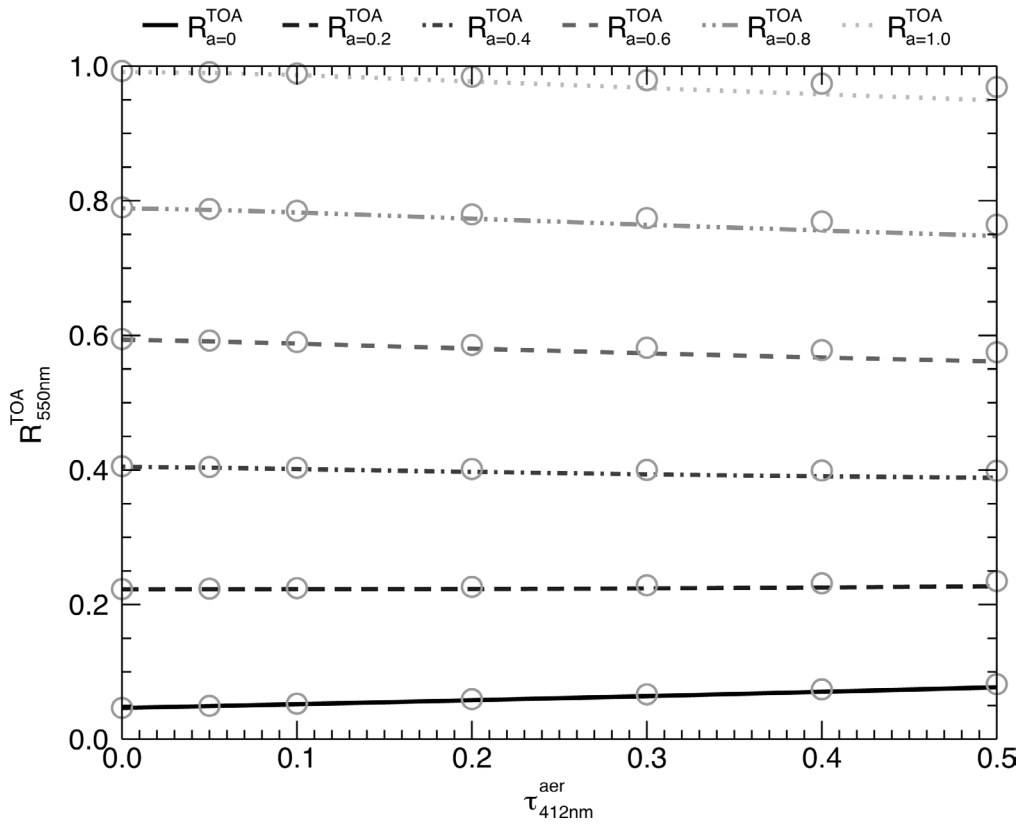

Figure 4.2.: *Reflectance $R^{TOA}_{550\,nm}$ as a function of AOD for surface albedo $a_{550\,nm} \in [0.0, 0.2, 0.4, 0.6, 0.8, 1.0]$. The lines were computed by Eq. (4.2) and the circles by using SCIATRAN as a benchmark. AOD inputs are given in Table 4.1. Both models used the same marine aerosol phase function (see Sect. 4.3.1 and Fig. 4.1).*

4.2.2. AOD retrieval with iSMART

iSMART is an extended version of SMART, which was developed for AOD retrievals from radiance measurements. iSMART initiates repeated SMART runs, until convergence with measured data is achieved. It uses *a priori* knowledge of a_λ, aerosol particle size distribution (PSD) and spectral aerosol refractive indices. The method uses the following Boolean function:

$$\begin{gathered}\left(R^{SMART}_{\tau^{aer}_\lambda} < R^{Data}_{\tau^{aer}_\lambda=?} \leq R^{SMART}_{\tau^{aer}_\lambda+i}\right) \\ \veebar \\ \left(R^{SMART}_{\tau^{aer}_\lambda} > R^{Data}_{\tau^{aer}_\lambda=?} \geq R^{SMART}_{\tau^{aer}_\lambda+i}\right)\end{gathered} \tag{4.8}$$

to search for the optimal solution with respect to the best fit between data and model. iSMART uses a decision tree with heuristically selected branches (see Fig. 4.3) allowing fast convergence on the most likely solution, which defines the AOD to be retrieved (τ^{aer}_λ =?). The AOD interval between two branches is defined by: $i = j \cdot 2^{(1-h)}$, where $h \in [1, 2, 3, 4]$ is the hierarchy and j is the initial AOD interval in the top hierarchy

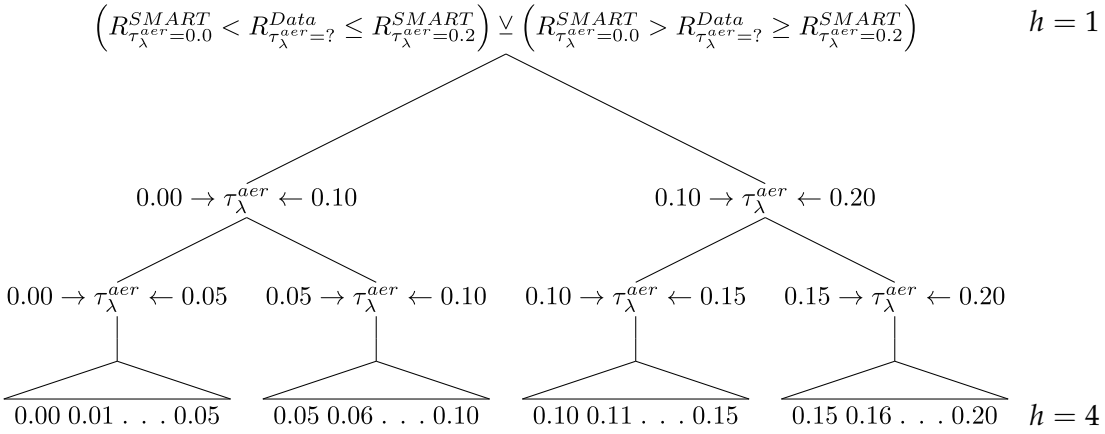

Figure 4.3.: *Part of the decision tree used in iSMART to retrieve AOD with a sampling interval of 0.01. It shows the case where Eq. (4.8) fulfills the condition with an initial AOD interval between 0.0 and 0.2. Boolean functions are used to quickly find the optimal solution without interpolation.*

($h = 1$). Thus, each subsequent hierarchy narrows down the search using halved AOD intervals. We used $j = 0.2$ and started the procedure at $\tau^{aer}_\lambda = 0.0$ and $\tau^{aer}_\lambda + i = 0.2$. If the conditions of Eq. (4.8) are met, the search in the subsequent hierarchy continues between $\tau^{aer}_\lambda = 0.0$ and $\tau^{aer}_\lambda + i = 0.1$ or $\tau^{aer}_\lambda = 0.1$ and $\tau^{aer}_\lambda + i = 0.2$ (see Fig. 4.3). Else, the search is continued in the same hierarchy between $\tau^{aer}_\lambda = 0.2$ and $\tau^{aer}_\lambda + i = 0.4$, and so forth. Note that $R_{\tau^{aer}_\lambda} < R_{\tau^{aer}_\lambda + i}$ is usually found over dark surfaces and $R_{\tau^{aer}_\lambda} > R_{\tau^{aer}_\lambda + i}$ over bright surfaces (see Sect. 4.4.1 and 4.4.3.1). After the initiation of the search, each step requires only one additional iteration, because one of the bounds is already known. In the lowest hierarchy ($h = 4$), only four out of six calculations are needed, because both bounds are already known. This leads to a minimum of eight consecutive SMART iterations. If $\tau^{aer}_\lambda > 0.2$ then the next node in the first hierarchy tests with one additional calculation at $\tau^{aer}_{550\,nm} = 0.4$ if the data fits the AOD interval $\tau^{aer}_\lambda \in [0.2, 0.4]$. If this is true, nine iterations are needed in total to find AOD, else one additional iteration per interval is needed. Twelve SMART iterations are needed to find an AOD, which is $\tau^{aer}_\lambda \in [0.8, 1.0]$. The AOD sampling interval is 0.01 and there is no interpolation of the results involved. $j = 0.2$ was chosen because $\tau^{aer}_\lambda \in [0.0, 0.2]$ represent typical vales for Western Europe (Ruckstuhl et al., 2008).

The current version of iSMART requires that the function from R^{Data}_λ to R^{SMART}_λ is bijective. Therefore, both sets of R_λ have to be a monotonically increasing or decreasing function with respect to AOD. If ambiguous solutions exist, such that one R^{Data}_λ can be related to more than one R^{SMART}_λ, the retrieval algorithm (Eq. 4.8) may choose a wrong branch in the decision tree (Fig. 4.3). Results with $\tau^{aer}_\lambda \notin [0.00, 1.20]$ are rejected.

SMART calculates approximately 20 results per second on a current CPU (Seidel et al., 2010). The retrieval of one AOD value, including non-RT operations, requires approximately between 0.5 $\left(\tau^{aer}_\lambda \in [0.0, 0.2]\right)$ and 0.8 seconds $\left(\tau^{aer}_\lambda \in [1.0, 1.2]\right)$.

Other retrievals are possible as well (e.g. surface albedo), though not implemented in the current version of iSMART. Multi-directional measurements are required to simultaneously retrieve AOD and surface albedo.

4.3. Data

4.3.1. Synthetic data

We used a synthetic dataset for testing the retrieval algorithm under controlled conditions. It was computed using the independent benchmark RT model SCIATRAN (Rozanov and Kokhanovsky, 2006; Kokhanovsky et al., 2010a,b). The inherent accuracy of SCIATRAN is better than 1% relative error as compared with other RT models (Kokhanovsky et al., 2010a).

The synthetic dataset accounts for a standard atmosphere comprising non-absorbing marine aerosols and an underlying Lambertian surface with monochromatic surface albedos $a_\lambda \in [0.0\,(0.1)\,1.0]$. Gaseous absorption is ignored. The SZA is 60° and the VZA is 0° (nadir). The aerosol PSD is modeled using the log-normal law:

$$f(r) = \frac{1}{\sqrt{2\pi}\sigma r} \exp\left[-\frac{\ln^2(r/r_0)}{2\sigma^2}\right], \tag{4.9}$$

where r is the radius of the spherical homogeneous particles. The geometrical radius $r_0 = r_m \exp(\sigma^2) = 100\,\text{nm}$ is assumed with a modal radius $r_m = 37\,\text{nm}$ and $\sigma = 1$. The effective radius and effective variance are defined in case of Eq. (4.9) as follows: $r_{\text{ef}} = r_0 \exp(2.5\sigma^2) = 1218\,\text{nm}$ and $v_{\text{ef}} = \exp(\sigma^2) - 1 = 1.7$ (Kokhanovsky, 2008, p. 5). The spectral extinction K_λ^{ext} and phase function $P_\lambda^{aer}(\Theta)$ are calculated using Lorenz–Mie scattering theory (Kokhanovsky, 2008). $P_{550\,nm}^{aer}(\Theta)$ is shown by the dashed line in Fig. 4.1. ω_λ^{aer} and the aerosol asymmetry parameter g^{aer} are set to 1.0 and 0.775, respectively. Reference values for the AOD retrieval using the synthetic dataset are given in Table 4.1. See Kokhanovsky, 2008, p. 2-6 and Kokhanovsky et al. (2010b) for details on complete input parameters. The $R_{550\,\text{nm}}^{Data}$ values of the synthetic dataset are shown in Fig. 4.2 (circles).

Table 4.1.: *τ_λ^{aer} denotes the spectral aerosol optical depth as input to the computation of the synthetic data using SCIATRAN as well as benchmark to evaluate the retrieval accuracy of iSMART. See Kokhanovsky, 2008, p. 2-6 and Kokhanovsky et al. (2010b) for further input parameters.*

λ, nm	τ_λ^{aer}					
412	0.0500	0.1000	0.2000	0.3000	0.4000	0.5000
550	0.0498	0.0995	0.1990	0.2986	0.3981	0.4976
865	0.0467	0.0935	0.1870	0.2805	0.3739	0.4674

4.3.2. Airborne remote sensing data

Measurements provide realistic data to validate the proposed AOD retrieval algorithm. We use data acquired by the imaging spectrometer Airborne Prism Experiment (APEX) (Itten et al., 1997; Schaepman et al., 1998; Itten et al., 2008) and concurrent *in-situ* reflectance measurements of surface reference targets in addition to independent aerosol reference data.

The latter were measured *in-situ* by the nearby Aerosol Robotic Network (AERONET, Holben et al., 1998) sunphotometer (Laegern; 47°28.6N, 8°21.9E; 735 m a.m.s.l.). The radiative properties of the aerosols during the APEX overflight are given in Table 4.3. The PSD was derived from AERONET inversions (Dubovik and King, 2000) using Eq. (4.9) with r =193 nm, r_0 =214 nm and σ =0.45. $P_\lambda^{aer}(\Theta)$ was determined using Lorenz–Mie scattering theory with the PSD as shown in Fig. 4.1. It should be noted that there was a hazy atmosphere with a presumably high aerosol concentration during the data acquisition.

The *in-situ* measurements of the surface reflectance were collected during the APEX overflight using portable field spectrometers (see Fig. 4.5). Each reference target is larger than nine APEX pixels (roughly 28 m^2; see Figs. 4.4b to 4.4e).

Table 4.2 provides the main APEX instrument specifications. Data were acquired in June 2010 close to Zurich, Switzerland (47°28.0N, 8°18.6E; 390 m a.m.s.l.). A true color subset of the data is shown in Fig. 4.4 with zooms on the surface reference targets.

Table 4.2.: *APEX instrument specifications (Itten et al., 1997; Schaepman et al., 1998; Itten et al., 2008).*

Type of instrument	Dispersive push-broom imaging spectrometerfication
Spectral range	380 – 2500 nm
Spectral bands (binned mode)	313
Spectral sampling interval	0.5 – 10 nm
Spectral resolution (FWHM)	0.6 – 11 nm
Spatial pixels (across-track)	1000
Field of view (FOV)	28°
Spatial resolution	1.75 m at 3500 m a.g.l.

Table 4.3.: *Independent* in-situ *measurements of optical and micro-physical aerosol properties from the Laegern AERONET site. τ_λ^{mlc} and τ_λ^{aer} denote the spectral molecular and aerosol optical thickness, respectively. ω_λ^{aer} is the aerosol single-scattering albedo and g^{aer} the aerosol asymmetry parameter.*

λ, nm	τ_λ^{mlc}	τ_λ^{aer}	refractive index	ω_λ^{aer}	g_λ^{aer}
440	0.224	0.619	$1.437-0.00157i$	0.990	0.732
675	0.039	0.304	$1.424-0.00156i$	0.987	0.664
870	0.014	0.185	$1.426-0.00155i$	0.985	0.601
1020	0.007	0.119	$1.422-0.00155i$	0.982	0.558

(a) *Subset of the APEX data. The reference target areas are marked within the boxes.*

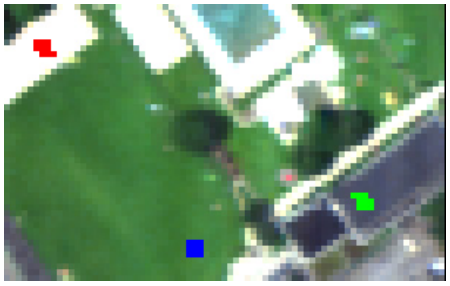

(b) *Zoom on the reference targets: grass (blue), sand (red), roof (green).*

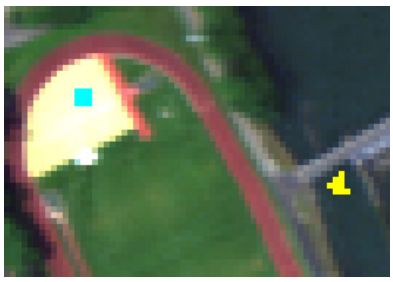

(c) *Zoom on the reference targets: water (yellow), track (cyan).*

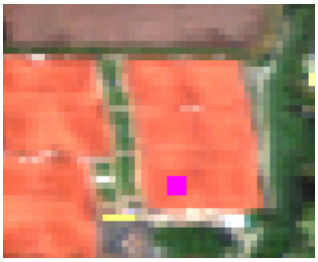

(d) *Zoom on the reference targets: tennis court (magenta).*

(e) *Zoom on the reference targets: asphalt (maroon).*

Figure 4.4.: *Subset of the APEX data with the surface reference targets in true color.*

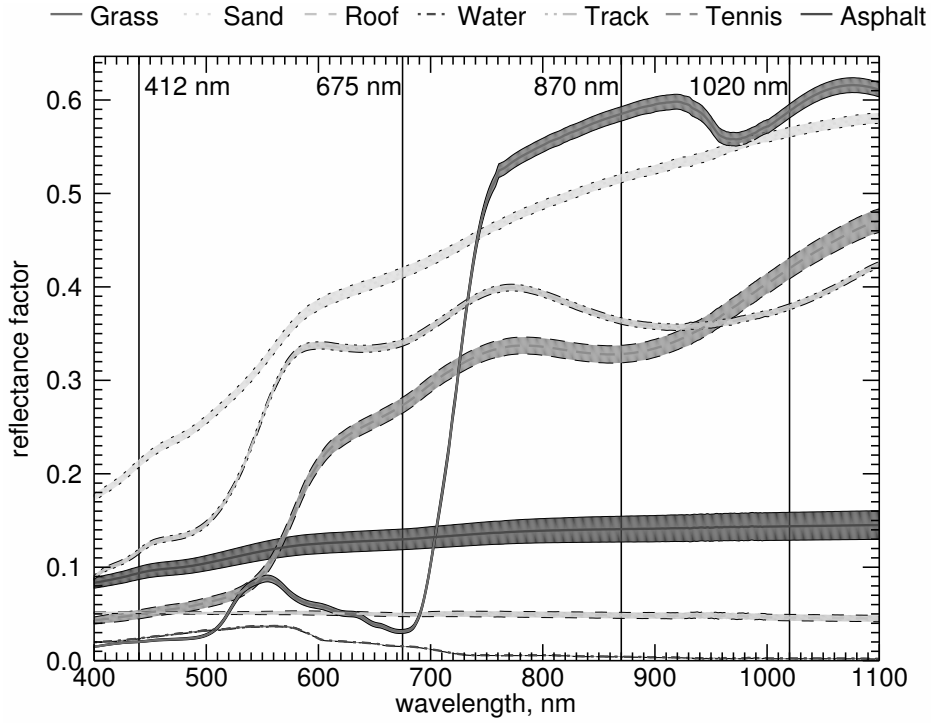

Figure 4.5.: *Measured reflectance factor of the surface reference targets. The variability is represented by* ± 1 *standard deviation around the average reflectance factor. The vertical lines denote the wavelengths for AOD retrieval.*

4.4. Results

4.4.1. AOD retrieval accuracy using synthetic data

The use of synthetic data (see Sect. 4.3.1 and Table 4.1) is important for an initial evaluation of iSMART's accuracy. In this formal study, we use the same input values $P_\lambda^{aer}(\Theta)$, ω_λ^{aer} and surface albedo a as they were used for the SCIATRAN benchmark calculations. We assess the absolute error of the retrieved AOD using iSMART as follows:

$$\Delta\tau_\lambda^{aer} = \tau_\lambda^{aer,SCIATRAN} - \tau_\lambda^{aer,iSMART}. \tag{4.10}$$

The Results are shown in Fig. 4.6 as a function of AOD and in Fig. 4.7 as a function of surface albedo[2]. The expected uncertainty of the MODIS "dark-target" AOD retrieval algorithm over land is given as a reference in the same figures. It is defined by: $\pm 0.05 \pm 0.15\tau_\lambda^{aer}$ valid at $a \leq 0.25$ (Remer et al., 2005; Levy et al., 2009, 2010). The aerosol optical properties are *a priori* known from the input parameters used to prepare the synthetic data.

Fig. 4.6a provides $\Delta\tau_\lambda^{aer}$ (Eq. 4.10) for a dark surface with $a = 0.1$. The error is small and mostly within the MODIS uncertainty envelope at all investigated wavelengths and AOD values. The small AOD overestimation is caused mainly due to the underes-

[2]See Appendix A.3 for additional results.

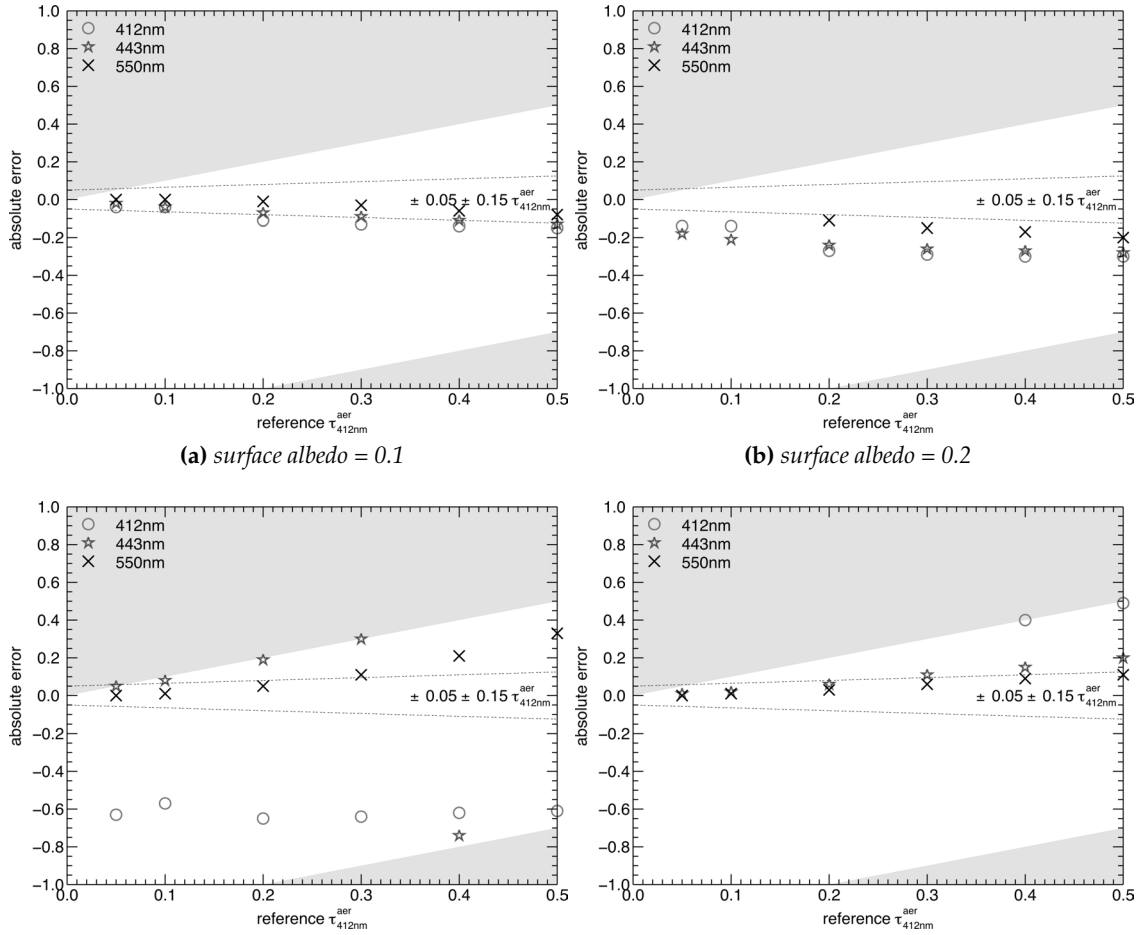

(a) *surface albedo = 0.1*

(b) *surface albedo = 0.2*

(c) *surface albedo = 0.3*

(d) *surface albedo = 0.7*

Figure 4.6.: *Absolute error of AOD retrieval as a function of AOD. Calculations were performed using iSMART and compared to SCIATRAN. Retrievals in colored areas are not feasible because either* $\tau_{412nm}^{aer} < 0$ *or* $\tau_{412nm}^{aer} > 1.2$*. The dotted lines denote the expected uncertainty range of the MODIS dark-target (*$0.01 \leq a \leq 0.25$*) AOD retrieval.*

timation of R^{TOA} by the aerosol scattering approximation (Eq. 4.5). The analysis shows larger $\Delta\tau_{\lambda}^{aer}$ for $a = 0.2$ (Fig. 4.6b) and 0.3 (Fig. 4.6c). The AOD is still overestimated by iSMART in the case of $a = 0.2$, except for 865 nm and $\tau_{412\,nm}^{aer} \leq 0.1$, where negative AOD values were rejected. iSMART strongly overestimates AOD at 412 nm and underestimates at 865 nm in case of $a = 0.3$. At 550 nm, there is a change from under- to overestimation for $\tau_{\lambda}^{aer} \in [0.3, 0.4]$. The errors are large, because R_{λ}^{TOA} is a very weak function of AOD at these surface albedos and the AOD retrieval is therefore very sensitive to small uncertainties, especially of surface albedo. This effect is discussed in Sect. 4.4.3.1. An example for results over brighter surfaces with $a \geq 0.4$ are shown in Fig. 4.6d with an underestimation of retrieved AOD. $\Delta\tau_{\lambda}^{aer}$ is for the most part within the MODIS expected uncertainties, except for the results at 412 nm.

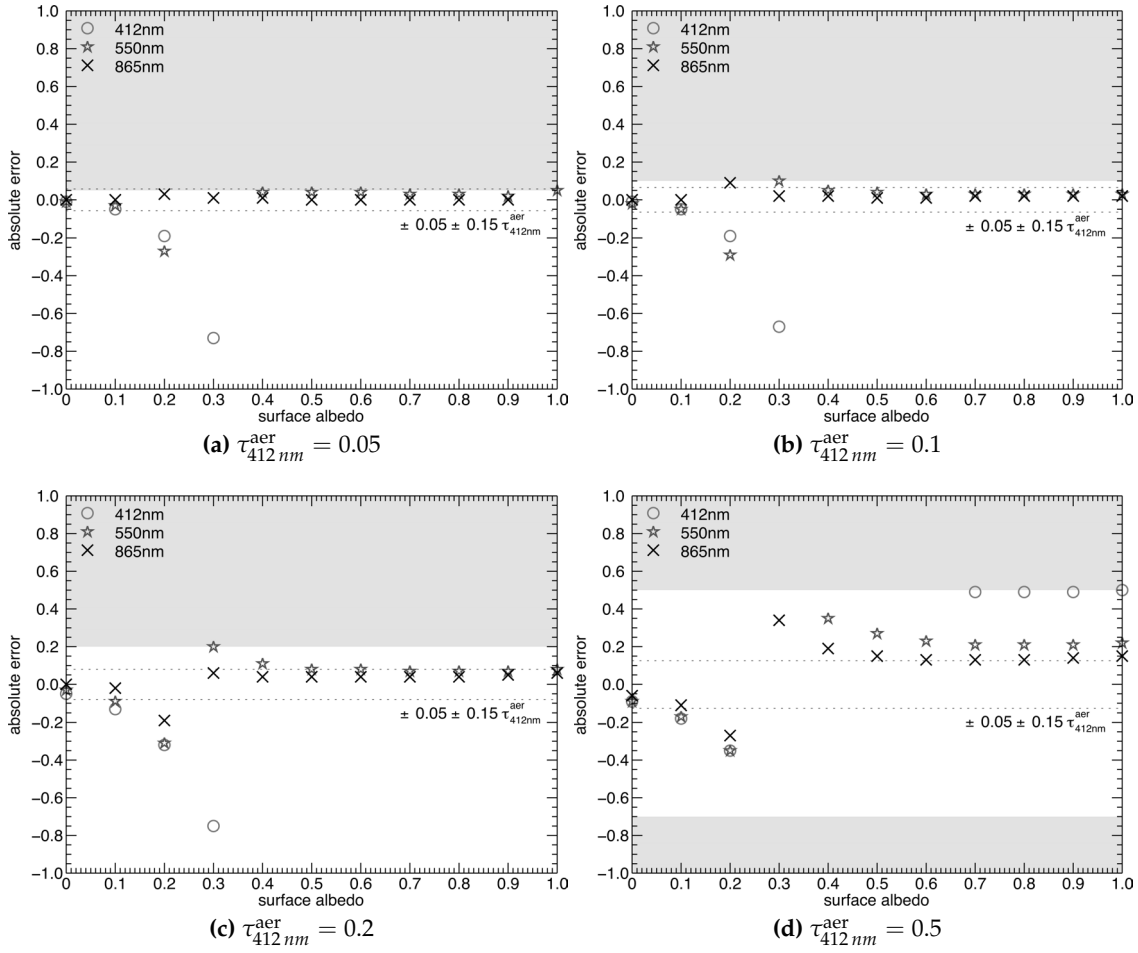

(a) $\tau^{\text{aer}}_{412\,nm} = 0.05$ **(b)** $\tau^{\text{aer}}_{412\,nm} = 0.1$

(c) $\tau^{\text{aer}}_{412\,nm} = 0.2$ **(d)** $\tau^{\text{aer}}_{412\,nm} = 0.5$

Figure 4.7.: *Absolute error of AOD retrieval as a function of surface albedo. Calculations were performed using iSMART and compared to SCIATRAN. Retrievals in colored areas are not feasible because either* $\tau^{aer}_{412nm} < 0$ *or* $\tau^{aer}_{412nm} > 1.2$*. The dotted lines denote the expected uncertainty range of the MODIS dark-target (*$0.01 \leq a \leq 0.25$*) AOD retrieval.*

Fig. 4.7 shows the same results as a function of a to emphasize the effect of surface albedo on the retrieval[3]. The retrievals at 550 nm and 865 nm are mostly within the MODIS expected uncertainties. It is obvious that the combination of short wavelengths ($\lambda \leq 500$ nm) with $a \geq 0.2$ leads to larger $\Delta\tau^{aer}_{\lambda}$ because the error due to SMART's scattering approximations is amplified by a. The influence of $a \approx 0.3$ on AOD retrievals (see Figs 4.6c and 4.7) is further analyzed in Sect. 4.4.3.1.

It may be noted that most land surfaces are generally dark in the blue part of the solar spectrum (see Fig. 4.5). The results of $\Delta\tau^{aer}_{412nm}$ at $a > 0.2$ in Figs. 4.6 and 4.7 are therefore more of theoretical interest.

[3]See Appendix A.3 for additional results.

4.4.2. AOD retrieval accuracy using airborne remote sensing data

The combined effects of all influences on the AOD retrieval were analyzed using airborne imaging spectrometer data, as well as surface and aerosol reference measurements (see Sect. 4.3.2). APEX's high spectral and spatial resolution data show that even water and artificial surfaces contain spectral features of e.g. vegetation due to adjacency effects by the hazy and strongly scattering atmosphere. We approximate this effects using the following simple linear forward mixing model for surface albedo with empirical coefficients: $a = a_{target} \cdot 0.8 + a_{surround} \cdot 0.2$, where $a_{surround}$ is estimated from the image data within a radius of 200 m around the targets.

Fig. 4.8 shows AOD results inverted from APEX data using iSMART[4]. The aerosol reference data were measured by AERONET on a nearby hill, which is 380 m above the APEX data. The measured AOD values (solid line) are therefore extrapolated to the level of the image data using the RT model 6S (dotted line). These results show that iSMART is feasible to determine AOD from APEX data. However, there is a relatively large spread in the retrieved AOD at 440 nm due to SMART's scattering approximations as well as neglected aerosol–molecule coupling and polarization. The results at 675 nm deviate significantly when using the *in-situ* reference targets sand, track and tennis court. Interestingly, these targets have an $a_{675\,nm}$ in the range of 0.25–0.4, which has already been found to be difficult for the AOD retrieval (see Fig. 4.7 and Sects. 4.4.1 and 4.4.3.1). Longer wavelengths provide good results, which is a further agreement to the previous findings in Sect. 4.4.1.

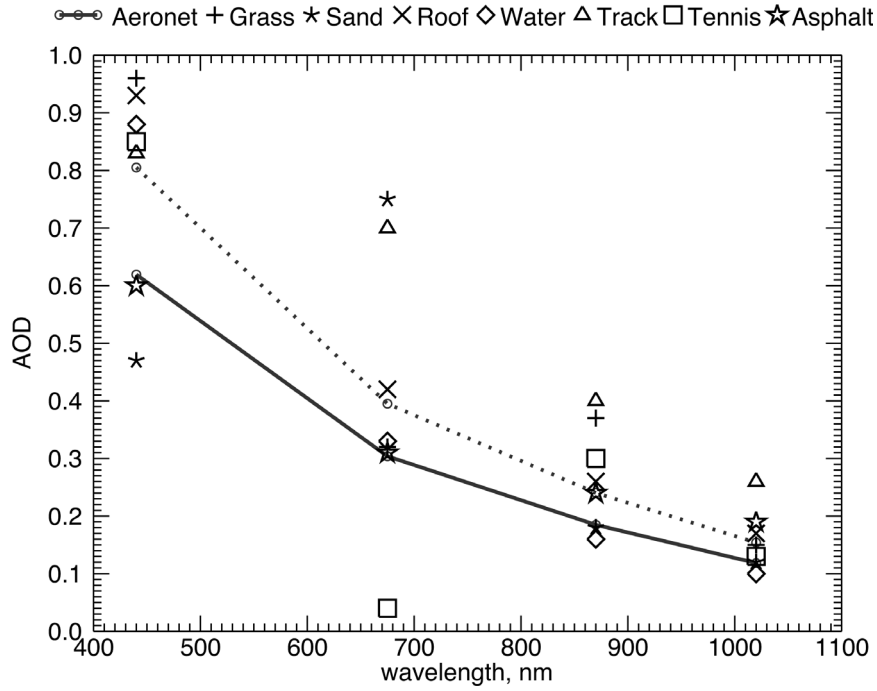

Figure 4.8.: *Results of the AOD retrieval using APEX data on various* in-situ *reference targets. The solid line shows the AERONET reference AOD, which was measured on a nearby hill. The dotted line shows the extrapolated AOD, which corresponds to the elevation of the image data.*

[4]See Appendix A.4 for the absolute retrieval error: $\tau_\lambda^{aer,AERONET} - \tau_\lambda^{aer,iSMART}$.

4.4.3. Sensitivity of the AOD retrieval to surface albedo

In the following, we analyze the sensitivity of the AOD retrieval to surface albedo using again the synthetic data introduced in Sect. 4.3.1.

4.4.3.1. Critical surface albedo

AOD retrieval problems are found in Figs. 4.6 and 4.7 for $a \approx 0.3 \pm 0.1$. For about the same a, there is almost no influence of AOD on $R^{TOA}_{550\,nm}$ (see Fig. 4.2). Such a is therefore posing difficulties for the AOD retrieval. The term critical surface albedo (CSA) was used in that sense by Fraser and Kaufman (1985), Hsu et al. (2004), Popp et al. (2007), Seidel et al. (2008), Zhu et al. (2011) and others. An example for the CSA is shown in Fig. 4.9 around $a_{550\,nm} = 0.3$, where all SMART calculations for $\tau^{aer}_{550\,nm} \in [0.0(0.2)0.6]$ provide almost the same R^{TOA}_{λ}. The aerosol absorption and backward scattering are reducing the transmittance at the same time as the forward scattering is increasing the signal from the atmosphere. Fig. 4.9 shows also that additional AOD increases R^{TOA}_{λ} for $a < CSA$ and *vice versa* (see also Fig. 4.2). Thus, the net effect is positive at dark surfaces, negative at bright surfaces and zero at $a = CSA$. The CSA depends mainly on ω^{aer}_{λ} (Fraser and Kaufman, 1985; Popp et al., 2007) , K^{ext}_{λ}, μ_0, μ, λ and slightly on aerosol particle concentration (Zhu et al., 2011).

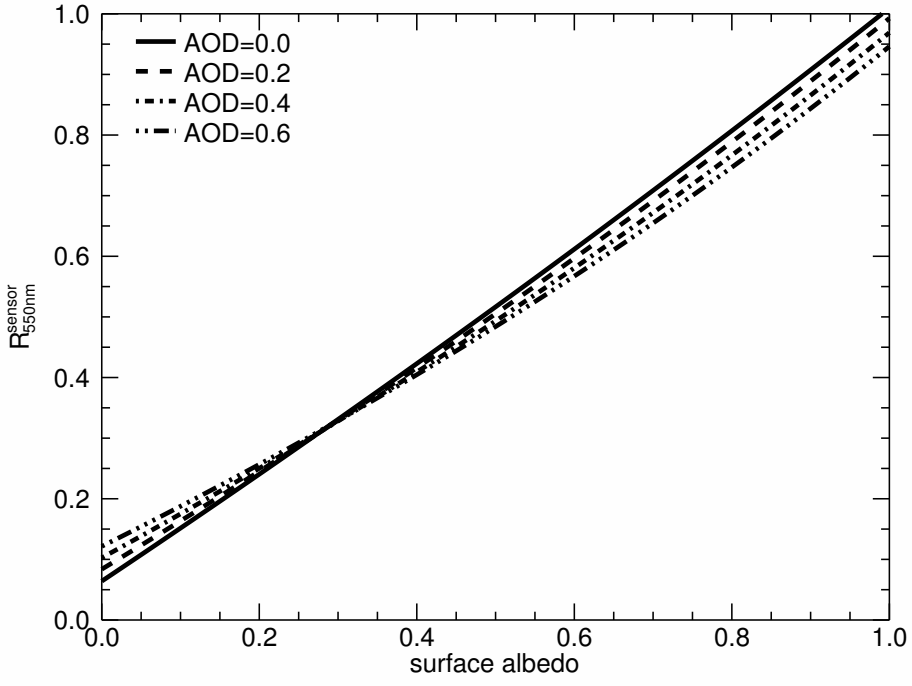

Figure 4.9.: *Reflectance $R^{TOA}_{550\,nm}$ using SMART (Eq. 4.2) with respect to surface albedo a at SZA=60° for average continental aerosols and different AOD levels. Additional AOD increases $R^{TOA}_{550\,nm}$ for $a < 0.3$ and* vice versa. *At $a \approx 0.3$ (critical surface albedo), $R^{TOA}_{550\,nm}$ does not depend strongly on AOD.*

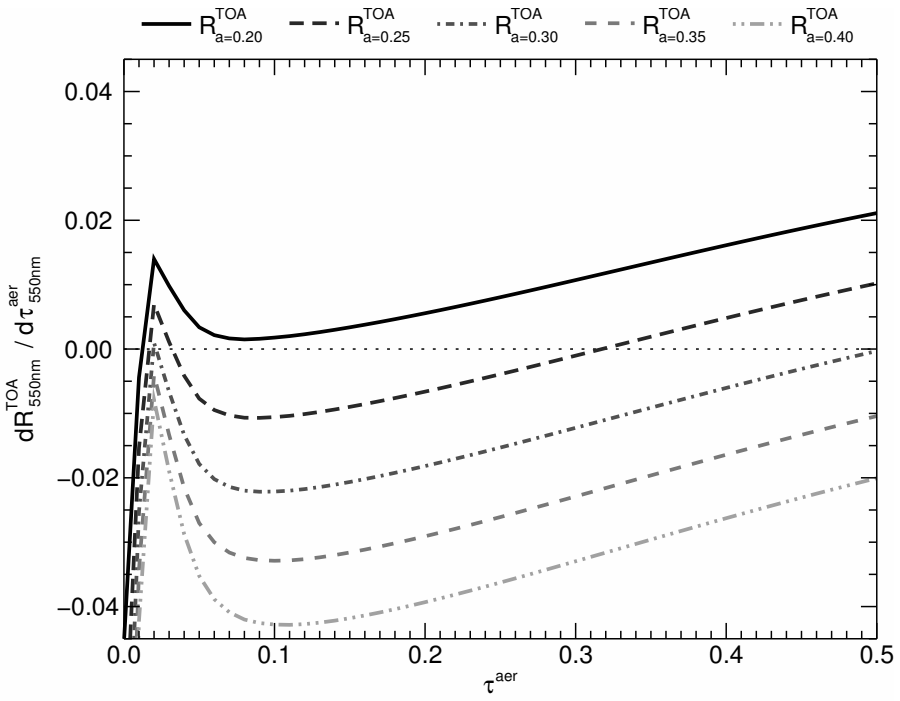

Figure 4.10.: *Derivative of reflectance $R^{TOA}_{550\,nm}$ with respect to AOD according to Eq. (4.11). Positive values indicate an increase of R^{TOA}_{λ} for an increasing AOD, and* vice versa. *Values close to zero indicate a weak dependence of $R^{TOA}_{550\,nm}$ on AOD and therefore, a small uncertainty in $R^{TOA}_{550\,nm}$ translates into a large AOD uncertainty.*

To understand better the relationship between R^{TOA}_{λ}, τ^{aer}_{λ} and a_{λ}, we use the derivative of the reflectance with respect to AOD:

$$\frac{dR^{TOA}_{\lambda}}{d\tau^{aer}_{\lambda}} \begin{cases} > 0 & \text{if aerosols increase reflectance.} \\ = 0 & \text{if aerosols have no effect on reflectance.} \\ < 0 & \text{if aerosols decrease reflectance.} \end{cases} \tag{4.11}$$

for different surface albedos. The results using Eq. (4.11) are given in Fig. 4.10, where aerosols increase R^{TOA} at all $a \leq 0.2$ and *vice versa* at $a \geq 0.3$. The aerosol effect on R^{TOA} is small for $a = 0.25 \pm 0.05$. The CSA in this range is found to be a function of AOD, where Eq. (4.11) is equal to zero.

Sensors are limited in sensitivity, which is defined by the noise equivalent reflectance difference $\mathrm{NE}\,dR = R^{TOA} \cdot \mathrm{Noise/Signal}$ (Schläpfer and Schaepman, 2002). Typical values of $\mathrm{NE}\,dR$ are found between 0.01 and roughly 0.002. $\pm\mathrm{NE}\,dR$ is an instrument specific envelope around the zero derivative of Eq. (4.11), where the aerosol induced signal is within the noise level and therefore impossible to be retrieved by the proposed method. See Seidel et al. (2008) for a further discussion on sensor performance requirements for AOD retrieval.

4.4.3.2. Influence of uncertainties in surface albedo

It follows from previous findings that the AOD retrieval is very sensitive to surface albedo, which is mostly not known *a priori* and has to be assumed by statistics, climatologies or retrieved by additional concurrent measurements. Airborne remote sensing campaigns (see e.g. Sect. 4.3.2) have the particular advantage that independent *in situ* measurements from field spectrometers can be collected. Nevertheless, even these measurements have an individual uncertainty(Milton et al., 2009), which may bias the retrieval of AOD.

We analyze this effect using iSMART and show the results in Fig. 4.11[5]. An uncertainty in a is simulated by a deviation d from the true surface albedo, such that $a_{error} = a_{true} \pm d$, where $d \in [0.005, 0.01, 0.05]$. The results confirm that the AOD retrieval at dark surfaces ($a \leq 0.1$) is more robust to surface albedo uncertainties than at bright surfaces. An uncertainty of 1% ($d = 0.01$) leads to a difference in retrieved AOD of roughly 0.2 at a dark surface (see Fig. 4.11a). For $a \leq 0.3$, an overestimation of the surface albedo causes an overestimation of AOD. Retrievals at 400 nm and at SZA=60° are more robust at dark targets than at 700 nm and at SZA=30°. Some retrievals were even rejected at $a = 0.3$. It is obvious from Sect. 4.4.3.1 that even small uncertainties in surface albedo close to the CSA are leading to large variations in the retrieved AOD as shown in Fig. 4.11d. The errors at $d = 0$, $a = 0.4$ and SZA=30° occurred because iSMART identified false local minima. In general, SZA=30° was found to be more sensitive to surface albedo uncertainties than SZA=60°.

4.5. Summary and conclusions

Fairly successful techniques and algorithms were developed for satellite aerosol remote sensing in the past three decades. Growing amounts of data are available for the study of aerosol distribution on the global scale. The corresponding advanced retrieval algorithms are often adapted for a specific satellite sensor and are mostly based on look-up-table approaches.

We therefore propose the fast, simple and flexible AOD retrieval algorithm iSMART. A short validation using synthetic data from SCIATRAN and airborne imaging spectrometer data from APEX have proven its feasibility. Retrieval errors using synthetic data were found to be in the same order of magnitude as the accuracy of the MODIS "dark target" AOD retrieval algorithm. The AOD retrieval using APEX data also generates promising results. The best retrieval accuracy is found in the near-infrared (e.g. 865 nm) for all surface albedo values using iSMART under the investigated conditions. The retrieval at 412 nm is less accurate due to neglected higher orders of aerosol scattering, as well as polarization and coupling of the aerosol–molecular scattering in the current version of SMART. Pronounced adjacency effects were observed by APEX due to haze in the lower atmosphere, which are not yet fully taken into account by SMART.

It was found that surface albedo and its associated uncertainty have a large influence on the AOD retrieval. A surface albedo between 0.25 and 0.4 can lead to large retrieval

[5]See Appendix A.6 for additional results.

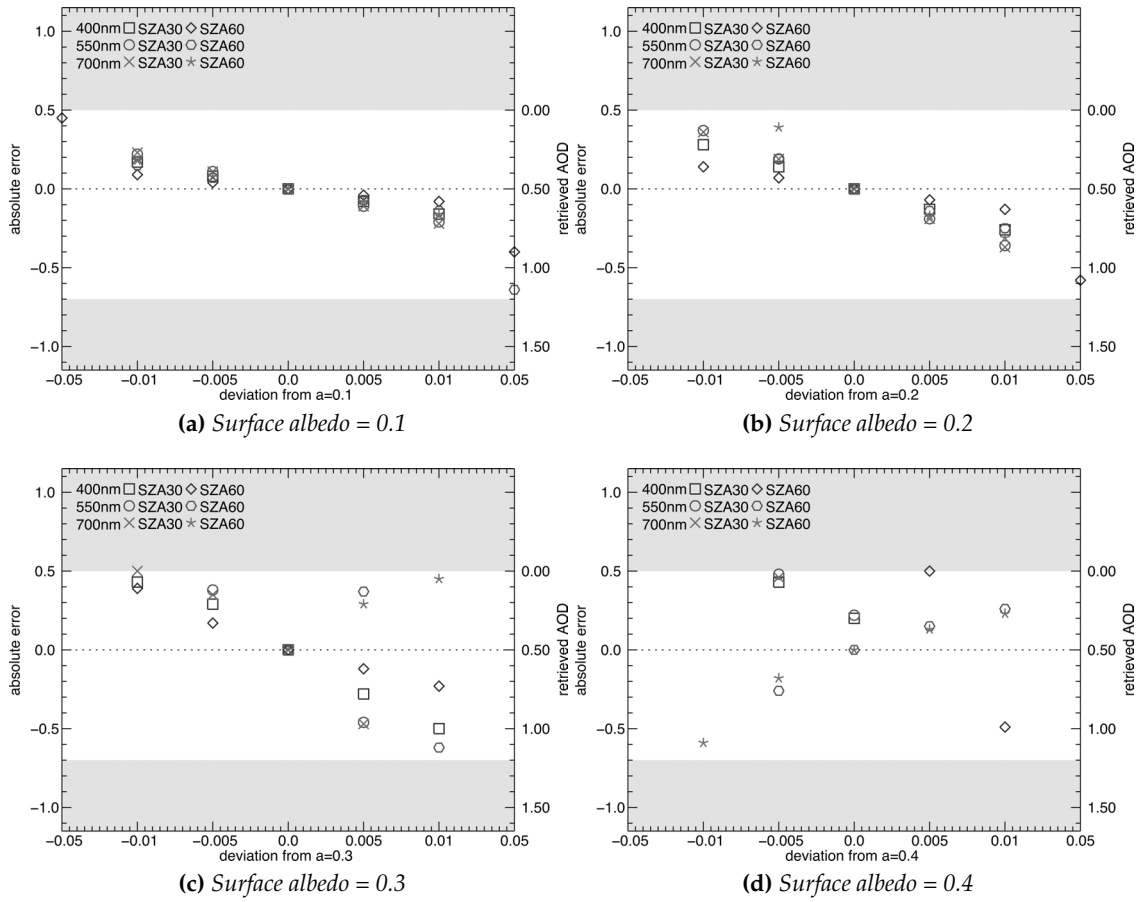

(a) *Surface albedo = 0.1* **(b)** *Surface albedo = 0.2*

(c) *Surface albedo = 0.3* **(d)** *Surface albedo = 0.4*

Figure 4.11.: *Absolute error of AOD retrieval using iSMART as a function of surface albedo uncertainties at* $\tau^{\text{aer}}_{412\,nm} = 0.5$. *The uncertainties are simulated by a deviation from the true surface albedo. Retrievals in the colored areas are not feasible because either* $\tau^{aer}_{412nm} < 0$ *or* $\tau^{aer}_{412nm} > 1.2$.

errors because the upwelling solar radiation does not depend strongly on AOD at the critical surface albedo(Fraser and Kaufman, 1985; Hsu et al., 2004; Popp et al., 2007; Seidel et al., 2008). It was found that an uncertainty in the surface albedo of 1% can translate in some cases to an AOD error of 0.2. The influence of uncertainties in the scattering phase function, size distribution and other parameters was not investigated.

Future versions of iSMART should account for three-dimensional radiative effects at the surface–atmosphere interface. Further extensions should comprise a statistically optimized inversion algorithm according to Dubovik et al. (2010), which would increase the retrieval accuracy and allow simultaneous retrievals of surface albedo and more complete aerosol properties. However, the latter requires multi-directional and polarized measurements to take advantage of the full information content of solar radiation.

We conclude that the proposed fast and simple algorithm is feasible for retrieving AOD with a promising accuracy from remote sensing data, given that the surface albedo is sufficiently known. iSMART is therefore particularly suited to applications requiring computational speed.

Acknowledgments

The work of A. A. Kokhanovsky was performed in the framework of DFG Project Terra. The Mie results were computed using a Mie code developed by the Sub-Department of Atmospheric, Oceanic and Planetary Physics, University of Oxford, UK. We thank C. Popp for the valuable discussions about the sensitivity of the surface albedo with regard to the aerosol retrieval. We also would like to thank the anonymous reviewers and A. Schubert for their valuable comments and suggestions, which helped to improve the manuscript.

5. Synopsis

As introduced in Chap. 1, aerosol remote sensing is very important to improve climate models by advancing our knowledge on the spatial distribution of atmospheric particles. Moreover, quantitative Earth observations requires the compensation of atmospheric influences on solar radiation in order to derive the reflectance factor at the surface or canopy level with less than 1% absolute error (Richter and Schläpfer, 2002). This atmospheric correction process requires an RT model and *a priori* knowledge on atmospheric constituents and state variables. It is shown in Chap. 2 that AOD should be known with an accuracy of about ± 0.01 to ± 0.05 to meet the 1% surface reflectance accuracy requirement.

5.1. Main findings

An AOD retrieval method using the RT model MODTRAN4 (Berk et al., 1989) and the APEX airborne imaging spectrometer was proposed in Seidel et al. (2005) and Itten et al. (2008). It follows the idea of a two-channel approach in the near-UV/Blue spectral range. Its general feasibility was proved in Seidel et al. (2006) using a dataset from the Portable Hyperspectral Imager for Low Light Spectroscopy (PHILLS) (Davis et al., 2002; Kohler et al., 2004; Bowles et al., 2005). But at the same time, it was found that the accuracy of the near-UV/Blue approach is limited by sensor calibration, which is usually better at longer wavelengths. It was also shown in Seidel et al. (2005) and Seidel et al. (2006) that MODTRAN4 may not be the optimal choice with respect to aerosol retrieval because it has only one rural aerosol model implemented.

All the above provides the context for the thesis's main objectives (see Sect. 1.3), which are the development of a fast and flexible RT algorithm (see Chap. 3 and Seidel et al. (2009)) and its elaboration to retrieve AOD using remote sensing data (see Chap. 4). Corresponding research questions were defined on page 5 in order to achieve this ambition. They are recapitulated in *italics* together with the corresponding main findings and conclusions.

What are the sensor performance requirements for aerosol retrieval with remote sensing instruments?

Chap. 2 has shown that the detection of aerosols is feasible with APEX for low, average and high spectral radiance levels under the evaluated conditions (ie. viewing and sensor configuration). The instrument sensitivity requirements for a successful AOD retrieval is met by the preflight sensor performance of APEX. It was also found that the spectral SNR is crucial for aerosol remote sensing and varies strongly with surface reflectance. The latter is strongly influencing the intensity of L_{λ}^{sensor} as a function of SNR. Dark surfaces ($a_{550\,nm} < 0.1$) have the lowest SNR demands for aerosol retrieval.

More critical are relatively bright surfaces ($0.4 < a_{550\,nm} < 0.6$) because $L^{sensor}_{550\,nm}$ is a weak function of $\tau^{aer}_{550\,nm}$. Generally, it was shown that an SNR of 300 or better will provide satisfying aerosol retrieval results for most surface reflectances considered in this analysis. Restricting the ranges to $\tau^{aer}_{550nm} < 0.25$ and $a_{550\,nm} < 0.2$, which are optimal and representative airborne remote sensing conditions, an SNR of 100 is adequate. This is a promising finding because most current instruments fulfill such SNR requirements under typical conditions. This theoretical results are confirmed by Chap. 4 using APEX data from the year 2010.

Is it feasible to simulate radiative transfer in the atmosphere faster and with less complexity than in existing algorithms? What is the trade-off between computational speed and accuracy?

Chap. 3 presents very promising results. It was found that even relatively simple equations combined with adequate approximations are capable of simulating most of the optical processes in the atmosphere. These equations are the basis to the fast and Simple Model for Atmospheric Radiative Transfer (SMART) implemented in the IDL computer language. SMART is validated against 6S benchmark results to verify its accuracy and performance. It was found that SMART fulfills its design principles: it is fast, flexible and simple, yet relatively accurate. It computes more than 20 reflectance results per second on a standard desktop computer. This is more than 25 times faster than the benchmark RT model. The overall relative error was found to be about 5% for spaceborne and 5–10% for airborne observational cases. SMART exceeds the desired accuracy goal of 5% in the spaceborne case only in the blue spectral region and for large AOD or SZA values.

How well can aerosol optical depth be retrieved with a simplified radiative transfer model? How large is the influence of the surface albedo on such a retrieval?

Chap. 4 proposes an AOD retrieval algorithm called iSMART. It is based on Chap. 3 with improved aerosol scattering using Mie theory. A concise validation verifies the feasibility of iSMART to retrieve AOD using both datasets: simulated (benchmark RT model SCIATRAN) and measured (APEX). Retrieval errors using synthetic SCIATRAN data are in the same order of magnitude as compared to the official uncertainty envelope of the MODIS "dark target" algorithm. Pointwise AOD retrieval using APEX data provides also promising results. Further, it was found that surface albedo and associated uncertainties have a huge influence on AOD retrieval. Especially for underlying surface albedo between roughly 0.25 and 0.5, where AOD has only a small influence on the measured upwelling solar radiation at sensor level (see also Chap. 2). It is shown that 0.01 uncertainty in surface albedo can turn into an AOD retrieval uncertainty of 0.2. Overall, the proposed algorithm of reduced complexity provides fast retrievals and promising accuracy, presuming that surface albedo is *a priori* known. iSMART can be used therefore especially for applications preferring fast computations.

Special attention should be given to the findings in Sect. 4.4.3 and especially to the results in Fig. 4.11 and Fig. A.12 in the following Appendix A.6. They support the conclusion that AOD retrievals should use only dark targets in order to remain less

sensitive to surface albedo uncertainties. Even then, surface albedo uncertainty of more than 1–5% may lead to wrong AOD results.

5.2. Synthesis

The dissertation has achieved both objectives and provides detailed answers to the corresponding research questions introduced in Sect. 1.3. A summary of the main findings is given in Sect. 5.1 with a link to the related research questions.

The performance of the newly developed fast RT algorithm SMART, as well as its inverse derivate for AOD retrieval iSMART, is very promising. iSMART by Seidel et al. (2011) and a similar approach by Katsev et al. (2010) are presumably amongst the first algorithms of a new aerosol retrieval generation reaching beyond classic LUT approaches by exploiting the remote sensing data themselves to directly infer certain aerosol properties. Similar algorithms are currently under development for the (airborne) Multiangle SpectroPolarimetric Imager (MSPI) being built by JPL (Diner et al., 2007, 2010), and the Aerosol Polarimetry Sensor (APS) on NASA's Glory satellite (Mishchenko et al., 2004) (David Diner, personal communication, May 6, 2010). This underlines the great potential of the fast and simple AOD retrieval algorithm iSMART, which is presented in this dissertation thesis.

Furthermore, it is with satisfaction to realize that some of the main findings in this thesis (see Chap. 4 and Sect. 5.1) can be linked to the latest IPCC report (Solomon et al., 2007) and its conclusions on the large uncertainties of aerosol radiative forcing (see Fig. 1.1). Important knowledge could be obtained on the influence of interactions between aerosols (i.e. AOD) and surface albedo on the upwelling visible radiance or R^{TOA}. These results may provide a small contribution to an increased level of scientific understanding with regard to the uncertainties in aerosol radiative forcing.

5.3. Outlook

This dissertation may provide the thin end of the wedge and more comprehensive research is certainly needed to address the above mentioned problems of aerosol radiative forcing. The findings in Sect. 4.4.3 on the strong influence of surface albedo and its uncertainty on AOD retrieval lead to new challenges and open questions. Initially, it was assumed that airborne remote sensing should be able to avoid such difficulties by using surface reference targets (Seidel et al., 2005, 2006). Chap. 4 has shown that adjacency effects due to a hazy atmosphere may challenge AOD retrievals, especially using high spatial resolution remote sensing data. Thus, more research on clever strategies to retrieve and implement three-dimensional effects at the surface-atmosphere interface should be performed in near future. It should consider non-Lambertian surfaces, adjacency effects (see Sects. 4.4.2 and 4.4.3) and ideally also the three-dimensional structure of the atmosphere with clouds. This would provide the key to the coupling with surface models (i.e. vegetation canopy RT models), which is an important issue also to climate models.

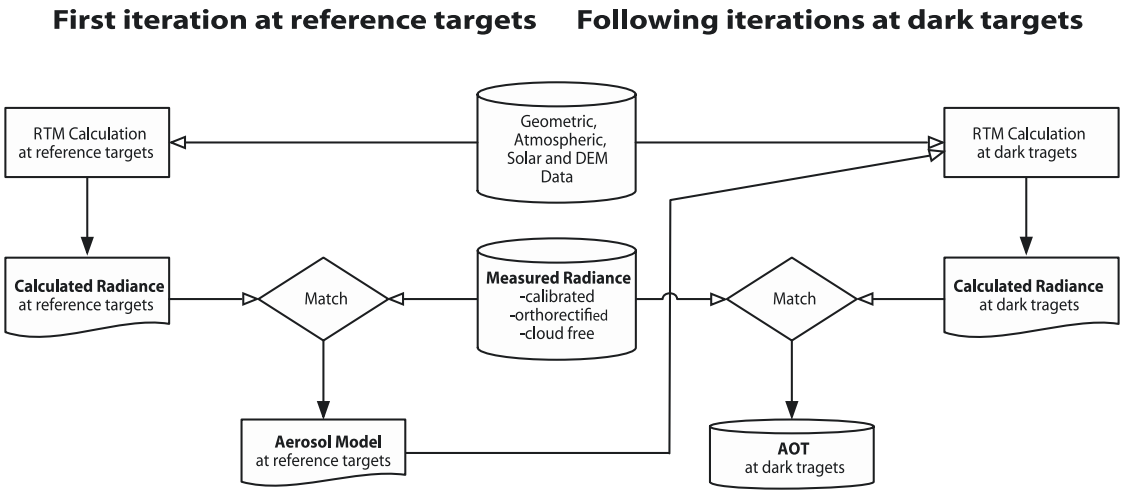

Figure 5.1.: *Processing flowchart of the proposed aerosol retrieval algorithm. The cylinder shapes denote the in- and output data. The rectangle symbolizes the RT model (RTM) calculation steps.*

In order to exploit SMART's and iSMART's full potential, it is suggested to implement the following: molecule-aerosol radiative coupling, additional atmospheric layers, gaseous absorptions (foremost ozone), higher orders of scattering and polarization by vector notation to infer information about the aerosol type (Emde et al., 2010). Further, the potential of APEX or comparable data should be analyzed in more details with regard to a multi-parameter (i.e. surface albedo and AOD) retrieval using more spectral bands and non-nadir observational angles.

The importance of RT modeling and AOD retrieval to the atmospheric correction and therefore to quantitative Earth observation was briefly stated in the beginning if this chapter. The dissertation provides a method for pointwise retrievals, but it would be helpful to have operational retrievals of spatial continuous AOD distribution. It is therefore suggested to extend iSMART by a retrieval strategy for airborne remote sensing as suggested in Seidel et al. (2005, 2006, 2008). The processing flow of the proposed two-dimensional AOD distribution retrieval is drafted in Fig. 5.1. The RT model stores the current atmospheric state with multiple scenarios of possible AOD and aerosol types. The first iteration requires *a priori* knowledge on surface albedo, which is given using field-spectrometer measurements (Goetz et al., 1985) or calibration targets. The RT results are then compared to the measured radiance L^{sensor} as described in Sect. 4.2.2. The algorithm is then searching for "dark" pixels for the following iterations to extend the retrieval to other areas in the image. We know from Chap. 4 that assumptions on the surface albedo of dark pixels have the smallest influence on the AOD retrieval uncertainty.

A. Appendix

A preliminary analysis of a potential aerosol retrieval for the APEX imaging spectrometer is published in Seidel et al. (2005). Its findings on the influence of aerosol type to the upwelling radiance at sensor level are recapitulated as additional information to this thesis in Appendix A.1. Appendices A.2 to A.6 provide complementing results to Chap. 4 because it was not possible to fit all figures into the submitted paper Seidel et al. (2011) on iSMART and the influence of surface albedo on aerosol retrieval.

A.1. Influence of aerosol types on simulated radiances using radiative transfer calculations

It can be concluded from Seidel et al. (2005) that the modeled radiance can significantly change by the use of different aerosol types. It is therefore clear that RT models with only a few fixed aerosol types, such as MODTRAN4 (Berk et al., 1989), may not be able to reproduce accurately radiative effects of real aerosols. RT models are limited by their flexibility in the definition of aerosol optical and microphysical properties. This topic was not discussed in this thesis, because SMART is designed to account for any type of aerosol, as along as it can be described by a log-normal PSD. Nevertheless, the results in Seidel et al. (2005) are recapitulated here to show the influence on RT results of the different aerosol types incorporated to MODTRAN4.

The first result is shown in Fig. A.1. Each dot represents a modeled at-senor reflectance value for a specific AOD (AOT≡AOD). This figure visualizes how the different AOD and different aerosol types are distinguishable from each other in the given plot. The further the different aerosol types are spread, the easier they can be distinguished with two spectral measurements of a remote sensing instrument. Since the rural type is equivalent to the tropospheric type in MODTRAN4, except for its vertical position in the atmosphere, the curves lie very close to each other. In that case, a distinct AOD retrieval would be very difficult for low aerosol concentrations. The maritime and especially the strongly absorbing urban aerosol types can easily be distinguished from each other, even for small aerosol loadings. Furthermore, Fig. A.1 shows the sensitivity of a two-channel retrieval approach to absorbing and non-absorbing aerosols, because the urban aerosol type does not induce a distinct at-sensor apparent reflectance change on a single spectral band. Note that only urban aerosols account for absorption in MODTRAN4 (56% water-soluble, 24% dust-like, 20% absorbing soot).

A further analysis on the effect of aerosol type with different AOD is presented in Figs. A.2 and A.3. The rural, maritime and tropospheric aerosol types induce nearly the same at-sensor signal for AOD=0.7 in near-UV spectral bands, while maritime particles increase the signal close to the O_2 absorption at 765 nm. If the AOD is increased from 0.5 to 2.0, rural types provide an increased signal due to increased scattering, while the

signal with urban particles remains almost the same. The increased absorption compensates the increased scattering in the near-UV spectral region.

Fig. A.3 shows that urban aerosols with AOD=2 lead to the same at-sensor signal as with rural aerosols and AOD=0.5 at roughly 750 nm. This finding emphasizes that a one-channel retrieval procedure may provide ambiguous RT solutions and consequently misinterpretations of the aerosol conditions.

Fig. A.4 shows results for different ground altitudes (0, 1 and 2 km). The rest of the model is kept constant with a sensor located at 5 km altitude. The 2 km difference in surface altitude lead to a difference of about 40% in at-sensor signal for rural aerosols in the blue spectral region (Fig. A.4a). The same is found for absorbing urban aerosols, but with a much lower difference in at-sensor signal (Fig. A.4b). The red spectral region is almost not influenced by changing distances between surface and sensor.

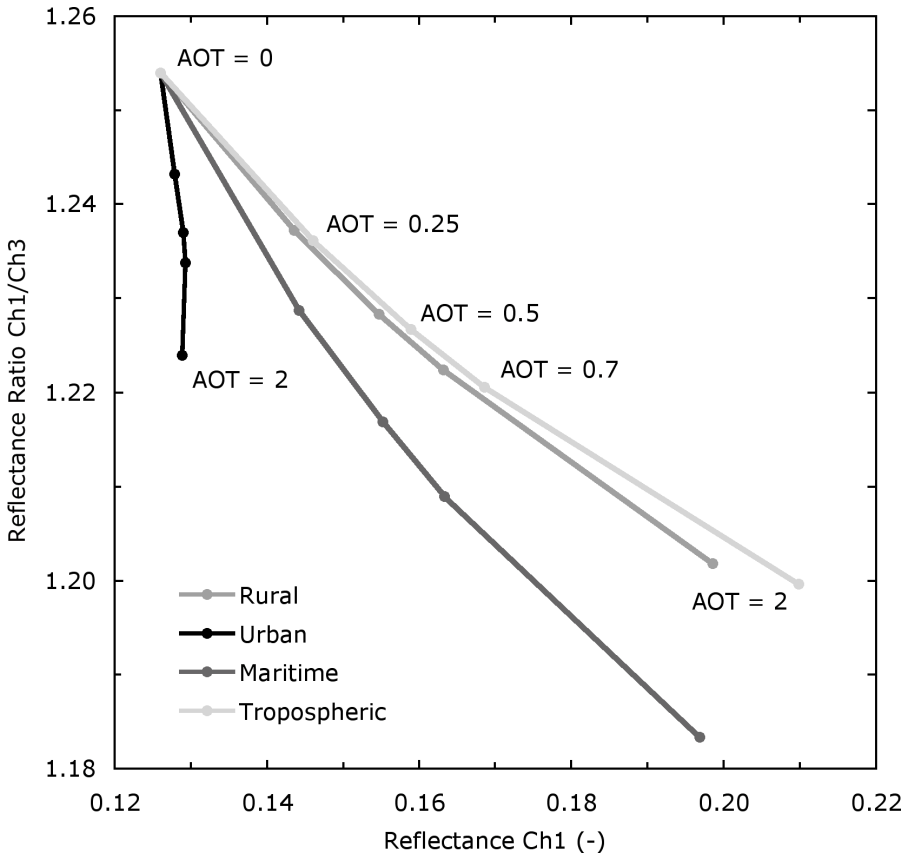

Figure A.1.: *Apparent at-sensor reflectance factor ratio between the two wavelengths 385 nm (Ch1) and 412 nm (Ch3) as a function of the apparent at-sensor reflectance factor at 385 nm. The dots represent different AOD values for each aerosol model (AOT≡AOD). This figure is published in Seidel et al. (2005).*

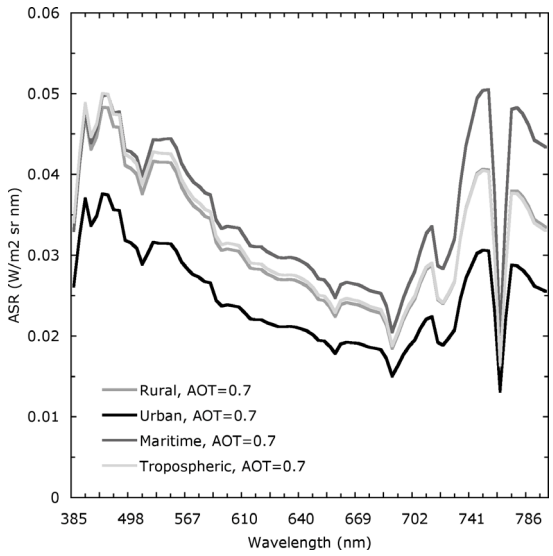

Figure A.2.: *At-sensor radiance (ASR) as a function of wavelength for different aerosol types. The rural and tropospheric types are identical, except for their vertical location in the atmosphere. The surface is a dark target within a green grass background. AOT≡AOD. This figure is published in Seidel et al. (2005).*

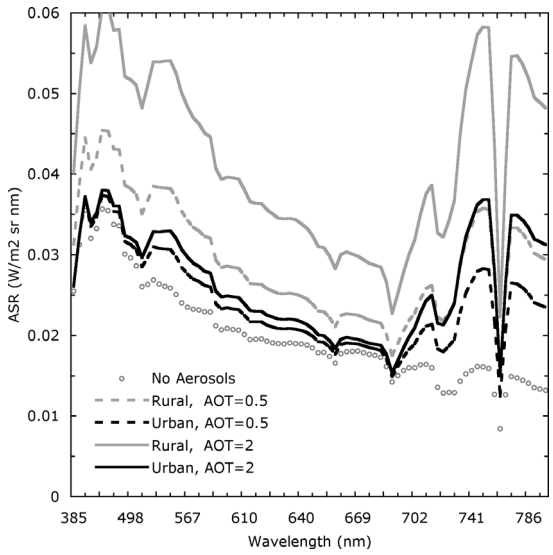

Figure A.3.: *At-sensor radiance (ASR) as a function of wavelength for different aerosol models and AOD. The surface is a dark target within a green grass background. AOT≡AOD. This figure is published in Seidel et al. (2005).*

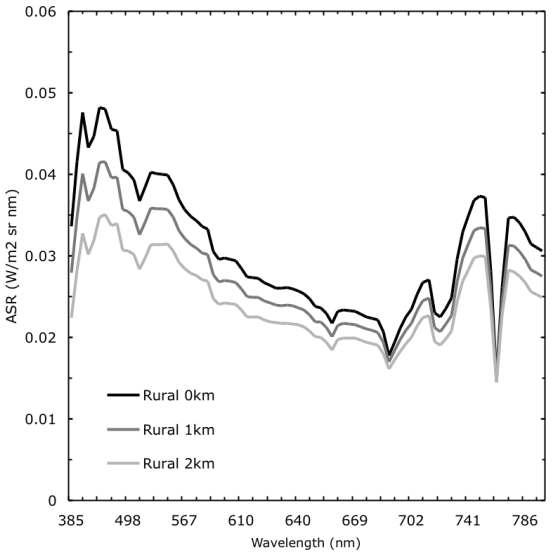

(a) *Rural aerosols*

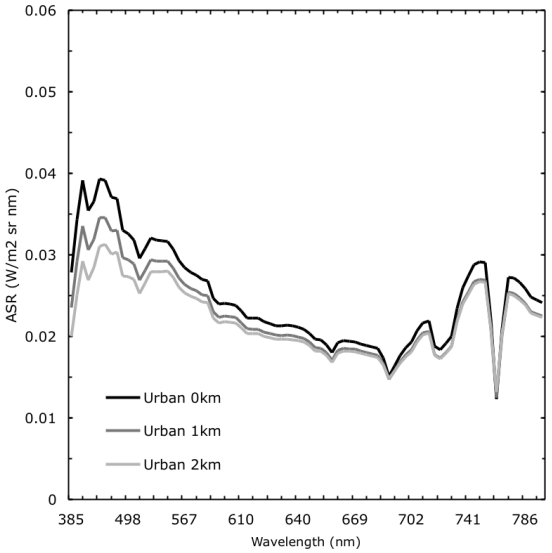

(b) *Urban aerosols*

Figure A.4.: *At-sensor radiance (ASR) as a function of wavelength for different surface altitudes. The surface is a dark target within a green grass background. The spectra are convolved to the bands of the APEX imaging spectrometer (Itten et al., 2008). This figure is published in Seidel et al. (2005).*

A.2. Additional results to section 4.2 on page 47 and 4.4.3.1 on page 59

Fig. A.5 shows calculations of the reflectance R_λ^{TOA} as a function of AOD for surface albedo $a_\lambda \in [0.20, 0.25, 0.30, 0.35, 0.4]$ at $\lambda \in [412\,nm, 550\,nm, 865\,nm]$. The lines were computed using SMART (Eq. 4.2) and the circles by using SCIATRAN as a benchmark. RT model inputs are given in Table 4.1. Both models used the same marine aerosol phase function as described in Sect. 4.3.1 and shown in Fig. 4.1. Fig. A.6 shows the derivative of the reflectance R_λ^{TOA} (see Fig. A.5) with respect to AOD, according to Eq. (4.11). Positive values indicate increasing R_λ^{TOA} for increasing AOD, and *vice versa*. Values close to zero indicate a weak dependence of R_λ^{TOA} on AOD and therefore, small uncertainties in R_λ^{TOA} translate to large uncertainties AOD retrieval. It is obvious that SMART correlates better to SCIATRAN at longer wavelengths because the effect of the scattering approximation is less dominant. It can be also concluded from this additional results that shorter wavelengths lead to more ambiguous R_λ^{TOA} with respect to AOD, especially for small AOD. In the presented case of non-absorbing marine aerosol particles, the critical surface albedo is found at higher albedo values for shorter wavelengths (i.e. $a^{crit}_{412\,nm} \approx 0.3 - 0.35, a^{crit}_{550\,nm} \approx 0.2 - 0.25, a^{crit}_{865\,nm} \approx 0.2$).

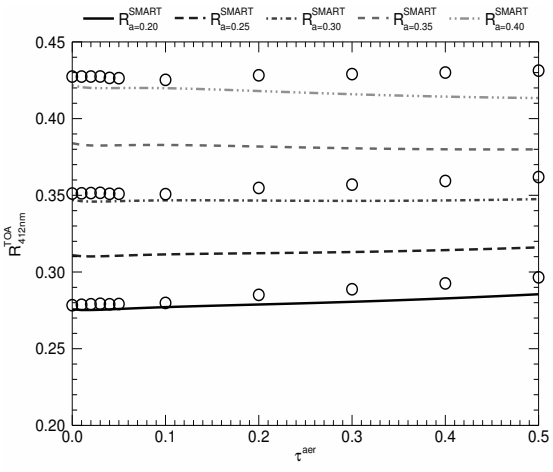

(a) $\lambda = 412\,nm$

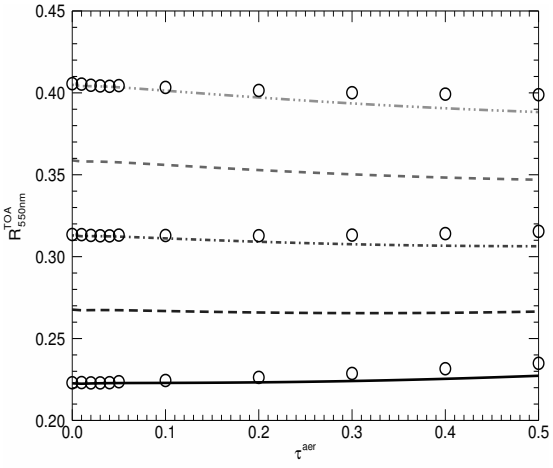

(b) $\lambda = 550\,nm$

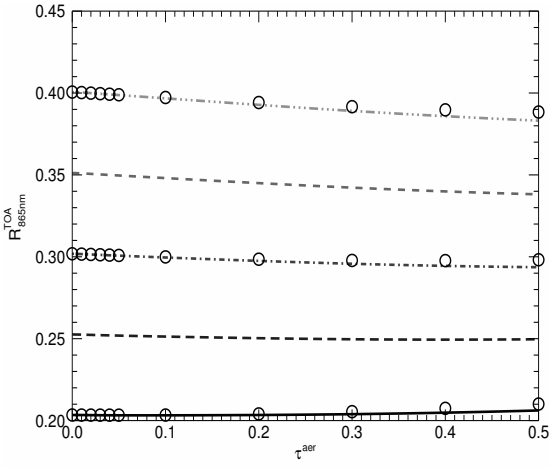

(c) $\lambda = 865\,nm$

Figure A.5.: *Same as Fig. 4.2 except for other surface albedo values.*

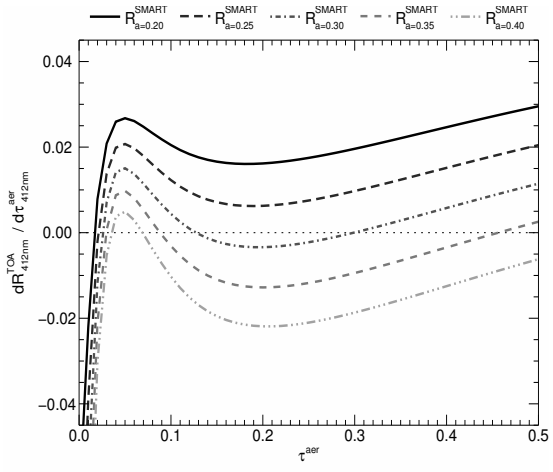

(a) $\lambda = 412\,nm$

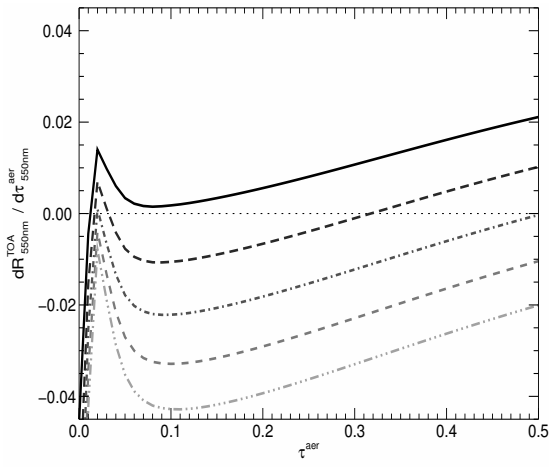

(b) $\lambda = 550\,nm$

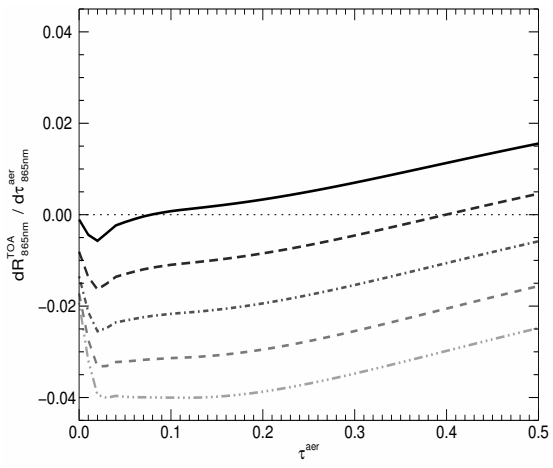

(c) $\lambda = 865\,nm$

Figure A.6.: *Same as Fig. 4.10 except for other surface albedo values.*

A.3. Additional results to section 4.4.1 on page 55

Fig. A.7 shows the absolute AOD retrieval error ($\Delta\tau_{\lambda}^{aer}$) as a function of AOD. Calculations were performed using iSMART and compared to SCIATRAN using Eq. (4.10). Retrievals in brownish areas are not feasible because either $\tau_{412nm}^{aer} < 0$ or $\tau_{412nm}^{aer} > 1.2$. The dotted lines denote the officially expected uncertainty range of MODIS dark-target AOD retrievals (valid for $0.01 \leq a \leq 0.25$) (Remer et al., 2005; Levy et al., 2009, 2010). Results for $a \in [0.1, 0.2, 0.3, 0.4]$ are given in Fig. 4.6. Results for $a \in [0.0, 0.5, 0.7, 0.9]$ are not shown because they are almost indistinguishable from the once with albedo ± 0.1. The interpretation of this additional results is the same as it is given in Sect. 4.4.1 for Fig. 4.6.

Fig. A.8 shows the same $\Delta\tau_{\lambda}^{aer}$ as Fig. A.7, but as a function of the surface albedo to emphasize its effect on AOD retrieval. The interpretation of Fig. A.8 is again the same as it is given in Sect. 4.4.1 for Fig. 4.7. Fig. A.8a provides the simple evidence that SMART was using the same τ_{λ}^{mlc} as SCIATRAN for this tests. Obviously, iSMART was able to find a correct match to SCIATRAN for $\tau_{412\,nm}^{\mathrm{aer}} = 0.00$.

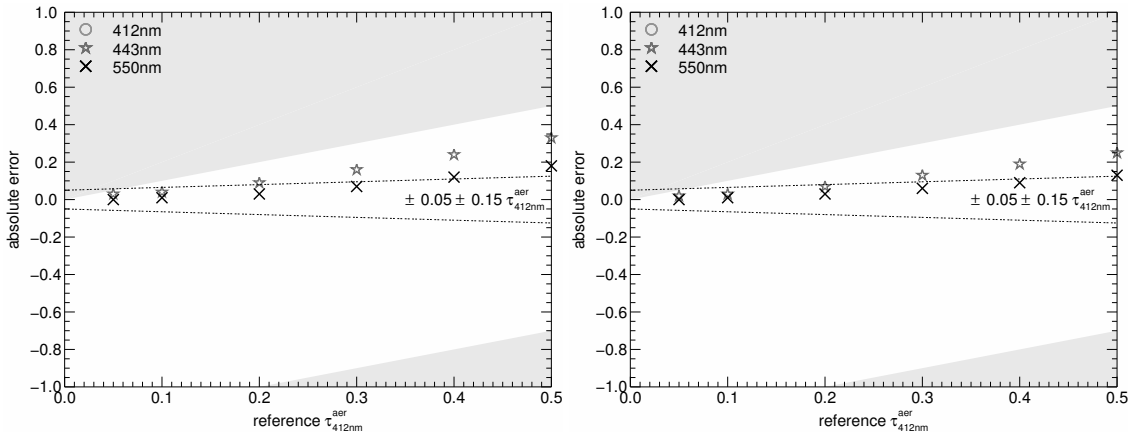

(a) *surface albedo=0.4* **(b)** *surface albedo=0.5*

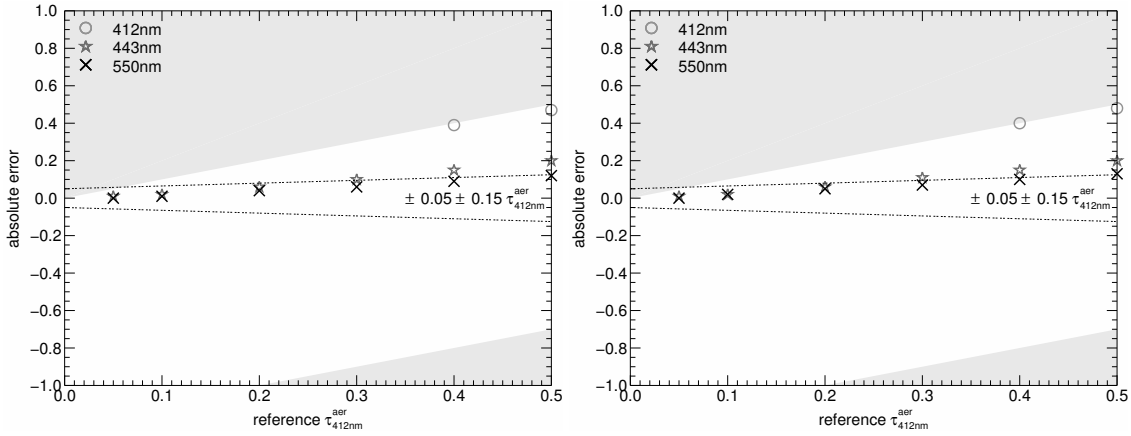

(c) *surface albedo=0.6* **(d)** *surface albedo=0.8*

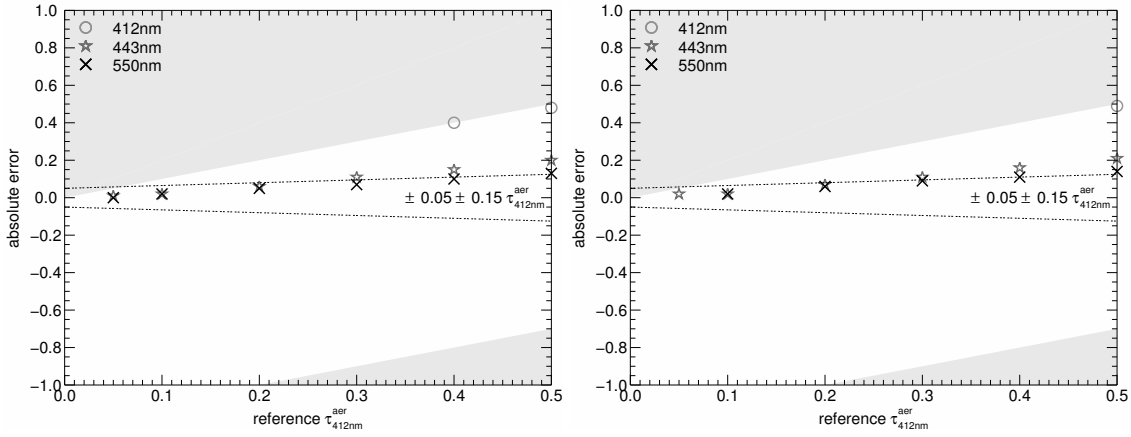

(e) *surface albedo=0.9* **(f)** *surface albedo=1.0*

Figure A.7.: *The absolute error of AOD retrieval with iSMART for different surface albedo. A retrieval in the blue areas is not possible because either $\tau_{412nm}^{aer} < 0$ or $\tau_{412nm}^{aer} > 1.2$. The dotted lines mark the expected uncertainty range of the MODIS dark-target AOD retrieval approach as a reference. (additional results to Fig. 4.6)*

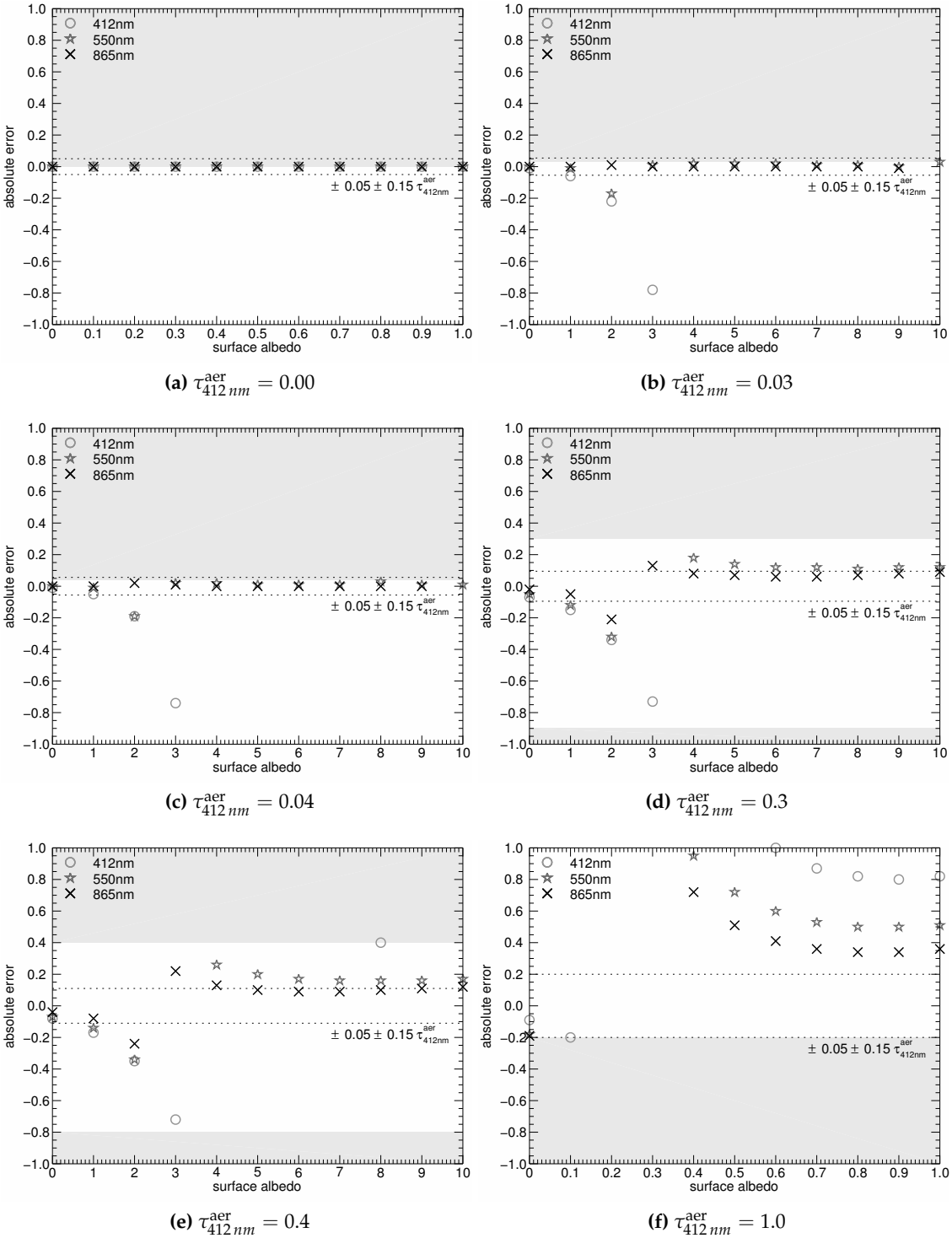

(a) $\tau^{\text{aer}}_{412\,nm} = 0.00$ **(b)** $\tau^{\text{aer}}_{412\,nm} = 0.03$

(c) $\tau^{\text{aer}}_{412\,nm} = 0.04$ **(d)** $\tau^{\text{aer}}_{412\,nm} = 0.3$

(e) $\tau^{\text{aer}}_{412\,nm} = 0.4$ **(f)** $\tau^{\text{aer}}_{412\,nm} = 1.0$

Figure A.8.: *Absolute error of AOD retrieval as a function of surface albedo. Calculations were performed using iSMART and compared to SCIATRAN. Retrievals in brownish areas are not feasible because either* $\tau^{aer}_{412nm} < 0$ *or* $\tau^{aer}_{412nm} > 1.2$*. The dotted lines denote the expected uncertainty range of the MODIS dark-target* ($0.01 \leq a \leq 0.25$) *AOD retrieval. (additional results to Fig. 4.7)*

A.4. Additional results to section 4.4.2 on page 58

Fig. A.9 provides iSMART's AOD retrieval results using airborne remote sensing data normalized by reference AOD from AERONET. The same interpretation applies as it is given in Sect. 4.4.2 for Fig. 4.8.

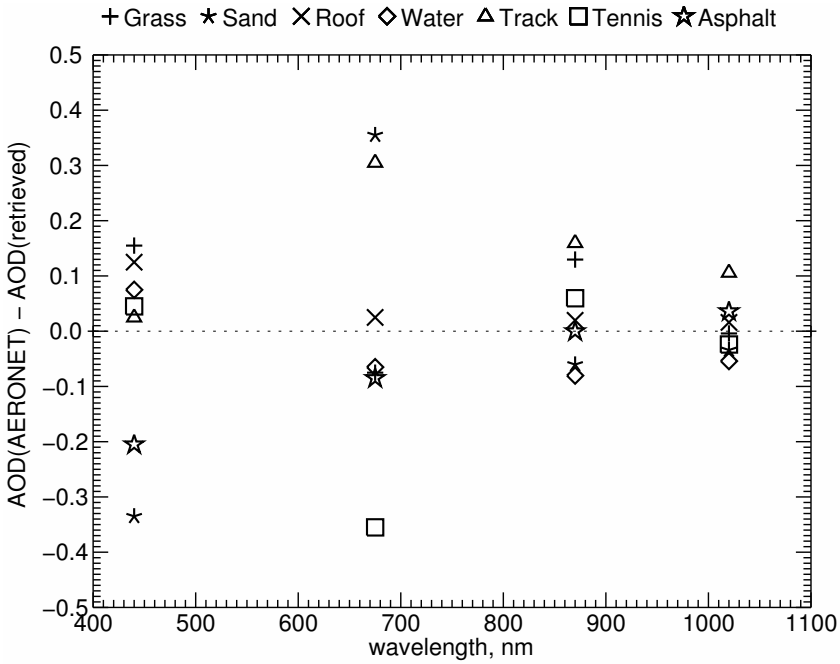

Figure A.9.: *Error-plot of AOD retrieval using airborne imaging spectrometer data on various in-situ reference targets. See also the corresponding Fig. 4.8.*

A.5. Additional results to section 4.4.3.1 on page 59

Sect. 4.4.3.1 explains the so-called critical surface albedo (CSA), which is posing difficulties for AOD retrieval due to low sensitivity of R^{TOA} to AOD. This is also shown by Figs. 4.10 and A.6. Another way to visualize the effect of CSA is given in Figs. 4.9, A.10 and A.11.

Fig. A.10 shows results calculated using SMART for average continental aerosols (Eq. 4.2). See Table A.1 for a list of input parameters used for this computations. Results are provided for combinations of SZA$\in$ [30°,60°] and $\lambda \in [400\,nm, 550\,nm, 700\,nm]$. They show that additional AOD is increasing R^{TOA}_{λ} and *vice versa.* Aerosol absorption and backward scattering reduces transmittance to a larger fraction than forward scattering increases upwelling radiation from the atmosphere. Thus, the net effect is negative over bright surfaces and positive over dark surfaces. The CSA is in between without a distinct change in R^{TOA}_{λ} due to aerosol scattering because both effects are equally effective (Fraser and Kaufman, 1985). The CSA depends mainly on ω^{aer}_{λ} (Fraser and Kaufman, 1985; Popp et al., 2007) and on K^{ext}_{λ}, μ_0, μ, λ, as well as aerosol particle concentration. It is interesting to see that calculations at SZA=60° provide more distinct CSA, while at SZA=30° the transition between increasing and decreasing signal due to AOD is more fuzzy with respect to surface albedo.

Fig. A.11 provides the same results as above, but with the absolute difference of at-sensor reflectance $\triangle R^{TOA} = R^{TOA}(\tau^{aer}_1) - R^{TOA}(\tau^{aer}_2)$ with respect to AOD, where $\tau^{aer}_1 \in$ [0.2, 0.4, 0.6, 0.8] and $\tau^{aer}_2 \in$ [0.0, 0.2, 0.4, 0.6]. It shows clearly that at SZA=60°, $\triangle\tau^{aer}$ lines are crossing $\triangle R^{TOA} = 0$ (CSA) close together, which corresponds to a relatively distinct crossing point or CSA. At SZA=30°, $\triangle\tau^{aer}$ lines spreading much more around $\triangle R^{TOA} = 0$, which means that the range of surface albedo, possibly leading to difficult AOD retrievals, is much broader. Especially for $a \geq 0.3$ and τ^{aer} in the range of a =0.3 to 0.5. It may be important not note that mid-latitude airborne remote sensing campaigns are typically performed during noon, where the SZA is close to 30°. It may be thus concluded that AOD retrieval from airborne remote sensing data with a SZA≈30° over bright surfaces and typical AOD values could be very challenging. Independent ground-based sunphotometer measurements are therefore still inevitable.

Table A.1.: *The input parameters to Figs. A.10 and A.11. SZA is the solar zenith angle and VZA the viewing or observation zenith angle (here nadir). τ^{mlc}_{λ} and τ^{aer}_{λ} denote the spectral molecular and aerosol optical thickness, respectively. ω^{aer}_{λ} is aerosol single-scattering albedo and g^{aer}_{λ} aerosol asymmetry parameter.*

λ, nm	SZA	VZA	τ^{aer}_{λ}	τ^{mlc}_{λ}	ω^{aer}_{λ}	g^{aer}_{λ}
400	30° and 60°	nadir	0.0, 0.2, 0.4 and 0.5	0.3595	0.964	0.657
550	30° and 60°	nadir	0.0, 0.2, 0.4 and 0.5	0.0969	0.960	0.639
700	30° and 60°	nadir	0.0, 0.2, 0.4 and 0.5	0.0363	0.953	0.620

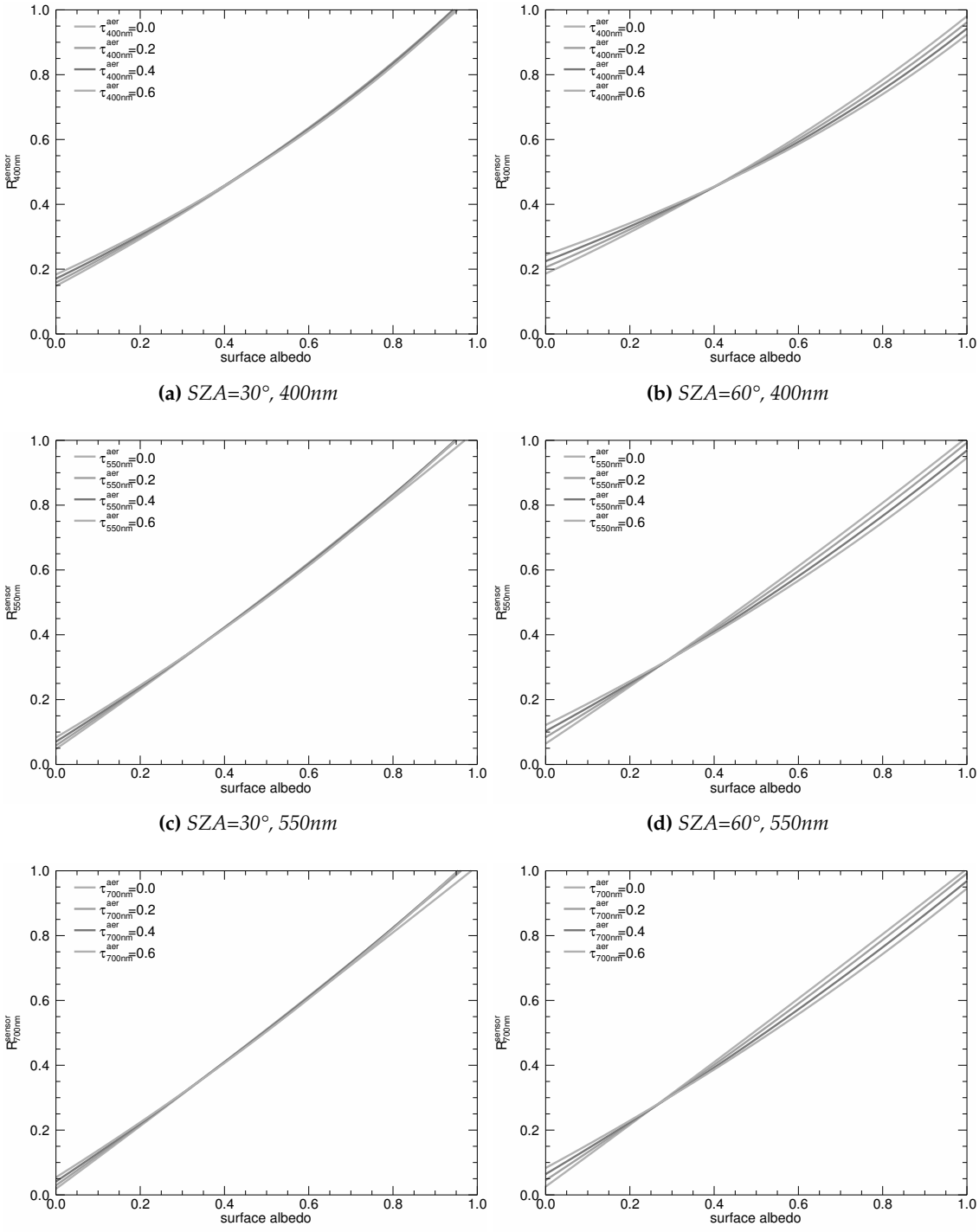

(a) *SZA=30°, 400nm* **(b)** *SZA=60°, 400nm*

(c) *SZA=30°, 550nm* **(d)** *SZA=60°, 550nm*

(e) *SZA=30°, 700nm* **(f)** *SZA=60°, 700nm*

Figure A.10.: *At-sensor reflectance (R^{TOA}_{λ}) as a function of the surface albedo for different AOD values. Calculations were performed using SMART for average-continental aerosols.*

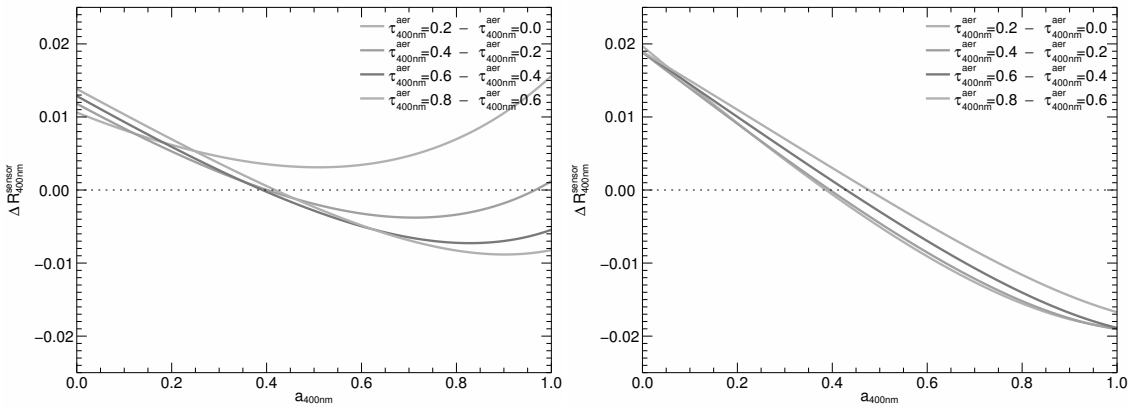

(a) *SZA=30°,400nm*

(b) *SZA=60°,400nm*

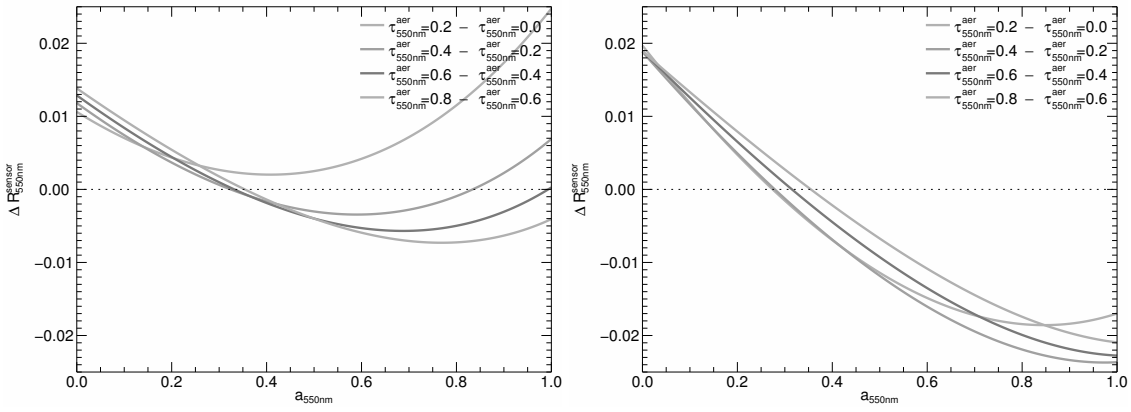

(c) *SZA=30°,550nm*

(d) *SZA=60°,550nm*

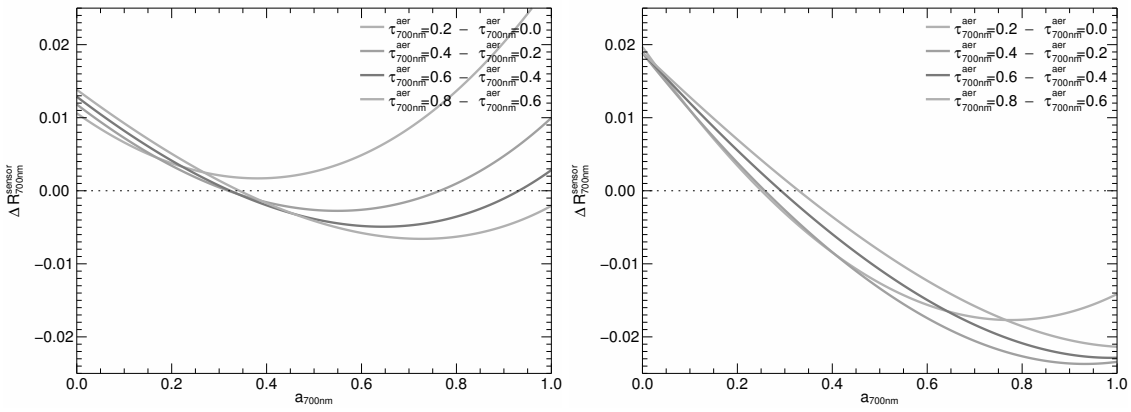

(e) *SZA=30,700nm*

(f) *SZA=60°,700nm*

Figure A.11.: *Same as Fig. A.10, but with the difference of the at-sensor reflectance* $\triangle R^{TOA} = R^{TOA}\left(\tau_1^{aer}\right) - R^{TOA}\left(\tau_2^{aer}\right)$*, where* $\tau_1^{aer} \in [0.2, 0.4, 0.6, 0.8]$ *and* $\tau_2^{aer} \in [0.0, 0.2, 0.4, 0.6]$*.* $\triangle R^{TOA} = 0$ *corresponds to the critical surface albedo.*

A.6. Additional results to section 4.4.3.2 on page 61

This section provides a complete set of figures discussing the influence of surface albedo uncertainties on AOD retrieval (see Sect. 4.4.3.2). These are important findings, because it is often assumed in RT models and atmospheric corrections that field spectrometer measurements are perfectly accurate. Unfortunately, this is not the case and uncertainties in the order of a few percent have to be taken into account (Milton et al., 2009). Sect. 4.4.3.2 shows with Fig. 4.11 that such uncertainties may have a strong influence on AOD retrieval accuracy. This findings are further supported by the following figures, where an assumed uncertainty in a is simulated by a deviation d from a, such that $a_{error} = a_{true} \pm d$, where $d \in [0.005, 0.01, 0.05]$. Fig. A.12 provides results on the left for $\tau^{\text{aer}}_{550\,nm} = 0.05$ and on the right for $\tau^{\text{aer}}_{550\,nm} = 0.5$. See Table A.1 for a list of input parameters used for this computations, while $\tau^{aer}_{\lambda} \in [0.05, 0.5]$.

The conclusions from Sect. 4.4.3.2 are valid also for Fig. A.12. They confirm that AOD retrieval at dark surfaces $(a \leq 0.1)$ is more robust to surface albedo uncertainties than at bright surfaces. An uncertainty of 1% ($d = 0.01$) leads to a difference in AOD of roughly 0.2 at a dark surface. For $a \leq 0.3$, an overestimation of surface albedo causes an overestimation of AOD. Retrievals at 400 nm and at SZA=60° are more robust at dark targets than at 700 nm and at SZA=30°. Some retrievals with $\tau^{aer} \notin [0.0, 1.2]$ values were rejected, especially in case of $\tau^{\text{aer}}_{550\,nm} = 0.05$, where even smallest underestimations lead to negative AOD values (see brownish areas in Fig. A.12).

See Sect. 5.1 for further interpretations on this interesting results, which may have an impact on the scientific understanding of the large uncertainties in aerosol radiative forcing.

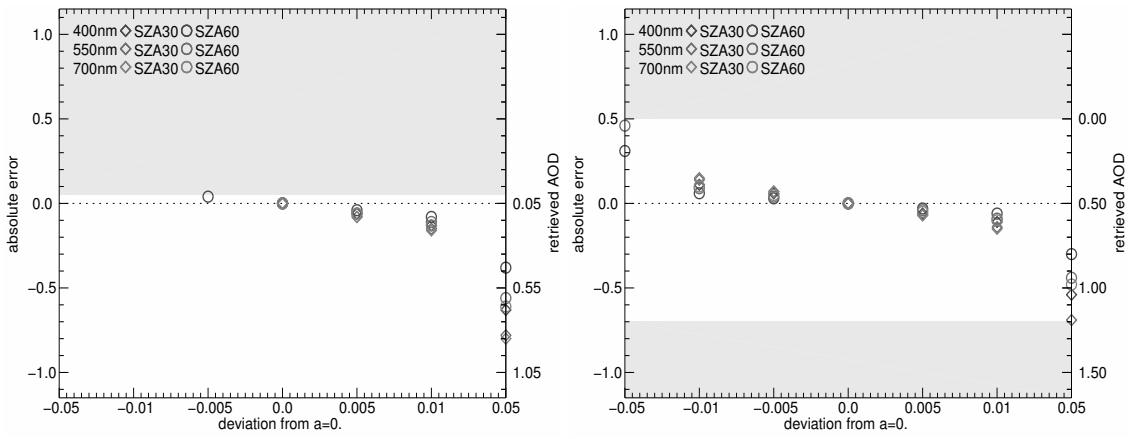

(a) $\tau^{\text{aer}}_{550\,nm} = 0.05$, $a_{550\,nm} = 0.0$ **(b)** $\tau^{\text{aer}}_{550\,nm} = 0.5$, $a_{550\,nm} = 0.0$

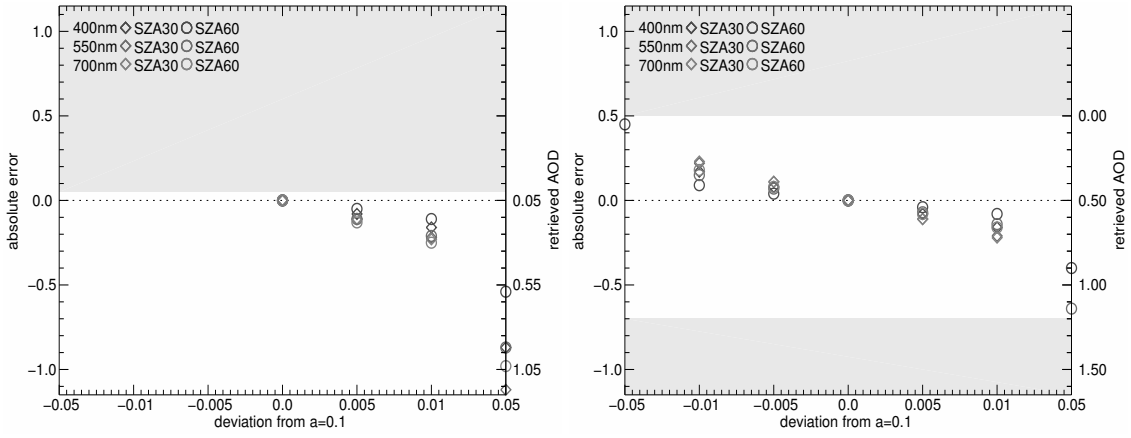

(c) $\tau^{\text{aer}}_{550\,nm} = 0.05$, $a_{550\,nm} = 0.1$ **(d)** $\tau^{\text{aer}}_{550\,nm} = 0.5$, $a_{550\,nm} = 0.1$

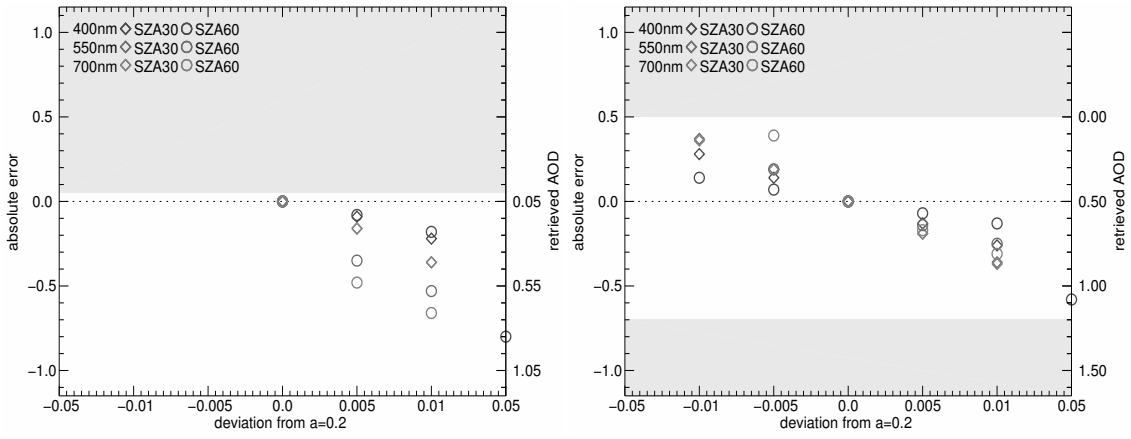

(e) $\tau^{\text{aer}}_{550\,nm} = 0.05$, $a_{550\,nm} = 0.2$ **(f)** $\tau^{\text{aer}}_{550\,nm} = 0.5$, $a_{550\,nm} = 0.2$

Figure A.12.: *Absolute error of AOD retrieval using iSMART as a function of surface albedo uncertainties at* $\tau^{\text{aer}}_{412\,nm} = 0.5$*. The uncertainties are simulated by a deviation from the true surface albedo. Retrievals in the brownish areas are not feasible because either* $\tau^{aer}_{412nm} < 0$ *or* $\tau^{aer}_{412nm} > 1.2$*.*

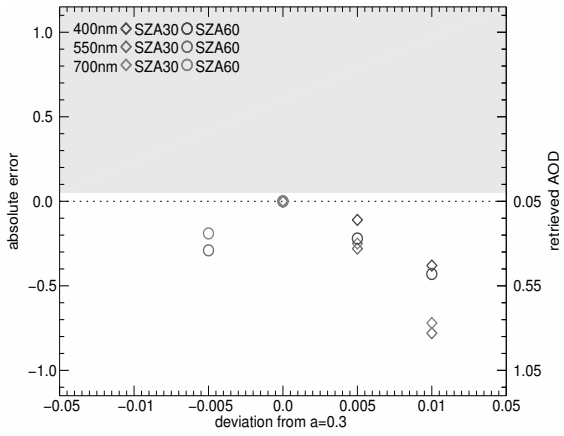

(g) $\tau^{\text{aer}}_{550\,nm} = 0.05$, $a_{550\,nm} = 0.3$

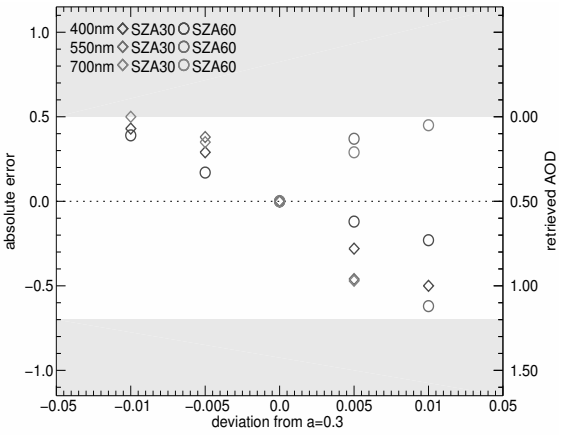

(h) $\tau^{\text{aer}}_{550\,nm} = 0.5$, $a_{550\,nm} = 0.3$

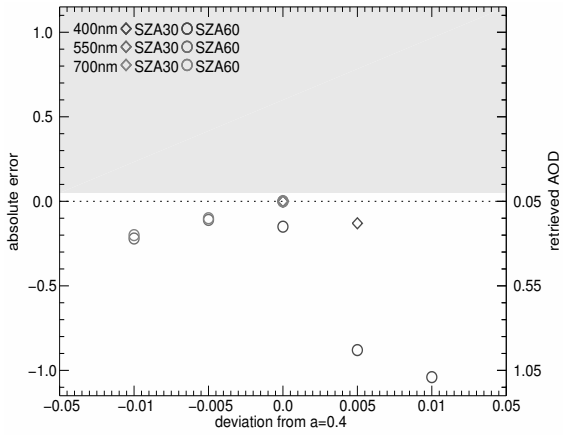

(i) $\tau^{\text{aer}}_{550\,nm} = 0.05$, $a_{550\,nm} = 0.4$

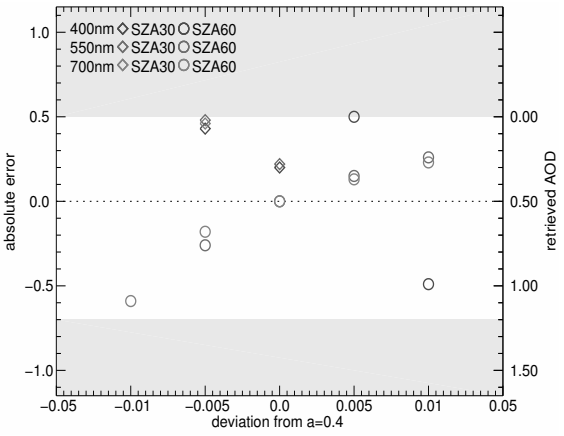

(j) $\tau^{\text{aer}}_{550\,nm} = 0.5$, $a_{550\,nm} = 0.4$

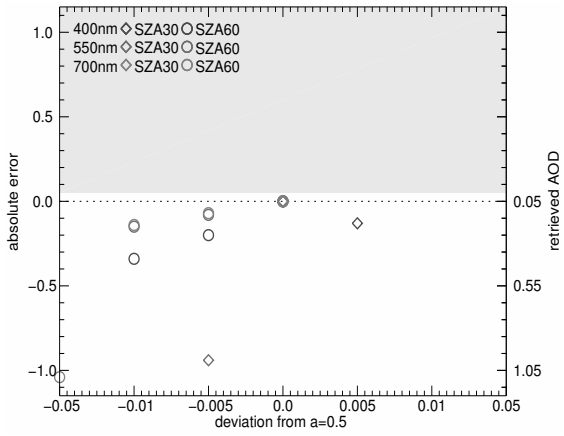

(k) $\tau^{\text{aer}}_{550\,nm} = 0.05$, $a_{550\,nm} = 0.5$

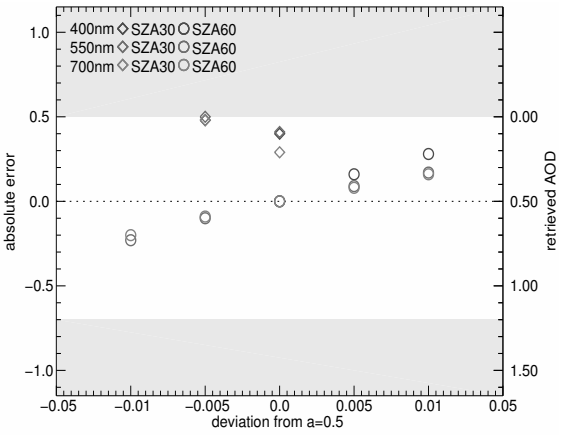

(l) $\tau^{\text{aer}}_{550\,nm} = 0.5$, $a_{550\,nm} = 0.5$

Figure A.12.: *Continued Fig. A.12.*

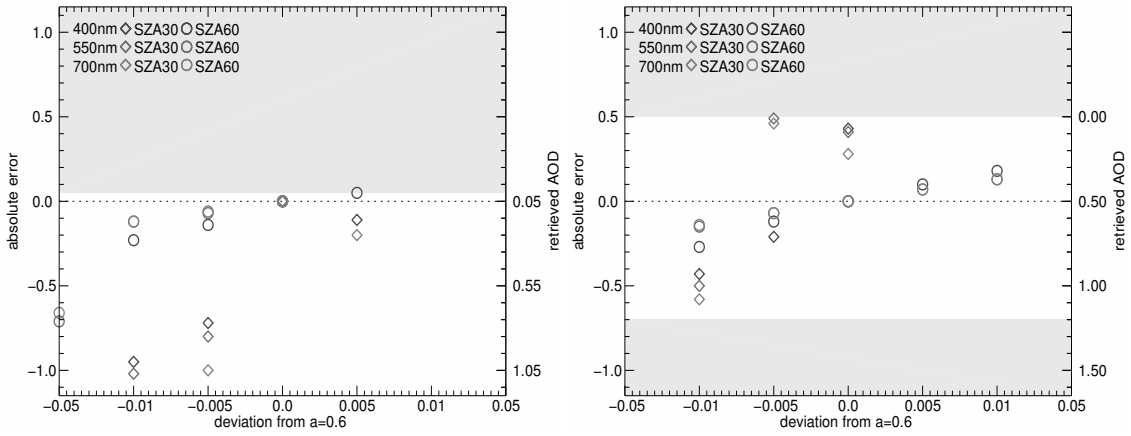

(m) $\tau^{\text{aer}}_{550\,nm} = 0.05$, $a_{550\,nm} = 0.6$ **(n)** $\tau^{\text{aer}}_{550\,nm} = 0.5$, $a_{550\,nm} = 0.6$

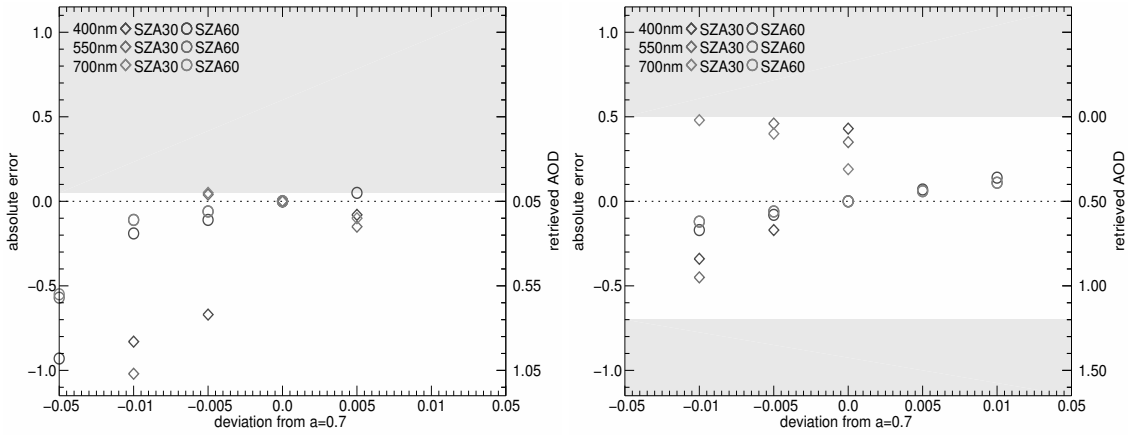

(o) $\tau^{\text{aer}}_{550\,nm} = 0.05$, $a_{550\,nm} = 0.7$ **(p)** $\tau^{\text{aer}}_{550\,nm} = 0.5$, $a_{550\,nm} = 0.7$

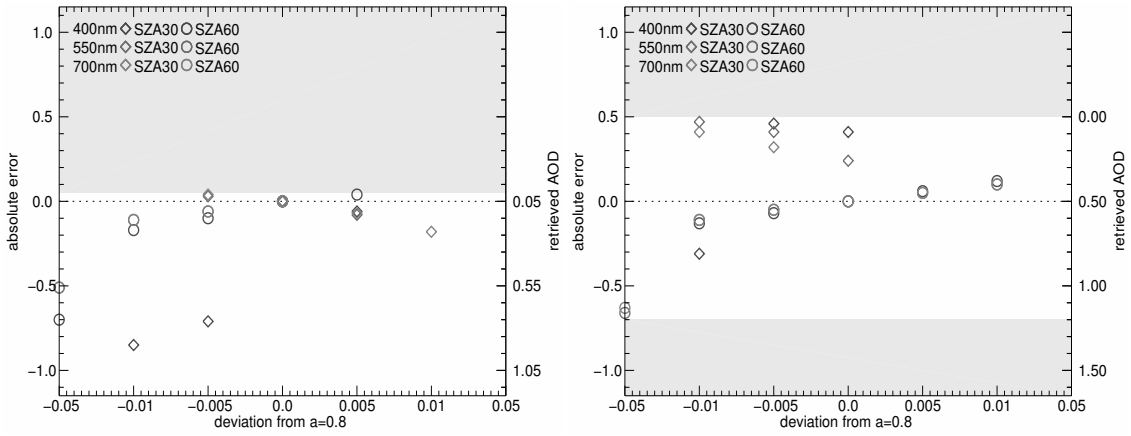

(q) $\tau^{\text{aer}}_{550\,nm} = 0.05$, $a_{550\,nm} = 0.8$ **(r)** $\tau^{\text{aer}}_{550\,nm} = 0.5$, $a_{550\,nm} = 0.8$

Figure A.12.: *Continued Fig. A.12.*

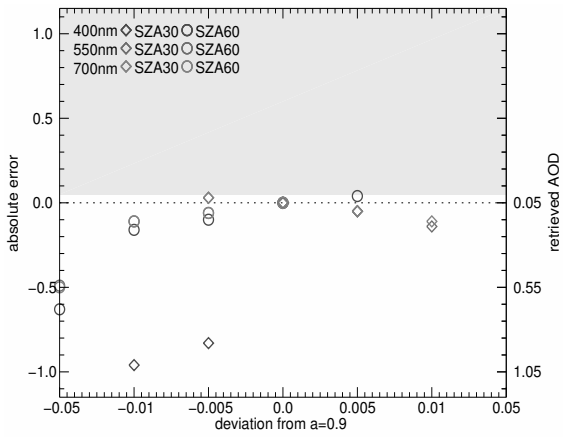

(s) $\tau^{\text{aer}}_{550\,nm} = 0.05$, $a_{550\,nm} = 0.9$

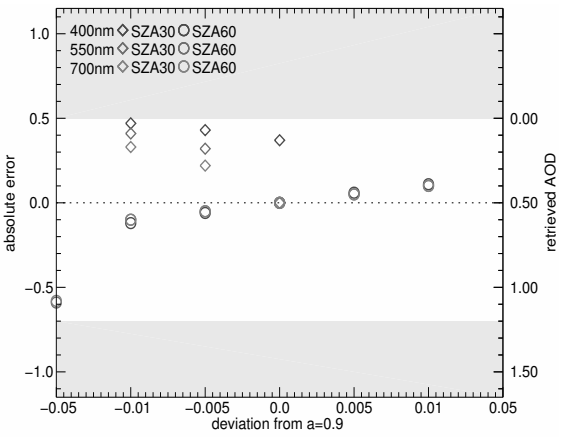

(t) $\tau^{\text{aer}}_{550\,nm} = 0.5$, $a_{550\,nm} = 0.9$

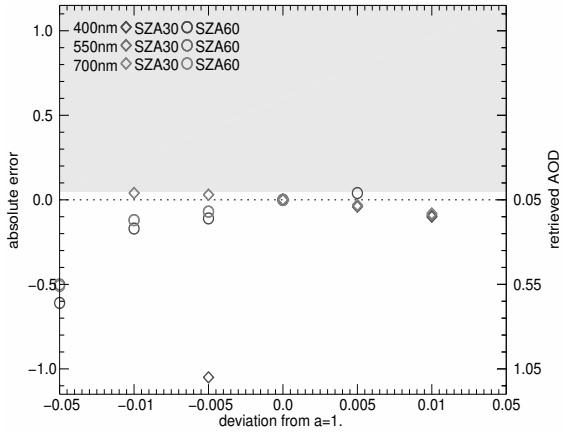

(u) $\tau^{\text{aer}}_{550\,nm} = 0.05$, $a_{550\,nm} = 1.0$

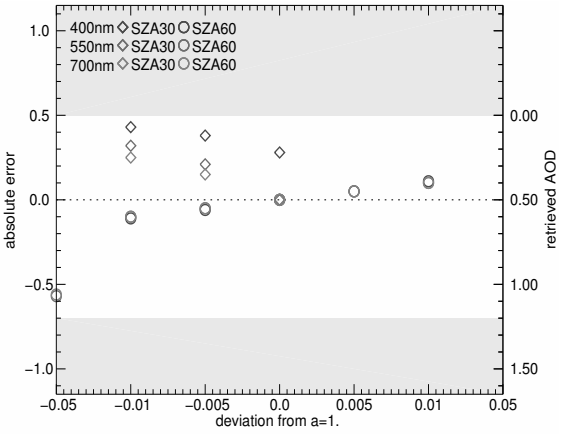

(v) $\tau^{\text{aer}}_{550\,nm} = 0.5$, $a_{550\,nm} = 1.0$

Figure A.12.: *Continued Fig. A.12.*

Bibliography

Ångström, A., 1925. The albedo of various surfaces of ground. Geogr. Ann. 7, 323–342.

Ångström, A., 1929. On the atmospheric transmission of sun radiation and on dust in the air. Geogr. Ann. 11, 156–166.

Ångström, A., 1930. On the atmospheric transmission of sun radiation. II. Geogr. Ann. 12, 130–159.

Bassani, C., Cavalli, R. M., Pignatti, S., 2010. Aerosol optical retrieval and surface reflectance from airborne remote sensing data over land. Sensors 10 (7), 6421–6438.

Berk, A., Bernstein, L. S., Robertson, D. C., 1989. MODTRAN: a moderate resolution model for LOWTRAN7. Tech. Rep. GL-TR-89-0122, Air Force Geophysics Lab, Hanscom AFB, Massachusetts, USA.

Bodhaine, B. A., Wood, N. B., Dutton, E. G., Slusser, J. R., 1999. On rayleigh optical depth calculations. J. Atmos. Ocean. Tech. 16 (11), 1854–1861.

Bowles, J. H., Maness, S. J., Chen, W., Davis, C. O., Donato, T. F., Gillis, D. B., Korwan, D., Lamela, G., Montes, M. J., Rhea, W. J., , Snyder, W. A., 2005. Hyperspectral imaging of an inter-coastal waterway. In: Ehlers, M., Michel, U. (Eds.), Remote Sensing for Environmental Monitoring, GIS Applications, and Geology V. Vol. Proc. of SPIE Vol. 5983. SPIE, p. 59830F.

Carrer, D., Roujean, J.-L., Hautecoeur, O., Elias, T., 2010. Daily estimates of aerosol optical thickness over land surface based on a directional and temporal analysis of SEVIRI MSG visible observations. J. Geophys. Res. 115 (D10).

Chandrasekhar, S., 1960. Radiative Transfer. Dover, New York, USA, 393 pp.

Charlson, R. J., Schwartz, S. E., Hales, J. M., Cess, R. D., Coakley, J. A., Hansen, J. E., Hofmann, D. J., 1992. Climate forcing by anthropogenic aerosols. Science 255, 423–430.

Collins, G. W., 2003; orig. 1989. The Fundamentals of Stellar Astrophysics, WEB Edition. NASA Astrophysics Data System Virtual Library, Ch. Solution of the Equation of Radiative Transfer. URL `http://ads.harvard.edu/books/1989fsa..book/AbookC10.pdf`

d'Almeida, G., Koepke, P., Shettle, E. P., 1991. Atmospheric Aerosols: Global Climatology and Radiative Characteristics. Deepak, Hampton, Virginia, USA, 561 pp.

Davis, C. O., Bowles, J., Leathers, R. A., Korwan, D., Downes, T. V., Snyder, W. A., Rhea, W. J., Chen, W., 2002. Ocean phills hyperspectral imager: design, characterization, and calibration. Opt. Express 10 (4), 210–221.

Diner, D. J., Davis, A., Hancock, B., Geier, S., Rheingans, B., Jovanovic, V., Bull, M., Rider, D. M., Chipman, R. A., Mahler, A.-B., McClain, S. C., 2010. First results from a dual photoelastic-modulator-based polarimetric camera. Appl. Opt. 49 (15), 2929–2946.

Diner, D. J., Davis, A., Hancock, B., Gutt, G., Chipman, R. A., Cairns, B., 2007. Dual-photoelastic-modulator-based polarimetric imaging concept for aerosol remote sensing. Appl. Opt. 46 (35), 8428–8445.

Diner, D. J., Martonchik, J. V., Kahn, R. A., Pinty, B., Gobron, N., Nelson, D. L., Holben, B. N., 2005. Using angular and spectral shape similarity constraints to improve MISR aerosol and surface retrievals over land. Remote Sens. Environ. 94 (2), 155–171.

Dubovik, O., Herman, M., Holdak, A., Lapyonok, T., Tanré, D., Deuzé, J. L., Ducos, F., Sinyuk, A., Lopatin, A., 2010. Statistically optimized inversion algorithm for enhanced retrieval of aerosol properties from spectral multi-angle polarimetric satellite observations. Atmos. Meas. Tech. Discuss. 3 (6), 4967–5077.

Dubovik, O., King, M. D., 2000. A flexible inversion algorithm for retrieval of aerosol optical properties from sun and sky radiance measurements. J. Geophys. Res. 105 (D16), 20673–20696.

Emde, C., Buras, R., Mayer, B., Blumthaler, M., 2010. The impact of aerosols on polarized sky radiance: model development, validation, and applications. Atmos. Chem. Phys. 10 (2), 383–396.

Evans, K. F., Stephens, G. L., 1991. A new polarized atmospheric radiative transfer model. Journal of Quantitative Spectroscopy and Radiative Transfer 46, 413–423.

Fraser, R. S., Kaufman, Y. J., 1985. The relative importance of aerosol scattering and absorption in remote sensing. IEEE Trans. Geosci. Remote Sens. GE-23 (5), 625–633.

Gao, B.-C., Montes, M. J., Davis, C. O., Goetz, A. F. H., 9 2009. Atmospheric correction algorithms for hyperspectral remote sensing data of land and ocean. Remote Sens. Environ. 113 (Supplement 1), S17–S24.

Goetz, A. F. H., Vane, G., Solomon, J. E., Rock, B. N., 1985. Imaging spectrometry for Earth remote sensing. Science 228 (4704), 1147–1153.

Govaerts, Y., 2006. RTMOM v0b.10 evaluation report. report EUM/MET/DOC/06/0502, EUMETSAT.

Guanter, L., Alonso, L., Moreno, J., 2005. A method for the surface reflectance retrieval from PROBA/CHRIS data over land: application to ESA SPARC campaigns. IEEE Trans. Geosci. Remote Sens. 43 (12), 2908–2917.

Hammad, A., Chapman, S., 1939. VII. The primary and secondary scattering of sunlight in a plane-stratified atmosphere of uniform composition. Philos. Mag. 28 (186), 99–110.

Hansen, J. E., Travis, L. D., 1974. Light scattering in planetary atmospheres. Space Sci. Rev. 16, 527–610.

Henyey, L. G., Greenstein, J. L., 1941. Diffuse radiation in the galaxy. Astrophys. J. 93, 70–83.

Hess, M., Koepke, P., Schult, I., 1998. Optical properties of aerosols and clouds: the software package opac. B. Am. Meteorol. Soc. 79 (5), 831–844.

Holben, B. N., Eck, T. F., Slutsker, I., Tanré, D., Buis, J. P., Setzer, A., Vermote, E., Reagan, J. A., Kaufman, Y. J., Nakajima, T., Lavenu, F., Jankowiak, I., Smirnov, A., 1998. AERONET–a federated instrument network and data archive for aerosol characterization. Remote Sens. Environ. 66 (1), 1–16.

Hsu, N. C., Tsay, S.-C., King, M. D., Herman, J. R., 2004. Aerosol properties over bright-reflecting source regions. IEEE Trans. Geosci. Remote Sens. 42 (3), 557–569.

Itten, K. I., Dell'Endice, F., Hueni, A., Kneubühler, M., Schläpfer, D., Odermatt, D., Seidel, F., Huber, S., Schopfer, J., Kellenberger, T., Bühler, Y., D'Odorico, P., Nieke, J., Alberti, E., Meuleman, K., 2008. APEX – the Hyperspectral ESA Airborne Prism Experiment. Sensors 8 (10), 6235–6259.

Itten, K. I., Schaepman, M. E., Vos, L. D., Hermans, L., Schlaepfer, H., Droz, F., 1997. APEX – airborne prism experiment a new concept for an airborne imaging spectrometer. In: Third International Airborne Remote Sensing Conference and Exhibition. Vol. 1. Copenhagen, Denmark, pp. 181–188.

Kahn, R. A., Gaitley, B. J., Garay, M. J., Diner, D. J., Eck, T. F., Smirnov, A., Holben, B. N., 2010. Multiangle Imaging SpectroRadiometer global aerosol product assessment by comparison with the Aerosol Robotic Network. J. Geophys. Res. 115 (D23).

Kahn, R. A., Garay, M. J., Nelson, D. L., Yau, K. K., Bull, M. A., Gaitley, B. J., Martonchik, J. V., Levy, R. C., 2007. Satellite-derived aerosol optical depth over dark water from MISR and MODIS: Comparisons with AERONET and implications for climatological studies. J. Geophys. Res. 112 (D18205).

Kanschat, G., Meinköhn, E., Rannacher, R., Wehrse, R. (Eds.), 2009. Numerical Methods in Multidimensional Radiative Transfer. Springer Berlin Heidelberg.

Katsev, I. L., Prikhach, A. S., Zege, E. P., Grudo, J. O., Kokhanovsky, A. A., 2010. Speeding up the aerosol optical thickness retrieval using analytical solutions of radiative transfer theory. Atmos. Meas. Tech. 3 (5), 1403–1422.

Katsev, I. L., Prikhach, A. S., Zege, E. P., Ivanov, A. P., Kokhanovsky, A. A., 2009. Iterative procedure for retrieval of spectral aerosol optical thickness and surface reflectance from satellite data using fast radiative transfer code and its application to meris measurements. In: Kokhanovsky, A. A., de Leeuw, G. (Eds.), Satellite Aerosol Remote Sensing over Land. Springer Praxis Books. Springer Berlin Heidelberg, pp. 101–133.

Kaufman, Y. J., Tanre, D., Boucher, O., 2002. A satellite view of aerosols in the climate system. Nature 419 (6903), 215–223.

Key, J. F., Schweiger, A. J., 1998. Tools for atmospheric radiative transfer: Streamer and FluxNet. Comp. and Geosci. 24, 443–451.

King, M. D., Kaufman, Y. J., Tanré, D., Nakajima, T., 1999. Remote sensing of tropospheric aerosols from space: Past, present, and future. Bull. Am. Meteorol. Soc. 80 (11), 2229–2259.

Kohler, D. D. R., Bissett, W. P., Steward, R. G., Davis, C. O., 2004. New approach for the radiometric calibration of spectral imaging systems. Opt. Express 12 (11), 2463–2477.

Kokhanovsky, A. A., 2004. Light Scattering Media Optics: Problems and Solutions, 3rd Edition. Springer-Praxis Books in Environmental Sciences.

Kokhanovsky, A. A., 2006. Cloud Optics. Vol. 34 of Atmospheric and Oceanographic Sciences Library. Springer.

Kokhanovsky, A. A., 2008. Aerosol Optics – Light Absorption and Scattering by Particles in the Atmosphere. Springer Praxis Books. Springer Berlin Heidelberg.

Kokhanovsky, A. A., Breon, F.-M., Cacciari, A., Carboni, E., Diner, D., Nicolantonio, W. D., Grainger, R. G., Grey, W. M. F., Höller, R., Lee, K.-H., Li, Z., North, P. R. J., Sayer, A. M., Thomas, G. E., von Hoyningen-Huene, W., 2007. Aerosol remote sensing over land: a comparison of satellite retrievals using different algorithms and instruments. Atmospheric Research 85, 372–394.

Kokhanovsky, A. A., Budak, V. P., Cornet, C., Duan, M., Emde, C., Katsev, I. L., Klyukov, D. A., Korkin, S. V., C-Labonnote, L., Mayer, B., Min, Q., Nakajima, T., Ota, Y., Prikhach, A. S., Rozanov, V. V., Yokota, T., Zege, E. P., 2010a. Benchmark results in vector atmospheric radiative transfer. J. Quant. Spectrosc. Radiat. Transf. 111 (12-13), 1931–1946.

Kokhanovsky, A. A., de Leeuw, G., 2009. Satellite Aerosol Remote Sensing over Land. Springer Praxis Books.

Kokhanovsky, A. A., Deuzé, J. L., Diner, D. J., Dubovik, O., Ducos, F., Emde, C., Garay, M. ., Grainger, R. G., Heckel, A., Herman, M., Katsev, I. L., Keller, J., Levy, R., North, P. R. J., Prikhach, A. S., Rozanov, V. V., Sayer, A. M., Ota, Y., Tanré, D., Thomas, G. E., Zege, E. P., 2010b. The inter-comparison of major satellite aerosol retrieval algorithms using simulated intensity and polarization characteristics of reflected light. Atmos. Meas. Tech. 3 (4), 909–932.

Kokhanovsky, A. A., Mayer, B., Rozanov, V. V., 2005. A parameterization of the diffuse transmittance and reflectance for aerosol remote sensing problems. Atmos. Res. 73 (1-2), 37–43.

Kondratyev, K. Y., Ivlev, L. S., Krapivin, V. F., Varotsos, C. A., 2006. Atmospheric Aerosol Properties: Formation, Processes and Impacts. Springer Berlin Heidelberg.

Kotchenova, S. Y., Vermote, E. F., Levy, R., Lyapustin, A., 2008. Radiative transfer codes for atmospheric correction and aerosol retrieval: intercomparison study. Appl. Opt. 47 (13), 2215–2226.

Kotchenova, S. Y., Vermote, E. F., Matarrese, R., Frank J. Klemm, J., 2006. Validation of a vector version of the 6S radiative transfer code for atmospheric correction of satellite data. part I: Path radiance. Appl. Opt. 45 (26), 6762–6774.

Lee, K. H., Li, Z., Kim, Y. J., Kokhanovsky, A. A., 2009. Atmospheric Aerosol Monitoring from Satellite Observations: A History of Three Decades. Springer Science+Business Media.

Lenoble, J., 1985. Radiative transfer in scattering and absorbing atmospheres: Standard computational procedures. Hampton, VA, A. Deepak Publishing.

Levy, R. C., Remer, L. A., Kleidman, R. G., Mattoo, S., Ichoku, C., Kahn, R., Eck, T. F., 2010. Global evaluation of the collection 5 MODIS dark-target aerosol products over land. Atmos. Chem. Phys. 10 (21), 10399–10420.

Levy, R. C., Remer, L. A., Mattoo, S., Vermote, E. F., Kaufman, Y. J., 2007. Second-generation operational algorithm: Retrieval of aerosol properties over land from inversion of Moderate Resolution Imaging Spectroradiometer spectral reflectance. J. Geophys. Res. 112 (D13211).

Levy, R. C., Remer, L. A., Tanré, D., Mattoo, S., Kaufman, Y. J., 2009. Algorithm for remote sensing of tropospheric aerosol over dark targets from MODIS: Collections 005 and 051: Revision 2. Tech. rep., NASA/GSFC.

Liou, K.-N., 1980. An Introduction to Atmospheric Radiation. Academic Press, New York, New York, USA, 392 pp.

Liou, K. N., Hansen, J. E., 1971. Intensity and polarization for single scattering by polydisperse sphere: a comparison of ray optics and mie theory. J. Atmos. Sci. 28 (6), 995–1004.

Lyapustin, A. I., 2001. Three-dimensional effects in the remote sensing of surface albedo. IEEE Trans. Geosci. Remote Sens. 39 (2), 254–263.

Lyapustin, A. I., 12 2005. Radiative transfer code SHARM for atmospheric and terrestrial applications. Appl. Opt. 44 (36), 7764–7772.

Marshak, A., Davis, A., 2005. 3D Radiative Transfer in Cloudy Atmospheres. Springer Berlin Heidelberg.

Martonchik, J. V., Kahn, R. A., Diner, D. J., 2009. Retrieval of aerosol properties over land using MISR observations. In: Kokhanovsky, A. A., de Leeuw, G. (Eds.), Satellite Aerosol Remote Sensing over Land. Springer Berlin Heidelberg.

Milton, E. J., Schaepman, M. E., Anderson, K., Kneubühler, M., Fox, N., 2009. Progress in field spectroscopy. Remote Sens. Environ. 113 (Supplement 1), S92–S109, imaging Spectroscopy Special Issue.

Mishchenko, M. I., Cairns, B., Hansen, J. E., Travis, L. D., Burg, R., Kaufman, Y. J., Vanderlei Martins, J., Shettle, E. P., 2004. Monitoring of aerosol forcing of climate from space: analysis of measurement requirements. J. Quant. Spectrosc. Ra. 88 (1-3), 149–161.

Mishchenko, M. I., Geogdzhayev, I. V., Cairns, B., Carlson, B. E., Chowdhary, J., Lacis, A. A., Liu, L., Rossow, W. B., Travis, L. D., 2007. Past, present, and future of global aerosol climatologies derived from satellite observations: A perspective. J. Quant. Spectrosc. Radiat. Transf. 106 (1-3), 325–347.

Mishchenko, M. I., Lacis, A. A., Travis, L. D., 1994. Errors induced by the neglect of polarization in radiance calculations for rayleigh-scattering atmospheres. J. Quant. Spectrosc. Ra. 51 (3), 491–510.

Mishchenko, M. I., Travis, L. D., Lacis, A. A., 2002. Scattering, absorption, and emission of light by small particles. Cambridge University Press, Cambridge.

Muldashev, T. Z., Lyapustin, A. I., Sultangazin, U. M., 1999. Spherical harmonics method in the problem of radiative transfer in the atmosphere–surface system. Journal of Quantitative Spectroscopy and Radiative Transfer 61 (3), 393–404.

Myhre, G., Stordal, F., Johnsrud, M., Ignatov, A., Mischenko, M. I., Geogdzhayev, I. V., Tanré, D., Deuzé, J.-L., Goloub, P., Nakajima, T., Higurashi, A., Torres, O., Holben, B., 2004. Intercomparison of satellite retrieved aerosol optical depth over the ocean. J. Atmos. Sci. 61, 499–513.

Nakajima, T., Tanaka, M., 1986. Matrix formulations for the transfer of solar radiation in a plane-parallel scattering atmosphere. J. Quant. Spectrosc. Radiat. Transf. 35 (1), 13–21.

Nieke, J., Seidel, F., Kaiser, J. W., Schläpfer, D., Itten, K. I., 2005. New retrieval capabilities for remote sensing of atmospheric parameters. In: Proceedings of the Conference of the Remote Sensing Society of Japan. Vol. 39. pp. 75–76.

Ota, Y., Higurashi, A., Nakajima, T., Yokota, T., 2010. Matrix formulations of radiative transfer including the polarization effect in a coupled atmosphere–ocean system. J. Quant. Spectrosc. Radiat. Transf. 111 (6), 878–894.

Popp, C., Riffler, R., Hauser, A., Wunderle, S., 2007. Approximation of aerosol type over land surfaces from MSG-SEVIRI data. In: Joint 2007 EUMETSAT Meteorological Satellite Conference and the 15th Satellite Meteorology and Oceanography Conference of the American Meteorological Society, Amsterdam, the Netherlands.

Remer, L., Kaufman, Y., Tanré, D., Mattoo, S., Chu, D., Martins, J., Li, R., Ichoku, C., Levy, R., Kleidman, R., Eck, T., Vermote, E., Holben, B., 2005. The MODIS aerosol algorithm, products, and validation. J. Atmos. Sci. 62 (4), 947–973.

Ricchiazzi, P., Yang, S., Gautier, C., Sowle, D., 10 1998. SBDART: A research and teaching software tool for plane-parallel radiative transfer in the Earth's atmosphere. Bulletin of the American Meteorological Society 79 (10), 2101–2114.

Richter, R., Schläpfer, D., 2002. Geo-atmospheric processing of airborne imaging spectrometry data. Part 2: atmospheric/topographic correction. Int. J. Remote Sens. 23 (13), 2631–2649.

Rind, D., Chin, M., Feingold, G., Streets, D., Kahn, R. A., Schwartz, S. E., Yu, H., 2009. Modeling the effects of aerosols on climate. In: Atmospheric Aerosol Properties and Impacts on Climate. A Report by the U.S. Climate Change Science Program and the Subcommittee on Global Change Research. National Aeronautics and Space Administration, Washington, D.C., USA.

Rozanov, A., Rozanov, V., Buchwitz, M., Kokhanovsky, A., Burrows, J., 2005. SCIATRAN 2.0 – a new radiative transfer model for geophysical applications in the 175-2400 nm spectral region. Adv. Space Res. 36 (5), 1015–1019.

Rozanov, V. V., Kokhanovsky, A. A., 2006. The solution of the vector radiative transfer equation using the discrete ordinates technique: Selected applications. Atmos. Res. 79 (3-4), 241–265.

Ruckstuhl, C., Philipona, R., Behrens, K., Collaud Coen, M., Dürr, B., Heimo, A., Mätzler, C., Nyeki, S., Ohmura, A., Vuilleumier, L., Weller, M., Wehrli, C., Zelenka, A., 2008. Aerosol and cloud effects on solar brightening and the recent rapid warming. Geophys. Res. Lett. 35 (12).

Ruggaber, A., Dlugi, R., Nakajima, T., 1994. Modelling radiation quantities and photolysis frequencies in the troposphere. J. Atmos. Chem. 18 (2), 171–210.

Schaepman, M. E., Schlaepfer, D., Mueller, A. A., 2002. Performance requirements for airborne imaging spectrometers. In: Descour, M. R., Shen, S. S. (Eds.), Proc. SPIE Vol. 4480, p. 23-31, Imaging Spectrometry VII. Vol. 4480 of Presented at the Society of Photo-Optical Instrumentation Engineers (SPIE) Conference. pp. 23–31.

Schaepman, M. E., Schläpfer, D., Itten, K. I., 1998. APEX – Airborne Prism Experiment: An airborne imaging spectrometer serving as a precursor instrument of the future esa land surface processes interactions mission. In: 1st Intl. EARSeL Workshop on Imaging Spectroscopy. EARSeL, Paris, pp. 45–52.

Schaepman-Strub, G., Schaepman, M., Painter, T., Dangel, S., Martonchik, J., 2006. Reflectance quantities in optical remote sensing–definitions and case studies. Remote Sens. Environ. 103 (1), 27–42.

Schläpfer, D., Schaepman, M., 2002. Modeling the noise equivalent radiance requirements of imaging spectrometers based on scientific applications. Appl. Opt. 41 (27), 5691–5701.

Seidel, F., Nieke, J., Schläpfer, D., Höller, R., Hoyningen-Huene, W., Itten, K., 2005. Aerosol retrieval for APEX airborne imaging spectrometer: a preliminary analysis. In: Schäfer, K., Comerón, A., Slusser, J. R., Picard, R. H., Carleer, M. R., Sifakis, N. (Eds.), Remote Sensing of Clouds and the Atmosphere X. Vol. Proc. of SPIE Vol. 5979. pp. 548–557.

Seidel, F., Nieke, J., Schläpfer, D., Itten, K., Bowles, J., 2006. Evaluation of near-uv/blue aerosol optical thickness retrieval from airborne hyperspectral imagery. In: Proc. IEEE-IGARSS, Denver, Colorado. pp. 2247–2250.

Seidel, F., Schläpfer, D., Itten, K. I., 2009. Efficient radiative transfer calculation and sensor performance requirements for the aerosol retrieval by airborne imaging spectroscopy. In: 6th Workshop on Imaging Spectroscopy, Tel Aviv, Israel, 16 March 2009 - 19 March 2009. pp. 1–6.

Seidel, F., Schläpfer, D., Nieke, J., Itten, K. I., 2008. Sensor performance requirements for the retrieval of atmospheric aerosols by airborne optical remote sensing. Sensors 8 (3), 1901–1914.

Seidel, F. C., Kokhanovsky, A. A., Schaepman, M. E., 2010. Fast and simple model for atmospheric radiative transfer. Atmos. Meas. Tech. 3 (4), 1129–1141.

Seidel, F. C., Kokhanovsky, A. A., Schaepman, M. E., 2011. Fast retrieval of aerosol optical depth and its sensitivity to surface albedo using remote sensing data. Atmos. Res. In Press.

Seinfeld, J. H., Pandis, S. N., 1998. Atmospheric Chemistry and Physics. Wiley, New York, New York, USA, 1326 pp.

Shore, S. N., 2002. Blue sky and hot piles: The evolution of radiative transfer theory from atmospheres to nuclear reactors. Historia Mathematica 29 (4), 463–489.

Sobolev, V. V., 1956. Radiative Transfer in Stellar and Planetary Atmospheres. Gostekhteorizdat, Moscow.

Sobolev, V. V., 1972. Light scattering in planetary atmospheres. Nauka, Moscow.

Solomon, S., Qin, D., Manning, M., Chen, Z., Marquis, M., Averyt, K. B., Tignor, M., Miller, H. L. (Eds.), 2007. Climate Change 2007: The Physical Science Basis. Contribution of Working Group I to the Fourth Assessment Report of the Intergovernmental Panel on Climate Change. Cambridge University Press, Cambridge, United Kingdom and New York, NY, USA.

Stamnes, K., Tsay, S.-C., Wiscombe, W., Jayaweera, K., 1988. Numerically stable algorithm for discrete-ordinate-method radiative transfer in multiple scattering and emitting layered media. Appl. Opt. 27 (12), 2502.

Tanré, D., 2010. Derivation of tropospheric aerosol properties from satellite observations. C. R. Geoscience 342 (4-5), 403–411.

Tanré, D., Herman, M., Deschamps, P., 1981. Influence of the background contribution upon space measurements of ground reflectance. Appl. Opt. 20 (20), 3676–3684.

Tanré, D., Herman, M., Deschamps, P. Y., de Leffe, A., 1979. Atmospheric modeling for space measurements of ground reflectances, including bidirectional properties. Appl. Opt. 18 (21), 3587.

Thomas, G. E., Stamnes, K., 2002. Radiative transfer in the atmosphere and ocean, 2nd Edition. Cambridge University Press, New York.

Torres, O., Tanskanen, A., Veihelmann, B., Ahn, C., Braak, R., Bhartia, P. K., Veefkind, P., Levelt, P., 2007. Aerosols and surface UV products from Ozone Monitoring Instrument observations: An overview. J. Geophys. Res. 112(D24).

van de Hulst, H. C., 1948. Scattering in a planetary atmosphere. Astrophys. J. 107, 220–246.

van de Hulst, H. C., 1980. Multiple light scattering. Vols._1_and_2. Academic Press, New York, NY (USA).

Vermote, E. F., Tanré, D., Deuzé, J. L., Herman, M., Morcrette, J.-J., 1997. Second simulation of the satellite signal in the solar spectrum, 6s: An overview. IEEE Trans. Geosci. Remote Sens. 35 (3), 675–686.

Wilson, R., Spengler, J. D., 1996. Particles in our air: concentrations and health effects. Harvard University Press, Cambridge, Massachusetts, USA, 259 pp.

Zege, E. P., Chaikovskaya, L., 1 1996. New approach to the polarized radiative transfer problem. J. Quant. Spectrosc. Radiat. Transf. 55 (1), 19–31.

Zhu, L., Martins, J. V., Remer, L. A., 2011. Biomass burning aerosol absorption measurements with MODIS using the critical reflectance method. J. Geophys. Res. 116(D7), D07202.

Curriculum Vitae

Short Biography

Education

2011 **Ph.D.**, University of Zurich, Department of Geography, Remote Sensing Laboratories. Thesis: Radiative Transfer and Aerosol Remote Sensing. Advisors: M.E. Schaepman, A.A. Kokhanovsky and K.I. Itten

2008 ESA Earth Observation Summer School on Earth System Monitoring and Modelling at ESRIN, Frascati, Italy

2004 **M.Sc.** (equivalent to Dipl. Natw. ETH) in Atmospheric and Climate Sciences (IAC), ETH Zurich. Thesis: Temporal and Spatial Variations in Remotely Sensed Atmospheric Water Vapor over North Africa from 1983 to 2003. Advisors: D. Grebner and U. Frei

2002 **B.Sc.** in Earth Sciences, ETH Zurich

Professional

2010 - Pres. **Research assistant** at University of Zurich, Department of Geography, Remote Sensing Laboratories

2009 - Pres. **Head of scientific NPOC** (Swiss National Point of Contact for Satellite Images)

2008 **Astronaut Applicant** for European Space Agency

2008 - Pres. **Chief-Pilot** Glider Tow

2004 - 2009 **Staff member of scientific NPOC** (Swiss National Point of Contact for Satellite Images)

2002 - 2004 **Staff member of Computer Support** at the Institute of Geology at ETH Zurich

2002 **Internship at the International Pacific Research Center**, University of Hawaii. Contribution to a study on the interactions of Sea Surface Temperature and surface wind speeds using satellite data. Advisors: R.J. Small and S.P. Xie

Teaching

2009 - Pres. Grundlagen Fernerkundung / Remote Sensing 1 (Lecture and Exercises), Subtopic: Data Archives & Repositories

2006 - Pres. Grundlagen Fernerkundung / Remote Sensing 1 (Lecture and Exercises), Subtopic: Time Series & Weather Satellites

2002 - Pres. Aviation Meteorology for Private-Pilots

Co-advised M.Sc. Theses

2008 Julia Walterspiel, Lidar Design, Construction and Measurements of Volcanic Aerosols on Hawaii. In collaboration with J.N. Porter at the Hawaii Institute of Geophysics and Planetology, SOEST, Univ. of Hawaii at Manoa

2008 Daniel Lachat, Fernerkundung von urbanen Aerosolen mittels LIDAR-Ceilometer. In collaboration with U.K. Krieger at Atmospheric and Climate Sciences (IAC), ETH Zurich

2007 Fabian Fusina, The impact of Ice Supersaturation Regions (ISSR) and Thin Cirrus Clouds on Radiation. In collaboration with P. Spichtinger at Atmospheric and Climate Sciences (IAC), ETH Zurich

Advised B.Sc. Theses (unpublished)

2009 Judith Buechel, Remote Sensing of the Global Change. (substitute title)

2008 Claudia Stocker, Remote Sensing of the Atmosphere. (substitute title)

2008 Stefanie von Büren, Remote Sensing of the Atmosphere. (substitute title)

2008 Sandra Meisser, Remote Sensing of the Atmosphere. (substitute title)

2007 Seraina Kauer, Remote Sensing of Natural Disasters. (substitute title)

2006 Patrick Staedeli, Remote Sensing of Natural Disasters. (substitute title)

2006 Sascha Gregori, Remote Sensing of Natural Disasters. (substitute title)

Memberships

2010 - Pres. European Geosciences Union (EGU)

2009 - Pres. Swiss interdepartmental coordination committee on space issues, working group GMES

2009 - Pres. Swiss interdepartmental working group remote sensing

2006 - 2011 IEEE

2005 - 2011 International society for optics and photonics (SPIE)

Publications

Peer reviewed journals

Seidel, F.C., Kokhanovsky, A.A., Schaepman, M.E., 2010. Fast retrieval of aerosol optical depth and its sensitivity to surface albedo using remote sensing data. Atmos. Res. (In Print to special issue on Remote Sensing of Clouds and Aerosols).
http://dx.doi.org/10.1016/j.atmosres.2011.03.006

Seidel, F.C., Kokhanovsky, A.A., Schaepman, M.E., 2010. Fast and simple model for atmospheric radiative transfer. Atmos. Meas. Tech. 3 (4), 1129–1141.
http://dx.doi.org/10.5194/amt-3-1129-2010

Seidel, F.C., Kokhanovsky, A.A., Schaepman, M.E., 2010. Fast and simple model for atmospheric radiative transfer. Atmos. Meas. Tech. Discuss. 3, 2225-2273.
http://dx.doi.org/10.5194/amtd-3-2225-2010

Itten, K.I., Dell'Endice, F., Hueni, A., Kneubühler, M., Schläpfer, D., Odermatt, D., **Seidel, F.**, Huber, S., Schopfer, J., Kellenberger, T., Bühler, Y., D'Odorico, P., Nieke, J., Alberti, E., Meuleman, K, 2008. APEX – the Hyperspectral ESA Airborne Prism Experiment. Sensors 8 (10), 6235–6259.
http://dx.doi.org/10.3390/s8106235

Seidel, F., Schläpfer, D., Nieke, J., Itten, K.I, 2008. Sensor performance requirements for the retrieval of atmospheric aerosols by airborne optical remote sensing. Sensors 8 (3), 1901–1914.
http://dx.doi.org/10.3390/s8031901

Other journals

Buehler, Y., **Seidel, F.**, Kellenberger, T., 2006. Unwetter 2005: Schnelle Schadenskartierung mit Satellitendaten zur Unterstützung des Katastrophenmanagements. Geomatik Schweiz 104 (9), 494–497

Conference contributions

Seidel, F.C., Kokhanovsky, A.A., Schaepman, M.E., 2011. Sensitivity of aerosol retrieval to surface albedo. In: Geophysical Research Abstracts. Vol. 13, EGU2011–1509. (Poster)

Seidel, F.C., Kokhanovsky, A.A., Schaepman, M.E., 2010. Concept of a Fast and Simple Atmospheric Radiative Transfer Model for Aerosol Retrieval. In: Geophysical Research Abstracts. Vol. 12, EGU2010–14489. (Poster)

Seidel, F.C., Kokhanovsky, A.A. Schläpfer, D., 2009. Parameterization of multiple-scattered light in an aerosol atmosphere for the use in a simple radiative transfer model. Determination of Atmospheric Aerosol Properties Using Satellite Measurements, Wilhelm and Else Heraeus Seminar, Physikzentrum Bad Honnef, Germany. (Poster)

Seidel, F.C., Schläpfer, D. Itten, K.I., 2009. Efficient Radiative Transfer Calculation and Sensor Performance Requirements for the Aerosol Retrieval by Airborne Imaging Spectroscopy. In proceedings: 6th EARSeL Imaging Spectroscopy SIG workshop, Tel Aviv, Israel. (Talk)

Seidel, F., Schläpfer, D., Nieke, J., Itten, K. I., 2008. Airborne Hyperspectral Remote Sensing of Aerosols: Radiation Transfer and Sensor Performance. 4th ESA Earth Observation Summer School on Earth System Monitoring and Modelling at ESRIN, Frascati, Italy. (Poster)

Walterspiel, J., Porter, J., Bates, D., **Seidel F.**, Sharma, S., 2007. Sensitivity Studies of Different Lidar Configurations. IEEE International Geoscience and Remote Sensing Symposium IGARSS, Barcelona, Spain. (Poster)

Seidel, F., Nieke, J., Bowles, J. H., Schläpfer, D., Itten, K. I., 2006. Aerosol retrieval technique for hyperspectral remote sensing with high spatial resolution. Conference on Visibility, Aerosols, and Atmospheric Optics, Vienna. (Poster)

Seidel, F., Nieke, J., Schläpfer, D., Itten, K. I., d Bowles, J. H., 2006. Evaluation of near-UV/blue aerosol optical thickness retrieval from airborne hyperspectral imagery. In: Proceedings-IEEE International Geoscience and Remote Sensing Symposium IGARSS. pp. 2247–2250. http://dx.doi.org/10.1109/IGARSS.2006.581 (Talk)

Seidel, F., Buehler, Y., Kellenberger, T., Perret, J.-P., 2006. Satellite response to the August 2005 floods in Switzerland: Charter call 100. In: Ammann, W. J., Haig, J., Huovinen, C., Stocker, M. (Eds.), Proceedings of the International Disaster Reduction Conference, Davos Switzerland. Vol. 3. Swiss Federal Research Institute WSL, pp. 531–533. (Talk & Poster)

Seidel, F., Nieke, J., (2006). Near-UV/blue aerosol retrieval for hyperspectral remote sensing with high spatial resolution: an evaluation. ISPRS Workshop on Remote Sensing of Aerosols, Berlin. (Poster)

Seidel, F., Nieke, J., Schläpfer, D., Höller, R., von Hoyningen-Huene, W., Itten, K. I., 2005. Aerosol retrieval for APEX airborne imaging spectrometer: a preliminary analysis. In: Schäfer, K., Comerón, A., Slusser, J. R., Picard, R. H., Carleer, M. R., Sifakis, N. (Eds.), Remote Sensing of Clouds and the Atmosphere X. Vol. 5979 of Proc. of SPIE. pp. 548–557. (Poster)

Nieke, J., **Seidel, F.**, Kaiser, J. W., Schläpfer, D., Itten, K. I., 2005. New retrieval capabilities for remote sensing of atmospheric parameters. In: Proceedings of the Conference of the Remote Sensing Society of Japan. Vol. 39. pp. 75–76.

Seidel, F., 2005. NPOC Response to Charter Call 100, Switzerland Flood. EURISY Conference "Benefits from Space for Sectorial Policy for High Mountain Security". (Poster)

Reports (unpublished)

Treichler, D., **Seidel, F.**, Schaepman, M., 2010. Geographische Informationen – Studie zu Bedürfnissen des EDA. Bericht zu Handen EDA, Remote Sensing Laboratories, University of Zurich, University of Zurich.

Seidel, F., Treichler, D., 2010. Evaluation der Nutzerbedürfnisse und Beiträge des Bundes an GMES Initial Operations (GIO) und GMES. Bericht zu Handen IKAR-GMES Arbeitsgruppe Nutzerstrategie - Erweiterte Befragung – GIO und GMES Operational Phase, National Point of Contact, University of Zurich.

Seidel, F., Treichler, D., 2009. Evaluation der Nutzerbedürfnisse und Beiträge des Bundes an GMES Initial Operations (GIO). Bericht zu Handen IKAR-GMES Arbeitsgruppe Nutzerstrategie, National Point of Contact, University of Zurich.

Seidel, F., Kellenberger, T., Buehler, Y., 2009. Fernerkundung in der Schweiz: Eine Übersicht. Bericht zu Handen SBF - Bereich Raumfahrt, National Point of Contact, University of Zurich.

Seidel, F., Kellenberger, T., Buehler, Y., 2008. Nutzerstrategie der Schweiz zur Europäischen Initiative "Global Monitoring for Environment and Security" (GMES). Bericht zu Handen IKAR-GMES Arbeitsgruppe Nutzerstrategie, National Point of Contact, University of Zurich.

Kellenberger, T., **Seidel, F.**, 2006. Verwendung von Fernerkundungsdaten zur raschen Kartendarstellung (Rapid Mapping). Bericht zu Handen Bundesamt für Bevölkerungsschutz BABS, National Point of Contact, University of Zurich.

Theses

Seidel, F.C., 2011. Radiative Transfer and Aerosol Remote Sensing. PhD thesis University of Zurich

Seidel, F.C., 2004. Temporal and spatial variations in remotely sensed atmospheric water vapor over North Africa from 1983 to 2003. Diploma thesis ETH Zurich